وزارة التعليم العالي و البحث العلمي

BADJI MOKHTAR UNIVERSITY- ANNABA

UNIVERSITE BADJI MOKHTAR - ANNABA

جامعة باجي مختار - عنابة

FACULTE DE TECHNOLOGIE

DEPARTEMENT DE GENIE CIVIL

Année: 2024

THESE

Présentée en vue de l'obtention du diplôme de DOCTORAT en Génie Civil

Thème

Flexural behavior of cold-formed steel beams: Development of generalized direct strength method and efficient built-up sections for local buckling

Option : Structure

Par :

MAIZI Salah-Eddine

Directeur de Thèse:

HADIDANE Yazid - Pr - Université de Badji Mokhtar, Annaba

Devant le jury:

Président:	**OUCIEF Hocine**	**Pr.**	**Univ. BADJI Mokhtar ANNABA**
Examinateurs:	**NAFAA Zahreddine**	**Pr.**	**Univ. 08 MAI 1945 GUELMA**
	GUENFOUD Mohamed	**Pr.**	**Univ. 08 MAI 1945 GUELMA**
	GOUIDER Nadia	**MCA.**	**Univ. BADJI Mokhtar ANNABA**

Abstract

This thesis investigates the flexural behavior of innovative cold-formed steel (CFS) built-up closed sections, focusing on cross-sectional buckling failure. A Finite Element (FE) model is developed and extensively validated against various built-up closed and open sections in bending. Three parametric studies are conducted, each exploring different aspects of the proposed built-up closed sections.

The first study compares different built-up box sections, revealing significant strength advantages for the DH section under certain thickness conditions. The second study examines the effect of fasteners on bending strength, demonstrating their importance in enhancing strength and deformation patterns, particularly in partially stiffened sections. The third study evaluates the Direct Strength Method (DSM) in predicting the strength of innovative built-up sections. It concludes that DSM tends to be unreliable for built-up members strength calculation, prompting the development of a Generalized Direct Strength Method (DSM-G). DSM-G incorporates a new equations based on a mathematical model derived from the study's results, significantly improving predictive accuracy. This new method relies on a convergence-based approach to extend the original DSM application on built-up members in bending.

The proposed DSM-G method is validated through extensive comparison with finite element analysis and experimental results from literature. A step-by-step diagram illustrates the application of DSM-G in built-up sections, emphasizing its gradual expansion and validation process.

Keywords: cold-formed steel, built-up sections, flexural behavior, buckling failure, Finite Element Analysis, Direct Strength Method, Generalized Direct Strength Method.

ملخص

تقدم هذه الأطروحة دراسة في سلوك الانحناء لمقاطع جديدة مركبة من القطاعات المشكلة على البارد مركزة على الانبعاج القطاعي لهذه العناصر. تم تطوير نموذج رقمي من العناصر المحدودة باستخدام برنامج أباكوس والتحقق منه بالمقارنة مع مجموعة متنوعة من الاختبارات التجريبية التي أجريت على المقاطع المركبة في الدراسات السابقة. تتلخص الدراسة في ثلاث دراسات معيارية تهدف إلى التحقيق في جوانب مختلفة من هذه المقاطع الجديدة.

تُقارن الدراسة الأولى بين مختلف المقاطع المركبة المغلقة، كاشفةً عن مزايا كبيرة من حيث المقاومة للمقطع (دش) تحت ظروف سمك معينة.

تفحص الدراسة الثانية تأثير البراغي على مقاومة الانحناء، مُظهرةً أهميتها في تحسين المقاومة وأنماط التشوه، خصوصاً في المقاطع المدعمة جزئيا.

تُقيّم الدراسة الثالثة طريقة الإجهاد المباشر (ط إ م) للتنبؤ بمقاومة المقاطع المركبة الجديدة. وتخلص إلى أن هذه الطريقة تميل إلى أن تكون غير موثوقة لحساب مقاومة العناصر المركبة، مما أدى إلى تطوير طريقة معممة للإجهاد المباشر (ط م إ م) تحتوي على معادلات جديدة مبنية على نموذج رياضي مستمد من نتائج الدراسة، مما يحسن بشكل كبير دقة تنبؤات المقاومة مقارنة بالطريقة الأصلية.

تم التحقق من صحة ط م إ م من خلال مقارنة واسعة مع نتائج تحليلات العناصر المحدودة والنتائج التجريبية المستمدة من الأدبيات، و النتائج المتحصل عليها كانت جد دقيقة و موثوقة، في الأخير يوضح مخطط خطوة بخطوة تطبيق ط م إ م على المقاطع المركبة، بالإضافة إلى دليل شامل لتطبيق الطريقة على المستوى البحثي و العملي.

الكلمات المفتاحية: القطاعات المشكلة على البارد، المقاطع المركبة، سلوك الإنحناء، الإنبعاج القطاعي، العناصر المحدودة، طريقة الإجهاد المباشر، الطريقة المعممة للإجهاد المباشر.

Résumé

Cette thèse présente une investigation sur le comportement flexionnel de nouvelle sections composées en profilé formé à froids en se basant sur le flambement sectionnelle de ces éléments. Un modèle d'éléments finis a été développé et vérifié par rapport à une variété de tests expérimentaux conduits sur des sections composées, issu de la littérature, l'étude se résume en trois études paramétrique conduites dans le but d'investiguer différents aspects de ces nouvelles sections. La première étude compare différentes sections composées fermées, révélant des avantages significatifs en termes de résistance pour la section DH sous certaines conditions d'épaisseur. La deuxième étude examine l'effet des boulons sur la résistance à la flexion, démontrant leur importance pour améliorer la résistance et les modes de déformation, en particulier dans les sections partiellement raidies. La troisième étude évalue la méthode de la contrainte directe (MCD) pour prédire la résistance des sections assemblées innovantes. Elle conclut que cette méthode a tendance à être peu fiable pour le calcul de la résistance des éléments composés, ce qui a conduit au développement d'une méthode généralisée de la contrainte directe (MCD-G). La MCD-G intègre de nouvelles équations basées sur un modèle mathématique dérivé des résultats de l'étude, améliorant considérablement la précision des prédictions. Cette nouvelle méthode repose sur une approche basée sur la convergence pour étendre l'application de la MCD originale aux sections assemblés en flexion soumise au voilement. La méthode MCD-G proposée est validée par une comparaison extensive avec des analyses par éléments finis et des résultats expérimentaux issus de la littérature. Un diagramme étape par étape illustre l'application de la MCD-G dans les sections assemblées, en mettant en avant son processus d'extension et de validation progressive.

Mots clés : Profils formés à froids, sections composées, flexion, flambement, Méthode de la contrainte directe, Méthode généralisé de la contrainte directe.

Acknowledgement

I would like to express my honest gratitude to Pr. Hadidane Yazid for suggesting this Ph.D subject and approving the investigations presented in this thesis, his patience, trust and supervision were the keys to the completion of this work. I ‘am also grateful to Dr. Mohammad Adil Dar for his co-guidance in giving advices and suggestions, and assuring the good presentation of the work. The challenges and difficulties encountered during the development of this research have been invaluable learning experiences that have helped me grow as a researcher.

I would like to express my gratitude to my mother, Dr. Benzannache Naziha, for initially introducing me to the field of Civil Engineering and later encouraging me to pursue my Ph.D. Her unwavering support and inspiration throughout my doctoral studies were pivotal. Her assistance was invaluable in helping me overcome laziness and complete this work on schedule.

Finally, I would like to take the liberty to express my gratitude in my native language:

من باب قول النبي صلى الله عليه و سلم (لا يشكر الله من لا يشكر الناس) أودُّ أن أعربَ عن امتناني الصادق للبروفيسور حديدان يزيد لاقتراحه موضوع هذه الأطروحة و الموافقة على ما قدم فيها من دراسات، إذ أن تأطيره و ثقته في البحث المقدم بالإضافة إلى صبره و سعة باله شكلت نقاطا مهمة في إتمام هذا العمل. إن شكري كذلك موصول إلى الدكتور محمد عديل على التوجيه المشترك والنصائح القيمة والاقتراحات التي ساهمت في جودة هذا العمل. إن التحديات و الصعوبات المواجهة خلال إنجاز هذه الأطروحة و ما احتوته من دراسات كانت تجربة تعليمية ثمينة ساعدتني بشكل رئيسي كي أصبح الباحث الذي أنا عليه اليوم.

إن شكري و امتناني كذلك موصولان لوالدتي الكريمة، الدكتورة بن زناش نزيهة، إذ كانت أول من عرفني بمجال الهندسة المدنية ثم امتد دعمها في تشجيعي لمواصلة الدكتوراه. إن حرصها و دعمها المتفانيان كانا مصدر إلهام رئيسي لي خلال مسيرتي في الدكتوراه. إن حرصها كان لا يقدر بثمن إذ ساعدني على تجاوز العقبات و إتمام هذا العمل في وقته. إن شكري هذا لا أستثني به عائلتي الكريمة، أبي أحمد، أختي لينة، أخي حسام، خالتي كميلة و جدتي فاطمة، و كل من دعمني من قريب أو بعيد و أراد لي النجاح و التوفيق

Table of Contents

List of Figures

List of Tables

List of Symbols

b_f = flange width;

b_l = lip depth;

C_p = reliability analysis correction factor;

E = young's modulus;

$f_{DM}(t)$ = Mathematical model for DM section;

$f_{DOW}(t)$ = Mathematical model for DOW section;

F_m = average value of fabrication factor;

f_y = yield stress;

h_w = overall web depth ;

l = width of the overlapped zone;

M_{crd} = critical elastic distortional buckling moment;

M_{crl} = critical elastic local buckling moment;

M_{DSM} = nominal bending strength using DSM equations;

$M_{\text{DSM-G}}$ = nominal bending strength using DSM-G equations;

M_{EXP} = maximum bending strength from experimental investigation;

M_{FEA} = maximum bending strength from finite-element analysis;

M_m = average value of material factor;

M_{nd} = nominal bending strength for distortional buckling;

M_{ne} = nominal bending strength for lateral-torsional buckling;

M_{nl} = nominal bending strength for local buckling;

M_p = cross-section plastic moment;

M_y = cross-section yield moment;

P_m = average value of experimental/FEA-to-predicted moment ratio;

r_i = inner radius of the round corner of sections;

S_f = cross-section modulus in the extreme fiber at first yield;

t = thickness of steel plate with coating;

t^* = base metal thickness.

V_F = coefficient of variation from fabrication factor;

V_M = coefficient of variation from material factor;

V_P = coefficient of variation of experimental/FEA-to- predicted moment ratio;

w_1, w_2, w_3 = plate width of stiffened M and Hat sections;

Z_f = plastic section modulus;

β_0 = target reliability index;

β_1 = reliability index using combination of 1.2 dead load

1.6 live load;

β_2 = reliability index using combination of 1.25 dead load

1.5 live load;

η = (shape/form) coefficient;

θ = angle of inclined web element from the vertical axis;

λ_d = slenderness limit for distortional buckling;

λ_l = slenderness limit for local buckling;

λ_{lf} = fictive slenderness limit for local buckling;

$\sigma_{0.2}$ = 0.2% proof stress (yield stress);

σ_u = ultimate stress;

ε_f = plastic strain (%);

ϕ_b = resistance factor for beams;

Chapter 1
Introduction

Cold-formed steel (CFS) sections of thicknesses from 0.5 mm to 6 mm have historically been employed as secondary frames in structures. Typical instances are roof purlins and wall girts fabricated from channels, zed and sigma sections, together with wall and roof cladding constructed from profiled sheets with thicknesses reaching 1.5 mm. CFS sections have been used in mezzanine flooring and as structural steel in small industrial building.

Production methods, such as roll forming or brake pressing, are dependent upon the number, length, and intricacy of the parts. In roll forming, a long steel strip is subjected to a sequence of rollers that incrementally shape it until the desired configuration is attained. This approach is used for the fabrication of substantial quantities of a certain form. Conversely, in the press-braking process, each curvature of the cross-section is achieved by bending the sheet along its whole length as it is pushed against a curved die. This method is used for low-volume manufacturing and for spans of up to 8 meters. Advancements in manufacturing techniques have facilitated higher production rates and permitted the roll forming of steel strips with a thickness of up to 25 mm, while sheets with a thickness of up to 12.5 mm may be brake-pressed. Furthermore, advancements in the application of zinc coatings on cold-formed steel sections have enhanced their corrosion resistance [1].

These enhancements, along with the benefits derived from the slim design of these sections, have considerably expanded their use. Their design facilitates nesting during storage, enabling compact packaging and minimizing shipping costs. They are also simply managed, with individual components and sub-frames readily positioned by operators, enabling rapid assembly. Furthermore, CFS sections are sustainable due to

their extended service life and ease of reuse or recycling, hence reducing trash production.

The effective use of materials in CFS sections results in a high strength-to-weight ratio, which simultaneously minimises the carbon footprint and offers a more cost-effective option by decreasing the structure's self-weight. This problem is not simply crucial for decreasing the overall cost of a project, but may also be critical in circumstances when it is required to add a new floor to a building, limiting the increased load on the current building and its foundations. This resulted in a growing utilisation of thin-walled members, not merely as secondary components but also as primary load-bearing elements, prompting the CFS industry to focus on manufacturing sections capable of accommodating wider spans and withstanding greater loads. Instances of this growth include multi-storey edifices and portal frames fabricated completely from CFS.

A rational approach to enhance the load-carrying strength of CFS members is the connection of two or more sections using welding or fasteners, including bolts, rivets, or screws, to create a built-up section. A broader variety of cross-sectional forms may thus be created with the presently accessible single shapes, allowing customization to fulfil certain specifications. Moreover, doubly symmetric cross sections may be readily formed by combining individual sections, hence mitigating certain buckling modes that often arise in members with singly symmetric cross sections, for instance flexural-torsional buckling. Double symmetry also minimizes the displacement of the effective centroid that individual sections may undergo during local or distortional buckling. Moreover, closed sections may be engineered to enhance torsional resistance. As built-up components may theoretically be assembled on-site, the benefits of convenient transit and handling mostly persist.

Due to their innovative nature in connecting individual CFS section, built-up sections are categorized into multiple categories, a primary category are built-up open sections, also known as back-to-back sections, are made up of two channel sections connected

together. These sections have been extensively studied for their flexural behavior and performance, altering key parameters like geometrical properties, slenderness, and screws spacing. Experiments have provided a global understanding of built-up I-beams and validated parametric studies in order to conduct extensive numerical analysis for particular aspects investigation.

Nevertheless, the range of built-up shapes available is limited to conventional I-sections with varying stiffener configurations. Moreover, the second category of built-up sections consisting of symmetrical closed sections, have proven effective in improving torsional buckling rigidity, a feature I-sections lack due to their free flanges. This limitation has been addressed by adopting built-up face-to-face sections, resulting in closed sectional profiles. These sections offer a diverse range of shapes by incorporating intermittent stiffeners in both the web and flanges, effectively preventing torsional buckling in extended members and laterally unrestrained spans.

1.1 Objective and scope

The present thesis aims to investigate the flexural behavior and design of novel CFS built-up sections developed through a new assembling concept in order to obtain an optimum design capable of satisfying the high strength to weight ratio criterion. The primary focus is to explore the elastic buckling in built-up closed sections, especially the cross-sectional instabilities (local and distortional buckling). A variety of built-up closed-sections profiles will be adopted, aiming to cover the behavioral response of the beams under various conditions, such as slenderness and cross-sectional slenderness variation, fasteners spacing and geometrical properties. The obtained flexural strength of the investigated built-up sections will be used to assess the prediction abilities of the Direct Strength Method (DSM) presented in the current (NAS) [2]. Depending upon the prediction adequacy of the current DSM, a new design method may be proposed, if necessary. This investigation will be divided based on the cross-sections adopted to investigate a particular aspect of the study.

1.2 Thesis layout

The present thesis will be divided into eight chapters as follows:

Chapter 2 presents the importance of CFS members in modern construction, it explores unique aspects related to these members such as the influence of the forming process on the mechanical properties, the determination and quantification of geometrical properties, it also addresses critical behavioral aspect such as warping and buckling modes. The chapter emphasizes the importance of adhering to the prescribed design guidelines to avoid instabilities. Finally, an overview into the different method used for analyzing the behavior of cold-formed steel members is presented.

Chapter 3 delve into exploring CFS built-up members under bending, it presents important investigations conducted on built-up open and closed sections subjected to different buckling modes, it addresses as well the stiffennig technics used to improve the overall behavior of these members,

Prior conducting the Finite Element parametric study to investigate the flexural behavior of novel CFS built-up sections, the modelling technic was validated against experimental tests conducted on a variety of built-up closed and open sections issued from literature. Chapter 4 discusses all particularities related to the finite element model development as well as the validation results obtained.

The first part of the global parametric study focuses on studying the efficiency of a new built-up closed section in enhancing the flexural strength and sustaining local buckling failure, the name attributed to this cross-section was DH, the design concept adopted was to consider the overlapped zone of the web as a connection part and bearing stiffeners intermittently as illustrated in Figure 1.1. The approach adopted for validating the section strength ability against local buckling failure, was achieved thought comparative study against two built-up box sections with different assembling concepts, as proposed in previous studies. Similar parameters were attributed to the

three sections to assess the flexural capacity and buckling performance of each cross-section. Details and results of this study are presented in Chapter 5.

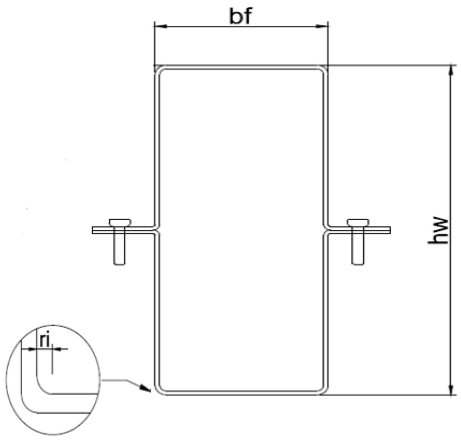

Figure 1.1: Built-up cross-sectional concept adopted (DH section).

This section of the parametric study treats the effect of fasteners spacing on the flexural capacity of built-up sections considering it an important external aspect present in these members, it comprises a parametric study conducted on three innovative built-up closed sections to assess the influence of fasteners on the bending capacity of these sections, the same assembling concept used for DH section is adopted, the followed approach to verify the impact of fasteners on this particular sectional configuration, was to variate the stiffening-degree of the sections, therefore, the overall cross-shapes of the three sections varies from partial to fully stiffened configurations, as shown in Figure 1.2, this allows for a better understanding of the contribution of fasteners in the overall behavior of the beams. Details and results of this investigation are summarized in Chapter 6.

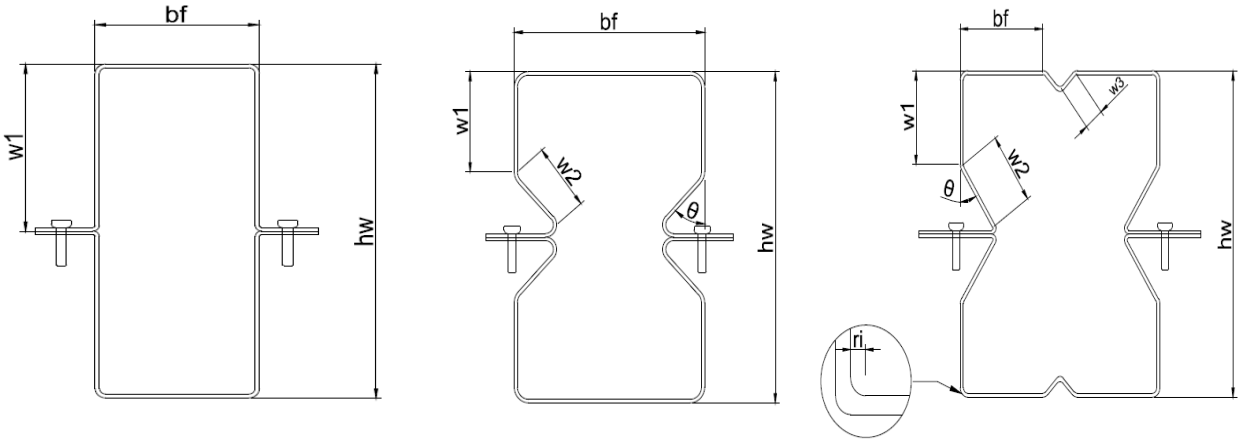

Figure 1.2: Built-up sections considered for fasteners effect on the strength, following stiffening-degree approach.

The analytical aspect of built-up sections subjected to bending is presented in Chapter 7, its main purpose is to assess the direct strength method (DSM) abilities in predicting the flexural behavior of built-up sections used in cold-formed steel design strength prediction, this method was primarily developed for cold-formed steel individual sections, therefore its applicability on built-up sections was a question addressed in limited studies, particularly for flexural members, this study delves more in this subject to contribute in developing a new design approach based on DSM, for built-up sections in bending, focusing notably on local buckling failure instability. The DSM was primarily applied on innovative built-up closed sections presented in Figure 1.3. The analysis of the obtained results, as well as the collection of previous DSM predictions on built-up sections, restricted to cross-sectional buckling failure, contributed in proposing a new design approach for built-up beams failing in local buckling. The detailed process as well as the outcome of the study will be presented in this chapter.

Chapter 8 concludes with relevant findings of this study, encompassing both numerical results related to the performance and behavior of the developed built-up sections, as well as the assessment of the current DSM, and successively the adoption of the novel

design approach for built-up members failed in local buckling, called the ‘Generalized Direct Strength Method’.

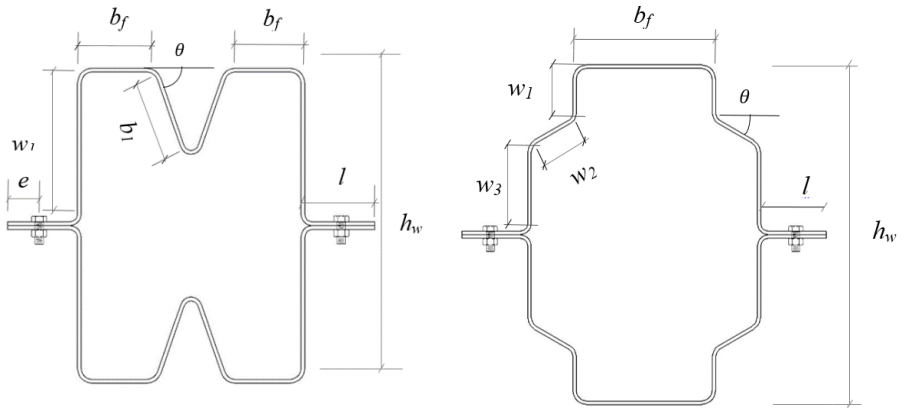

Figure 1.3: Stiffened built-up closed sections used in the design part [106].

1.3 Publications

The following papers have resulted from the research presented in this thesis:

S.-E. Maizi, Y. Hadidane, and M. A. Dar, “Flexural design of cold-formed steel built-up sections failing by local buckling: Development of generalised direct strength method” Engineering Structures, vol. 308, p. 117967, Jun. 2024, doi: 10.1016/j.engstruct.2024.117967.

S.-E. Maizi, Y. Hadidane. (2021) “Comparative study between two box CFS sections assembled in different ways in bending”, *2nd International Symposium on Construction Management and Civil Engineering (ISCMCE), University of Skikda Algeria.*

S.-E. Maizi, Y. Hadidane. (2021) “Comparative study between two box CFS sections assembled in different ways in bending”, *Geotechnical, structural and material engineering First International Conference held at Biskra University, Algeria.*

S.-E. Maizi, Y. Hadidane. (2021) “Comparative study between two box CFS sections assembled in different ways in bending”, *3ème Conférence Internationale de Construction Métallique et Mixtes, CICOMM, Oran.*

S.-E. Maizi, Y. Hadidane. (2023) “Effect of Screws Spacing on the Flexural Strength of Innovative Cold Formed Steel Built-up Sections”, *Congrès National de Génie Civil et Hydraulique (CNGCH), Guelma.*

S.-E. Maizi, Y. Hadidane. (2023) “Effect of Screws Spacing on the Flexural Strength of Innovative Cold Formed Steel Built-up Sections”, *1st International Conference on Civil and Earthquake Engineering (ICCEE), Annaba.*

S.-E. Maizi, Y. Hadidane. (2024) “Influence of Connectors on the Bending Resistance of Cold-Formed Sections Partially and Fully Stiffened”, *1er Colloque National sur l’Hydraulique et le Génie Civil (CNHGC), Bouira*.

Chapter 2
Generalities on cold-formed steel members

2.1 Introduction

Steel construction encompasses two primary categories of structural elements. The first, refers to well-known categories of shapes and members that are formed by hot-rolling process. The second, less-known but increasingly significant method involves the creation of sectional profiles through the cold-forming process of steel materials such as sheet, strip, plates, or flat elements, using roll-forming machines or press brake operations [1]. The thickness of steel sheets or strip commonly employed in cold-formed steel structural members varies from 0.4 mm to approximately 6.4 mm. Structural shapes can be successfully cold-formed from steel plates and bars with a thickness of up to 25 mm [2].

The focus of the discussions in this document is primarily on the use of cold-formed steel sections in building construction, although they are also commonly used in car bodies, railway coaches, various types of equipment, storage racks, grain bins, highway products, transmission towers, transmission poles, drainage facilities, and bridge construction (Figure 2.1). For non-building structures, it may be important to consider allowances for dynamic effects, fatigue, and corrosion [2].

The utilization of cold-formed steel elements in the construction of buildings began in the 1850s in both the United States and Great Britain. Nevertheless, the utilization of such steel components in structures did not become prevalent until approximately 1940. Winter has conducted a comprehensive analysis of the initial progress in constructing steel buildings [3]. The issue of successive editions of the 'Specification for the Design of Cold-Formed Steel Structural Members' by the American Iron and Steel Institute (AISI) [3], has expedited the use and development of thin-walled cold-

formed steel construction in the United States since 1946. The initial versions of the standard were primarily derived from the research funded by AISI at Cornell University, led by George Winter, starting in 1939. It has been subsequently changed to incorporate the latest technology advancements and findings from ongoing research.

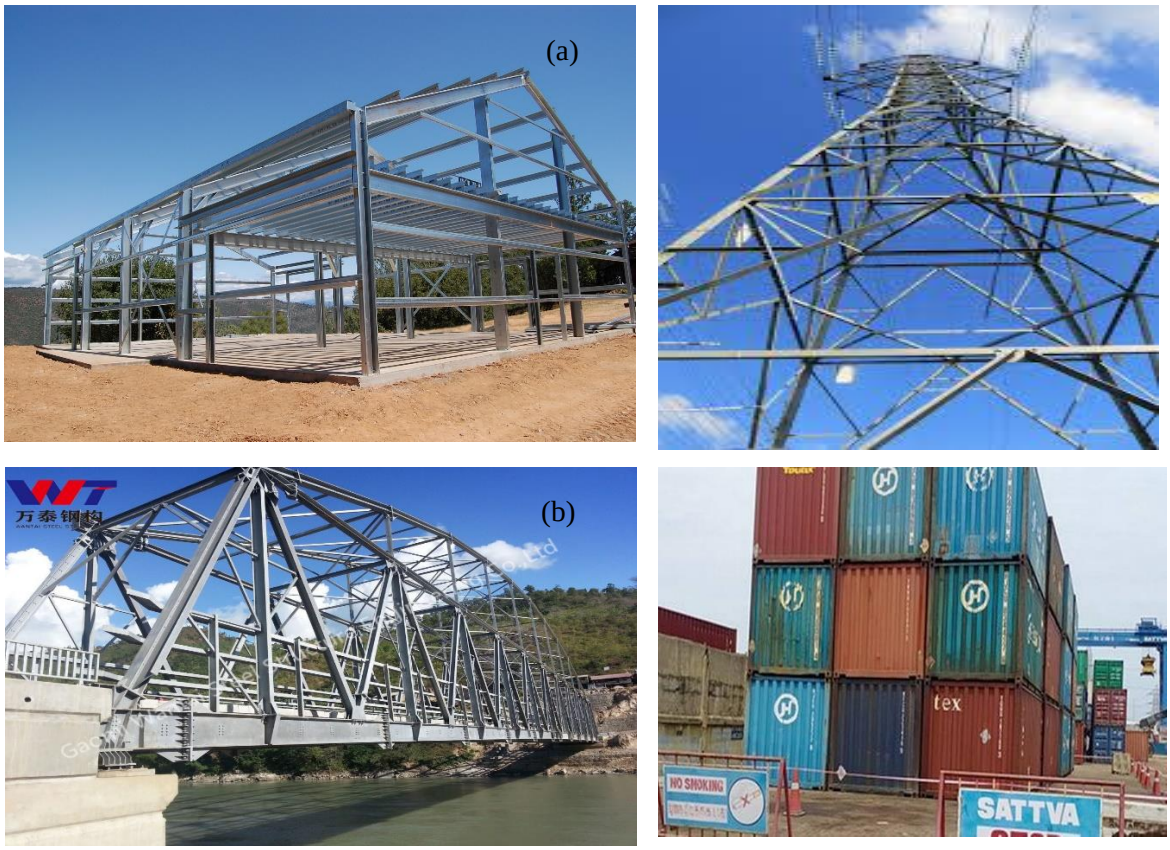

Figure 2.1: Domain of utilization of cold formed steel, (a) construction frame (https://www.mcelroymetal.com/cold-formed-steel-buildings); (b) small bridge (https://fr.made-in-china.com), [accessed on November 2024].

2.2 Application of cold formed steel sections in construction

Cold-formed steel structural elements can be categorized into two main categories based on their orientation in the construction:

2.2.1 Main Framing members

This category encompasses a wide range of sectional shapes, such as the usual shapes like channel section, Z section, Hat sections, angle sections, I sections, T sections, and

hollow members etc..., Typically, the cold-formed individual framing members have a depth ranging from 51 to 305 mm, and a material thickness from 1.2 to approximately 6.4 mm. In certain instances, the individual members can have a depth of up to 457 mm (if met with the geometrical limits prescribed in design codes), and the thickness of the member can be 13 mm or greater in transportation and building construction. Cold-formed steel sections with thicknesses ranging from approximately 19 to 25 mm have been utilized in buildings, transmission poles, and highway-sign support structures.

Design priorities center on ensuring structural strength and stiffness, as load bearing is the primary purpose of these individual framing members, these sections can be utilized as the primary members of the frame, on the condition that the structure does not exceed a maximum height of six stories. A building consisting of two stories and completely constructed in cold formed steel members is depicted in Figure 2.2. In addition, cold formed steel could be used as secondary frame members in a construction that combines between hot rolled and cold formed members where they both complement each other. In this case cold-formed sections are utilized as chord and web members in open web steel joists, space frames (Figure 2.3), arches, and storage racks.

Figure 2.2: Two story residential building entirely built in cold formed members (https://framecad.com/blog/accelerate-the-construction-of-mid-rise-buildings-with-cold-formed-steel-and-framecad [accessed on November 2024]).

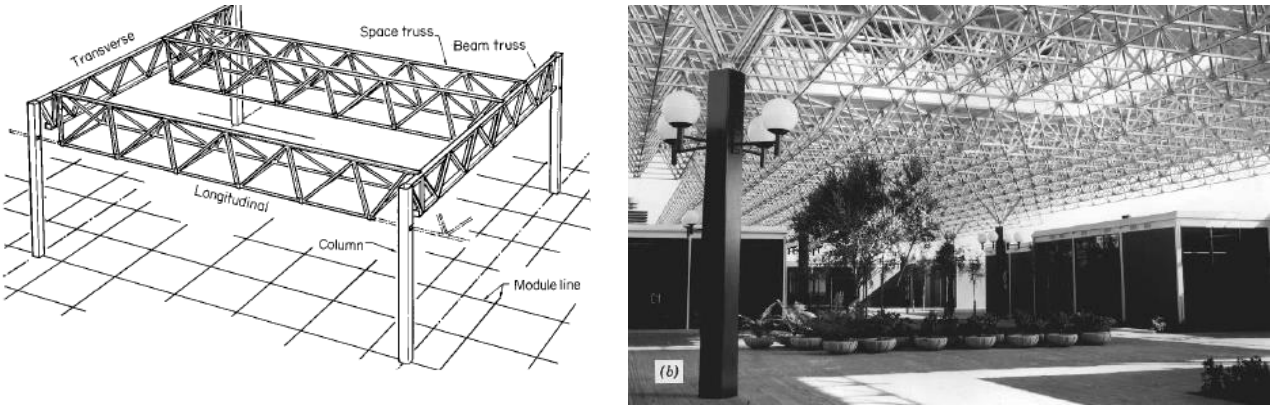

Figure 2.3: Space frames built in cold formed members [1].

2.2.2 Panels and Decks

Figure 2.4(a) shows another type of cold-formed steel application in construction. These corrugated sheet sections are typically employed for building roof decks, floor decks, wall panels, and various types of bridges. Web stiffeners are used in cold-forming deeper panels and decks. The panels typically have a depth ranging from 38 to 191 mm, and the materials used have a thickness ranging from 0.5 to 1.9 mm. It is important to note that there are situations when the utilization of 0.3 mm steel ribbed sections as load-bearing components in roof and wall construction may not be permissible.

Steel panels and decks serve a dual purpose by offering both structural stability for bearing loads and a platform for the application of flooring, roofing, or concrete fill, as depicted in Figure 2.4(b). In addition, it has the ability to offer room for electrical components, conduits, or it can be perforated and paired with sound absorption materials to provide an acoustically conditioned ceiling. The cells of cellular panels serve as conduits for heating and air conditioning.

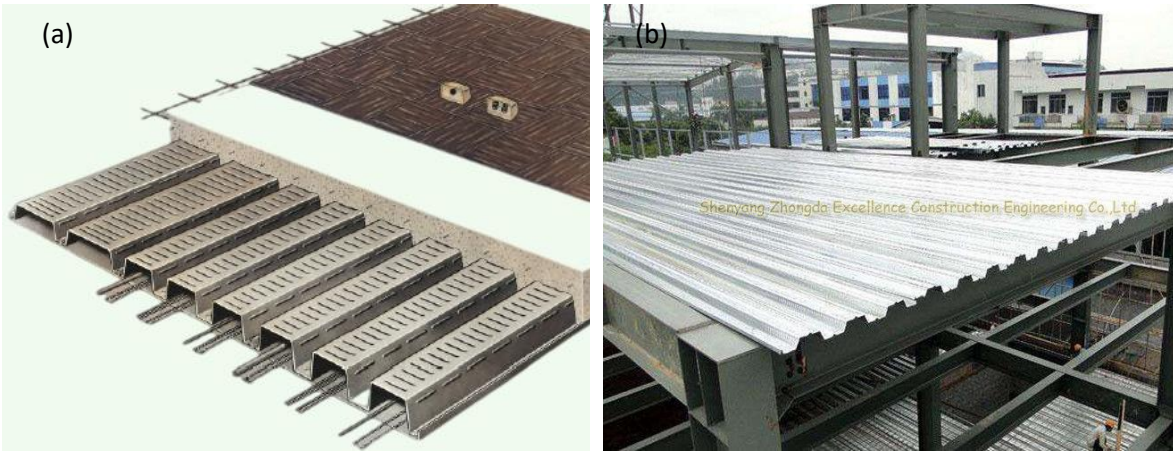

Figure 2.4: Panels corrugated profiles (a) with concrete [1], (b) without concrete (https://www.prefabricatedsteelstructures.com/sale-9458035-aisi-astm-corrugated-steel-floor-decking-sheet-steel-structure-0-5mm-1-2mm.html [accessed on November 2024]).

2.3 Built-up sections

The performance of cold-formed steel differs significantly from that of conventional hot-rolled steel due to its thickness profile and light weight. Low in rigidity and high in strength, cold-formed steel is susceptible to deformation due to its inherent properties. Therefore, the industrial sector lacked the conviction to generalize the usage of cold-formed steel members to a large range until the 1940s, when a greater understanding of the cold-formed steel material behavior began. Since then, cold-formed steel members have gained widespread acceptance and application. The first studies focused on examining the behavior of individual CFS sections made with typical sectional shapes such as channels and Z sections. Over time, individual sections ceased to be adequate in meeting the demands of construction. To effectively allow the utilization of these members as load-bearing members, designers tested a variety of reinforcement strategies for columns. Constructing a built-up column by connecting two separate columns is among the effective methods proposed. Therefore, built-up sections were developed in response to the requirement to carry larger loads; they are now among the most commonly employed sections. built-up member consists of two or more structural members mechanically joined together via intermediate fasteners such as screws, self-drilling screws, bolts or weld connections. Figure 2.5 show different connection establishments between individual CFS sections.

For many low to medium-rise commercial and residential buildings, built-up members are a popular choice due to their structural feasibility and accommodation with installation requirements of current construction projects. Open sections and closed sections are the two main ways to classify built-up sections.

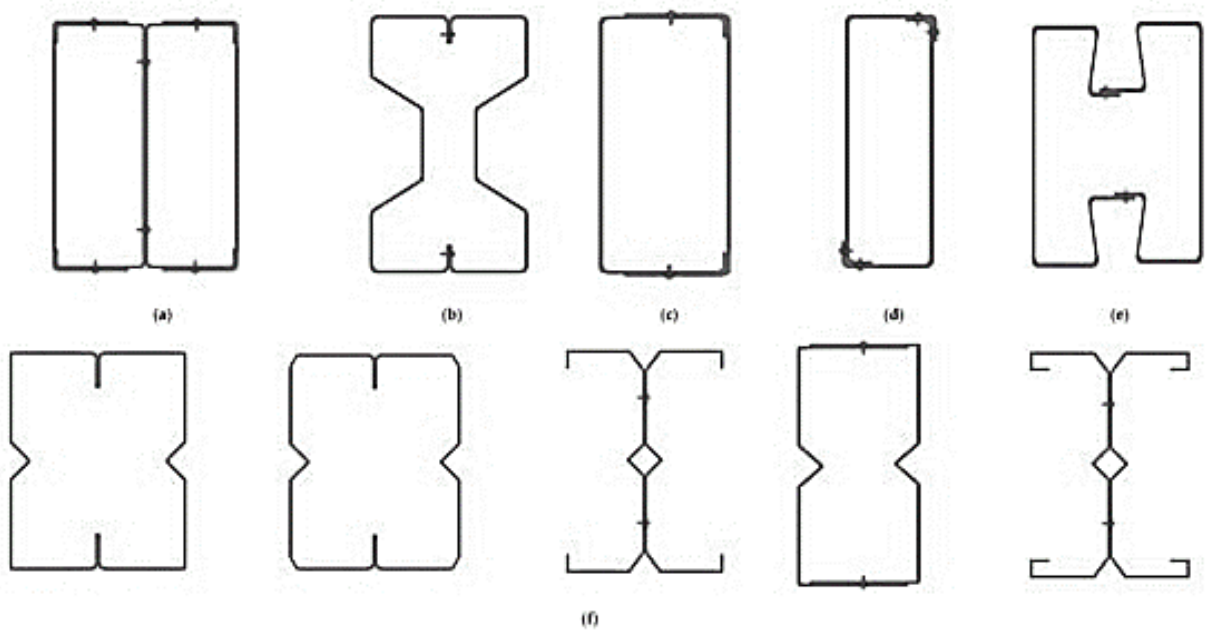

Figure 2.5: Cold formed steel built-up section with different shapes and stiffeners.

2.4 Material properties

2.4.1 Steel types allowed for members cold forming

The yield point or yield strength determines the strength of cold-formed steel structural members, with the exception of connections and situations where elastic local buckling or general buckling are dominant. The yield points of the steels specified in the AISI-S1000 [2] range from (165 to 552 MPa), the steels grades prescribed in the ASTM norm used in members cold forming must fall under the following categories:

2.4.1.1 Steels with a specified minimum elongation of ten percent or greater (Elongation ≥ 10%)

Steel sheets grades used for structural purposes, can be utilized without any limitations according to the rules stated in AISI-S1000 specification [2], as long as the following conditions are met:

(i) The ratio of tensile strength to yield stress must be at least 1.08.

(ii) The minimum elongation must be either 10 percent in a 50 mm gauge length or 7 percent in a 200 mm gauge length standard specimen, as measured following the guidelines of ASTM A370 or ASTM A1058.

2.4.1.2 Steels with a specified minimum elongation from three percent to less than ten percent (3% ≤ Elongation < 10%)

Steel sheets used for structural purposes must have a minimum elongation of 3% in a 50 mm gauge length standard specimen, as tested according to either ASTM A370 or ASTM A1058. These sheets are allowed to be used if the available strengths of structural members and connections are calculated following the guidelines in Chapters B through M (excluding welded connections in Chapter J), Appendices A and B, and Appendices 1 and 2 of AISI-S1000 [2] specifications. In these calculations, the yield stress F_{sy} will be replaced with a lowered value of 0.9 F_{sy}, and the tensile strength Fu will be replaced with a reduced value of 0.9 F_u.

2.4.1.3 Steels with a specified minimum elongation of less than three percent (Elongation < 3%)

Steel sheet grades that fail to meet the standards of 3.1.1 or 3.1.2 can only be utilized for multiple web configurations, while these steel grades may not satisfy the standards for specific structural applications, they are nonetheless permissible for use in such applications where a significant level of elongation is not essential. Nevertheless, modifications must be implemented to the design specifications in order to guarantee

satisfactory performance of the steel in non-structural, web-related applications such as roofing, siding, and floor decking. These modifications may involve changing the design, thickness, or other characteristics to account for the steel's ductility.

N.B: It should be mentioned that there are exceptions to the standards given, and specific steel grades while meeting the requirement are not allowed for structural application (refer to AISI-S1000 for more details).

2.4.2 Effect of cold working on mechanical properties of steel

The mechanical properties of CFS sections might vary significantly from those of the steel sheets prior to forming. This is because cold-forming enhances yield point and tensile strength while decreasing ductility. The percentage increase in tensile strength is substantially lower than the rise in yield strength, resulting in a significant reduction in the spread between yield point and tensile strength. Because the material in the section's corners is cold-worked to a far greater extent than the material in the flat portions, the mechanical properties vary throughout the cross section. [4] tested the channel section and joist chord after the cold forming process. As a result of the material's lower yield point in flat regions, buckling or yielding always starts in the flat region. Any additional load supplied to the section will be distributed to the corners.

[4-7] found that cold work affects mechanical qualities primarily through strain hardening and strain aging, as seen in Figure 2.6 [5]. where curve A depicts the stress-strain curve of virgin material. Curve B shows strain-hardening unloading, curve C shows instantaneous reloading, and curve D shows the stress-strain curve of reloading following strain aging. Curves C and D have higher yield points than virgin material, and ductility decreases with strain hardening and strain aging.

As the cold work process alters mechanical properties through strain hardening and strain aging, it can cause the direct and inverse Bauschinger effect. The Bauschinger effect shows that stretched steels have lower longitudinal compression yield strength

than longitudinal tension yield strength. In counterpart situation the inverse Bauschinger effect creates the opposite condition in the transverse direction.

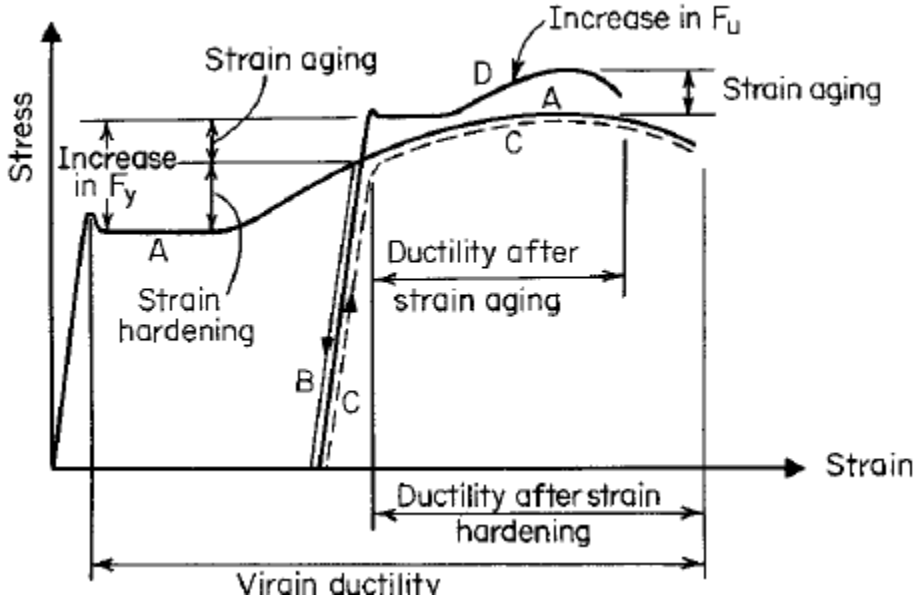

Figure 2.6: Effects of stress hardening and strain aging on stress-strain relationship [1].

2.5 Geometrical limits for cold formed steel members

Before addressing the geometrical limits for cold formed steel applicability, it is important to note that precise adherence to geometrical limits is critical for preventing instable behavior and premature deformations. Maintaining exact dimensions, tolerances and shape, ensures homogeneous loads, straightness, and a consistent cross-sectional profile. It also promotes good alignment and connection integrity, lowering the likelihood of misalignment-induced deformations during assembly. Before applying geometrical limits to a specific cold formed section we must differentiate between three types of cold-formed elements:

Unstiffened elements: are structural components that do not have any additional reinforcement or stiffeners along their length. They are defined by their fundamental, unmodified shapes and profiles such as C, Z..etc (Figure 2.7), lacking any additional attributes in flanges, lips, or ribs that would augment their ability to withstand lateral-torsional buckling or other forms of deformation.

Figure 2.7: Unstiffened C and Z sections.

Edge stiffened elements: In this category, a flat compression element with only one edge stiffened perpendicular to the stress direction is called an unstiffened compression element. Egg: (Figure 2.8) illustrates an example of an edge stiffened elements consisting of adding one lip to the section flanges.

Figure 2.8: Edge stiffened C and Z sections.

Stiffened elements: are structural components that are reinforced by using intermediate stiffeners in web, flange, or attributing shapes with additional edge and lip stiffeners, aligned parallel to the direction of stress (Figure 2.9).

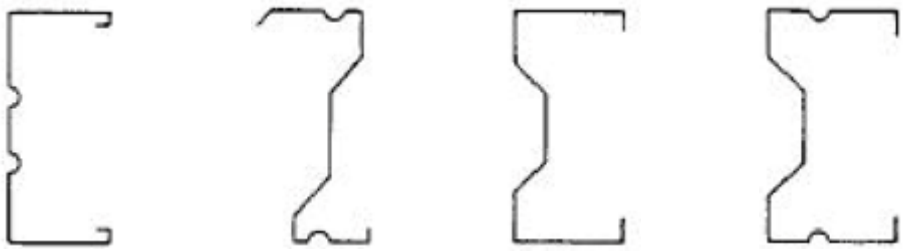

Figure 2.9: Stiffened sections.

When designing cold formed steel members there are two main methods, the Effective Width Method (EWM) and the Direct Strength Method (DSM), definition and specifications of the two methods will be further discussed in 1.10.3 section of this Chapter, the AISI-S1000 [2] differentiates between the two methods in geometrical

limits applicability, Table 2.1 Illustrates the limits of applicability for member's design using the (EWM) and (DSM) as follows:

Table 2.1: Geometrical limits for cold formed steels section applications [2].

Criteria	Geometrical limits	Effective Width Method	Direct Strength Method
Stiffened element in compression	w/t[b]	≤ 500	≤ 500
Edge-stiffened element in compression	b/t	≤ 90 for $I_s \geq I_a$ ≤ 60 for $I_s < I_a$	≤ 160
Unstiffened element in compression	d/t[b]	≤ 60	≤ 60
Stiffened element in bending (e.g. a *web*)	h/t	< 200 for unstiffened *web* ≤ 260 for bearing stiffener[c] ≤ 300 for bearing and intermediate stiffener[c]	≤ 300
Inside bend radius	R/t	≤ [10d]	≤ 20

[a] Geometrical limits definitions:
w = *Flat width* of stiffened compression element (disregard intermediate stiffeners)
t = *Thickness* of element
b = *Flat width* of element with edge stiffeners (disregard intermediate stiffeners)
d = *Flat width* of unstiffened element (disregard intermediate stiffeners)
h = Depth of flat portion of *web* measured along plane of *web* (disregard intermediate stiffeners)
R = Inside bend radius

[b] Stiffened compression elements with w/t > 250 and unstiffened compression elements with d/t > 30 are likely to have noticeable deformations prior to developing their full strength.

[c] Bearing and intermediate stiffener requirements in accordance with Section F5.1.

[d] For inside bend R/t ratios larger than 10, *rational engineering analysis* is permitted.

e See Section A3 for additional limitations.

2.6 Generalities on the behavior of cold formed steel members

2.6.1 Warping of thin-walled sections

Thin-walled structures preserve particularities which must be considered in their analysis. The classic hypothesis, known as the BERNOULLI hypothesis, is in fact no longer applicable, when a certain thin-walled beam is twisted, the out-of-plane distortion of the cross-section of the beam in the direction of the axial axis occurs, which makes BERNOULLI's theory unable to capture the behavior. This out-of- plane distortion is commonly called warping. If the twist is uniform, all the cross sections warp by the same amount, this is the SAINT-VENANT twist, the warping in this case only causes tangential stresses; no normal constraints appear. Whereas if warping is

prevented, the non-uniform twisting in this case brings normal and tangential stresses, as illustrated in Figure 2.10.

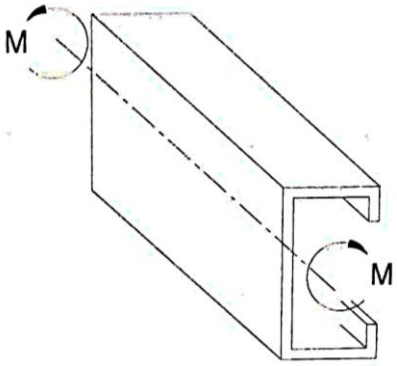

a. C section beam under torsion

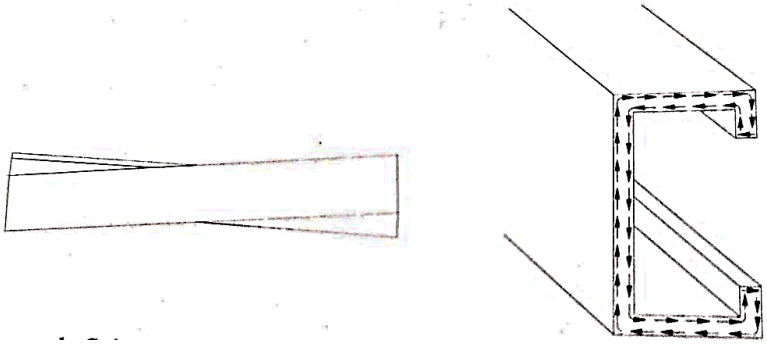

b. Tangential stresses caused by Saint-Venant torsion. Normal stresses due to warping are equal to zero, because all the cross sections exhibit the same torsion values along the length

Tangential stresses of Saint-Venant on the C cross-section

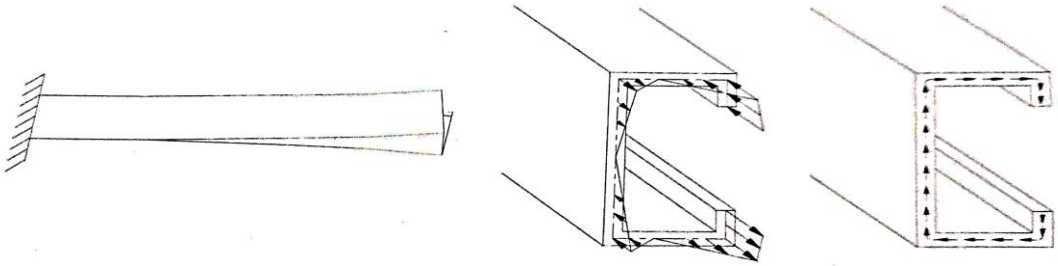

c. Using boundary conditions result in normal and tangential stresses due to warping

Normal and tangential stresses of Saint-Venant on C cross-section

Figure 2.10: Warping in cold-formed steel Channel section [30].

2.6.2 Buckling modes

When approaching thin-walled structures, one must immediately consider the buckling phenomena inherent to their behavior. CFS sections can be subject to local, distortional or global buckling, these buckling modes are caused by the compressive loading applied on these members.

Local buckling is a buckling mode that involves only out-of-plane deformation of the flat portions of CFS sections, without deformation of the lines at the plate junction (edges), Figure 2.11(a) shows a local buckling deformation on C section. In the longitudinal direction, local buckling is characterized by relatively short buckling half-wave length of the individual plates Figure 2.12(a) shows the distribution of local buckling half-wave length along the length of the member. In distortional buckling, the member is subjected to both in-plane and out-of-plane deformations, it is determined by changes in shape of the cross-section; causing relative torsional movements of the individual plates as shown in Figure 2.11(b). The distortional buckling half-wave length is of an average value, as shown in Figure 2.12(b). The global buckling as the term suggests, is a buckling mode which occurs along the whole length of the member, in the context of CFS members, this mode could happen in different global sub-modes, such as Euler buckling and lateral torsional buckling, the differentiation between these sub-modes is realized by the consideration of different parameters such as cross-sectional shape and length of the member, in the global buckling the member deforms similar to a rigid body without any distortion in the cross-section, the global buckling half-wave length is the longest among the buckling modes.

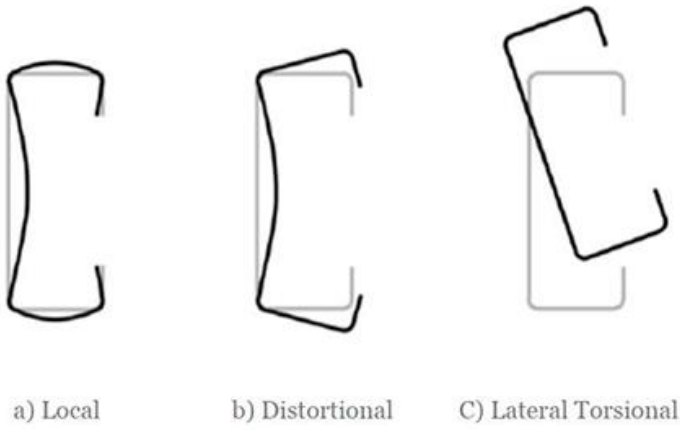

Figure 2.11: Buckling modes on cross-sectional profile of a lipped channel section.

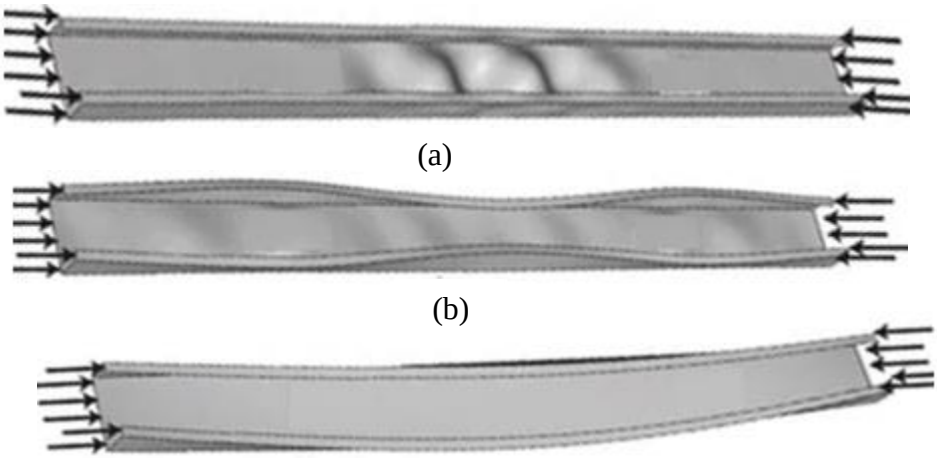

Figure 2.12: Buckling modes in longitudinal profiles of a lipped channel section;
a) local buckling, b) distortional buckling, c) lateral torsional buckling.

Signature curve is a curve used in the semi-analytical analysis of CFS sections behavior, it plots the relationship between the ultimate buckling stress and the correspondent buckling half-wave length, this curve permits the differentiation between the three buckling modes, and determines the ultimate stress for each mode, it is produced from the post-processors of a software using the finite strip method deformable in shear, which will be detailed in section 2.10.4 of this Chapter. Figure 2.13 & 2.14 show signature curves for a lipped channel section subjected to uniform compression and uniform bending, respectively.

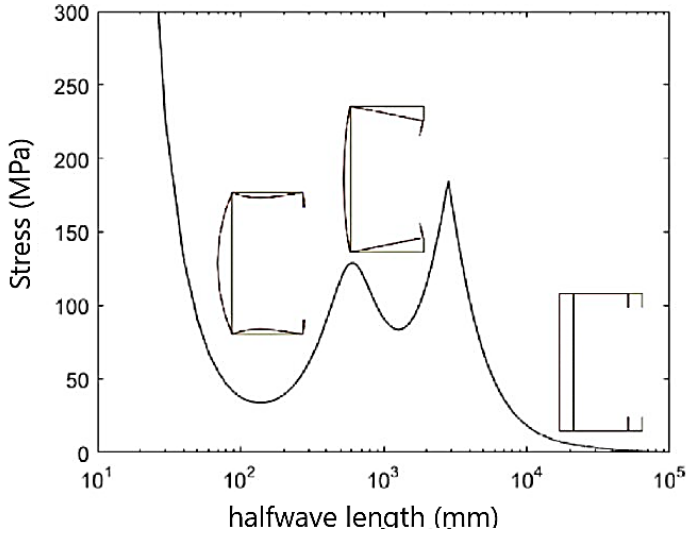

Figure 2.13: Signature curve for a lipped channel section in compression.

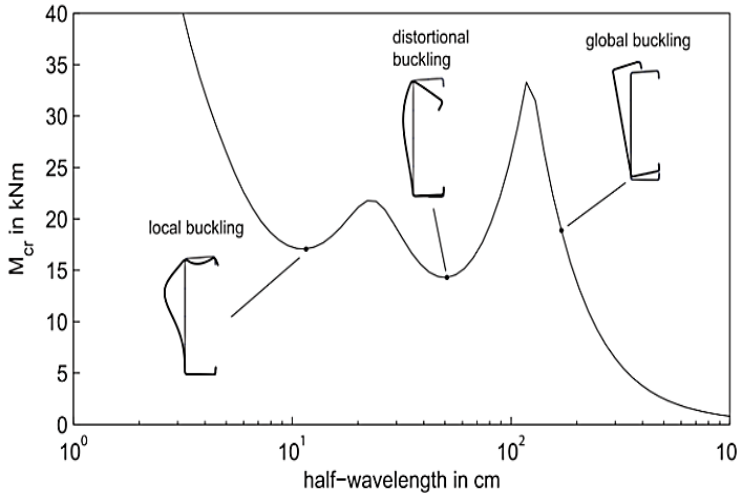

Figure 2.14: Signature curve for a lipped channel section in bending.

The occurrence of an interaction between buckling modes is possible, in this case an examination between the interaction of the different modes is recommended to capture the true behavior of the member, this interaction could happen between local and distortional, local and global, or global and distortional buckling, the next section will address more this aspect.

2.6.3 Buckling modes interaction

2.6.3.1 Local-distortional buckling interaction

Buckling modes interaction can impact the structural response of members depending on the length. Members with short-to-intermediate lengths may typically undergo local distortional buckling interaction (L-D) when their critical buckling moments, M_{crL} and M_{crD}, are close. When designing such members, it's important to consider the behavioral characteristics of the coupling phenomenon since they can cause significant ultimate strength erosion (especially when $M_{crL} \approx M_{crD}$) this unpredictable failure may result in the inability of the designs provisions to predict the true strength [8]. In the current DSM there are two cases of predicting the critical buckling stresses (i) The use of individual local and distortional DSM curves; this procedure offers expressions tailored for using in a pure buckling mode (local or distortional) influencing the member. (ii) The second procedure concerns more elaborated DSM expressions for capturing the effect of local-distortional buckling modes interaction, this procedure called the NLD approach was developed by [9,10], and offers expressions for capturing L-D interaction or D-L interaction modes.

Local-distortional interaction in columns

Experimental tests have been conducted on 26 fixed ended channel columns in order to obtain an experimental evidence of the apparition of L-D modes interaction, Figure 2.15 highlights this interaction from tests and numerical simulation [11], Figure 2.16 show the relationship between the applied axial load, and (i) mid-height web-flange junction (distortional) displacements, and (ii) mid-height mid-web displacements. It is important to note that web transverse bowing can be caused by both local and distortional deformations. Significant local and distortional deformations occur about a stress of 35kN, indicating local-distortional interaction in specimens. The experimental and numerical findings of this study were used to assess the performance of the two mentioned DSM approaches, eventfully, [11] proposed a more accurate procedure for L-D interaction.

In a similar study [12] conducted a numerical analysis comprising 111 specimens to capture the interactive buckling behavior on ended lipped channel columns, the differences between the two studies resides on the buckling stresses ratio between local and distortional buckling (f_{crD}/f_{crL}) of the specimens, in [11],

$1.1 < f_{crD}/f_{crL} < 1.7$, was considered, whereas in [12] $f_{crD}/f_{crL} < 1.1$.

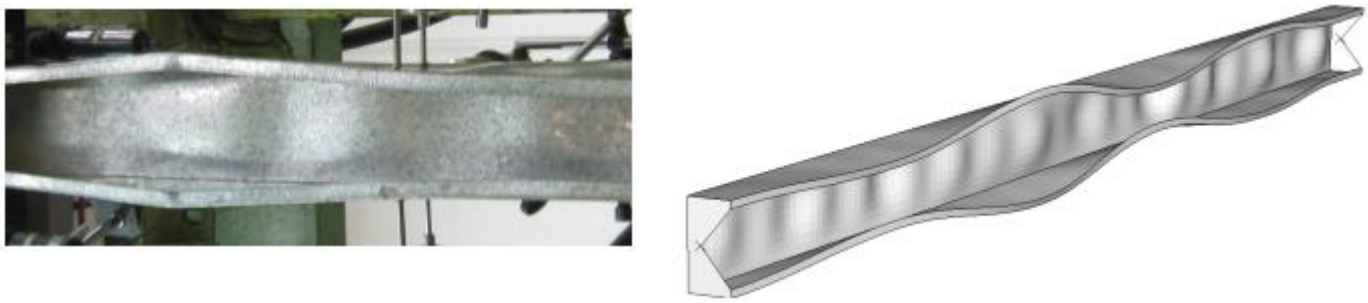

Figure 2.15: Local-distortional interaction in experimental tests and numerical simulation [11].

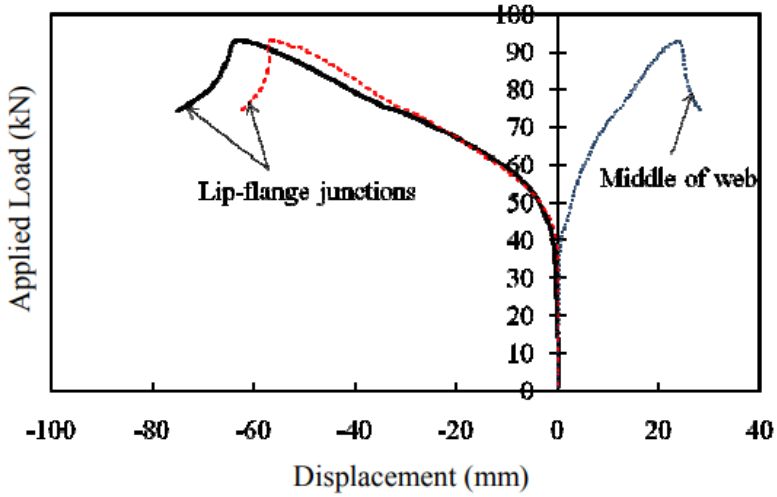

Figure 2.16: Influence of applied load on flange and web displacements [11].

From analyzing the presence of L-D interaction for fixed-ended lipped channel reported in the previous mentioned works, the following conclusion could be drawn:

(i) Columns exhibiting relevant L-D interaction effects may belong to two distinct families: (i1) columns with close local and distortional critical buckling stresses, such

as the ones investigated by [12,13]. (i2) columns with distortional buckling stresses considerably higher than their local counterparts, provided that the yield stress is "high enough" (with respect to the distortional critical buckling stress) to allow for the development of significant L-D interaction along the local post-buckling equilibrium path. These columns category was investigated by [11].

(ii) Columns with low λ_g (global slenderness) and high λ_d (distortional slenderness) were found to be extremely vulnerable to L-D interaction, regardless of f_{crd}/f_{crl} value.

Local-distortional interaction in beams

Researchs primarily focused on examining the impact of L-D interaction on the behavior and strength of CFS columns. However, there is a limited number of studies that have investigated this coupling modes in CFS beams. In the 90s, BERNARD et al. conducted experimental investigations on L-D interaction on trapezoidal steel decks at the University of Sydney. They tested 14 out of 27 specimens, showing evidence of L-D interaction [14,15]. Later, [16] conducted a study on CFS C-section beams with various lip configurations, observing several failure modes, including local, distortional, and L-D interactive failures. 13 of the 24 specimens collapsed in L-D interactive modes, confirming the detrimental effects of this coupling phenomenon on the bending strength of specimens. The interaction between local and distortional buckling may result in a detrimental effect on specimens' bending strength.

Recently, [17] investigated the behavior and strength of CFS lipped channel (LC) beams experiencing local-distortional interaction. 20 tests were conducted on beams with G450-G500 high-strength steel grades. All specimens failed in expected L-D interactive modes and exhibited critical distortional-to-local buckling moment ratios. Figure 2.17 shows the evidence for capturing L-D interaction mode.

As for columns, the design part codifying L-D interactive mode using DSM design curve [2] in beams, affirmed that this method produced unconservative predictions,

and consecutively propositions and suggestions has been provided to the current design codes [18-20].

Figure 2.17: Evidence for L-D interactive mode from different perspective in Lipped-C beams [17].

2.7 Imperfections

The post-critical response of thin-walled sections is difficult to predict due to geometric and material nonlinearity. Notably when using numerical predictive methods such as finite element and finite strip methods, while these methods have reached a level of maturity such that many of them can successfully describe the non-linear behavior up to the failure of thin-walled profiles. The fundamental lack of knowledge of the initial state of the profile and the non-unification in the determination of quantities and distributions to model initial imperfections present a tedious job in predicting the true behavior of members. The initial state of a thin-walled profile can be characterized by local and global geometrical imperfections, residual stresses, and change of elastic limit and ultimate limit on the cross-section of the profile.

2.7.1 Geometric imperfections

A Geometric imperfection is the deviation of the profile from perfect geometry. It includes non-straightness along the profile, non-flatness of the walls and twisting of

the section along the length. The commonly adopted technique to define the distribution of initial imperfections, is to carry out a linear buckling analysis and then use one of the dominant eigenmodes, chosen according to a specific criterion, such as the initial shape. The use of maximum imperfections for an eigenmode of buckling is a conservative estimate, because the maximum imperfections are not periodic along the element. The worst mode of imperfection which causes the greatest reduction in bearing capacity is often linked to the first buckling mode. The nodal displacements in the buckling mode are normalized using the maximum displacement in the structure and this maximum displacement is taken equal to unity. By multiplying the normalized displacements by an appropriate factor, which is the amplitude, the initial imperfections attached to the eigenmode considered can be calculated.

2.7.1.1 Local imperfections

After carrying out several experimental measurements, [21] showed that the wall flatness imperfection can be classified into two categories: type ‘1’, the maximum local imperfection is located at the core of the profile and type 2, the maximum deflection is located at the stiffened or unstiffened flange Figure 2.18(a&b) shows both type’1’ (local imperfection) and type’2’ (distortional imperfection). As a result, to this investigation, simple equations were proposed to determine the magnitude of the considered imperfection.

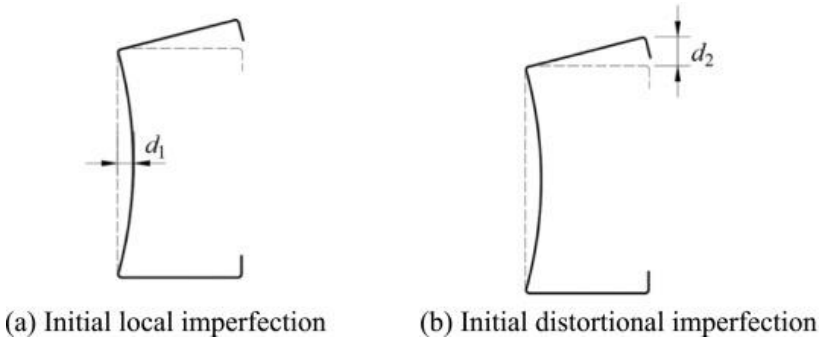

Figure 2.18: Locals imperfections types.

The following equations presented herein in relative forms, are applied for profiles with a thickness less than 3mm.

For type '1' when the height-to-thickness ratio (h/t) is less than 200:

$$\frac{d_1}{h} = 0.006 \quad \text{Eq 2.1}$$

Another expression is also recommended:

$$\frac{d_1}{t} = 6e^{-2t} \quad \text{Eq 2.2}$$

For type '2', when the width-to-thickness ratio (b/t) is less than 100, the maximum deviation is taken approximately equal to the thickness of the plate:

$$\frac{d_1}{t} = 1 \quad \text{Eq 2.3}$$

Type '1' can be considered suitable for local plate buckling and Type '2' characterizes distortional buckling of the flange. It should be noted that Eq (2.1-2.3) give the maximum values for imperfections with regular undulations.

The distribution of local imperfections in a cold-formed column can be assumed to be analogous to the local buckling mode. For local buckling of a member composed of plates, a plate buckles in a half-wave in the transversal direction and in a series of waves in the longitudinal direction. Thus, a double sinusoidal distribution can be used to model the local geometric imperfections of the web wall (type '1', Figure 2.18(a)) [22]. A formula retained in the British standard BS 5950 [23] for the upper limit of the amplitude of the flatness defect of compressed plates was suggested by [24]:

$$\frac{d_1}{t} = 0.145\left(\frac{h}{t}\right)\sqrt{\frac{f_y}{E}} \quad \text{Eq 2.4}$$

This equation was applide for the non-linear analysis of axially compressed C-section members and approximately estimated the length of the longitudinal half-wave using the widths of the web and the flange. Eq 2.4 appear to be more general than Eq 2.1 & 2.2 because it does not limit the domain of validity of the height-to-thickness ratio (h/t) and it considers not only the slenderness of the wall, but also material properties, such as the elastic limit (f_y), and young modulus (E). If the values of the yield strength for cold-formed steel requirements (As presented in section 2.4 of this Chapter) are replaced in Eq 2.4 using a young modulus E =2100000 N/mm², the amplitude obtained d_1 is of an order of that given by equation Eq 2.1.

It should be noted that the initial geometric imperfections in the numerical simulation can be used not only to represent the imperfect geometry but also to take into account other imperfections such as the contains of material non-homogeneity account of eccentric loading, and residual stresses. if the latter, especially the residual stresses, are not explicitly modeled. Because of the uncertainty associated with its magnitude and distribution, their influence can be taken into account in the numerical modeling by an appropriate increase of the initial geometric imperfections. [25] proposed to use the amplitude of the local imperfection of the web in C-sections, and used it in the non-linear analysis of compression members at ambient and high temperatures. He found an acceptable accuracy compared to the experimental results of other authors. The reason for this simplified modeling is that the influence of residual stresses is negligible at high temperature. The expression for the amplitude could be written in simple form such as Eq 2.1:

$$\frac{d_1}{h} = \frac{1}{200} = 0.005 \qquad \text{Eq 2.5}$$

Another formula applicable to C, L and U-shaped CFS members which are made of stainless steel was proposed by [26]:

$$\frac{d_1}{t} = 0.023 \frac{\sigma_{0.2}}{\sigma_{cr}} \qquad \text{Eq 2.6}$$

where $\sigma_{0.2}$ is the stress corresponding to the plastic deformation of 0.2% and identified from the specimens taken from the faces of the profiles, σ_{cr} is the critical stress of the plate.

[21,27] proposed a probability treatment to evaluate the amplitude and frequency of imperfections, the maximum imperfection data shows a wide range of values. Simple rules of thumb (imperfection type 1 & 2) cannot fully describe the magnitude of imperfections, one option, is to consider the maximum imperfection magnitude as a random variable. Any trend in the data related to the plate's slenderness or thickness is now ignored, the probabilistic study was realized by carrying a statistical analysis on measuring the geometric imperfections on multiple specimens, the goal was to determine the cumulative distribution function CDF, which gives the chances of an imperfection magnitude occurrence in relation to the target imperfection, using the following expression P($\Delta < d$), where Δ is a randomly selected imperfection and d is the target imperfection. Table 2.2 illustrates CDF values based on measured imperfections magnitudes reported in Figure 2.19 for type '1' imperfection, the same procedure was followed for imperfection type '2'.

Table 2.2: CDF values for type 1 imperfection [21].

P($\Delta < d_1$)	Type 1
	d_1/t
0.25	0.14
0.50	0.34
0.75	0.66
0.95	1.35
0.99	3.87
Mean	0.5
St.dev.	0.66

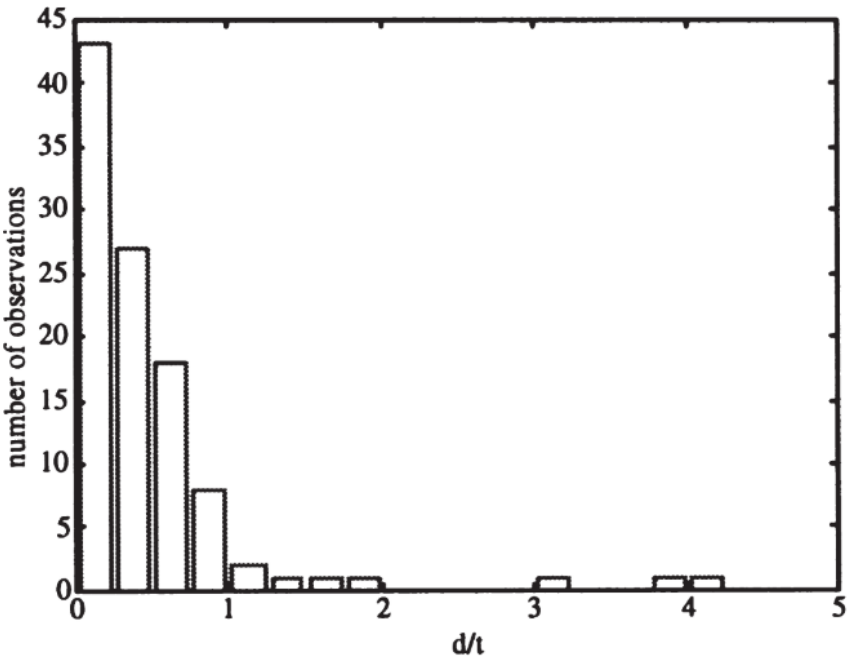

Figure 2.19: Histogram of type 1 imperfection [21].

2.7.1.2 Global imperfections

One of the intriguing characteristics of the behavior of thin-walled members is the coupling between local and global buckling modes. The introduction of this interaction into the non-linear analysis is made by the intermittent simulation of local and global imperfections in the corresponding buckling eigenmodes. [25] showed that the size of the global imperfection has a more unfavorable influence on the failure load of a C-section column than the local imperfection. Global imperfections include flexural (camber and bow) and torsional imperfection (twisting) as shown in Figure 2.20, [28] collected findings of various authors concerning the measurement of CFS profiles imperfections, Tables 2.3 & 2.4 illustrates results for flexural and torsional imperfections respectively.

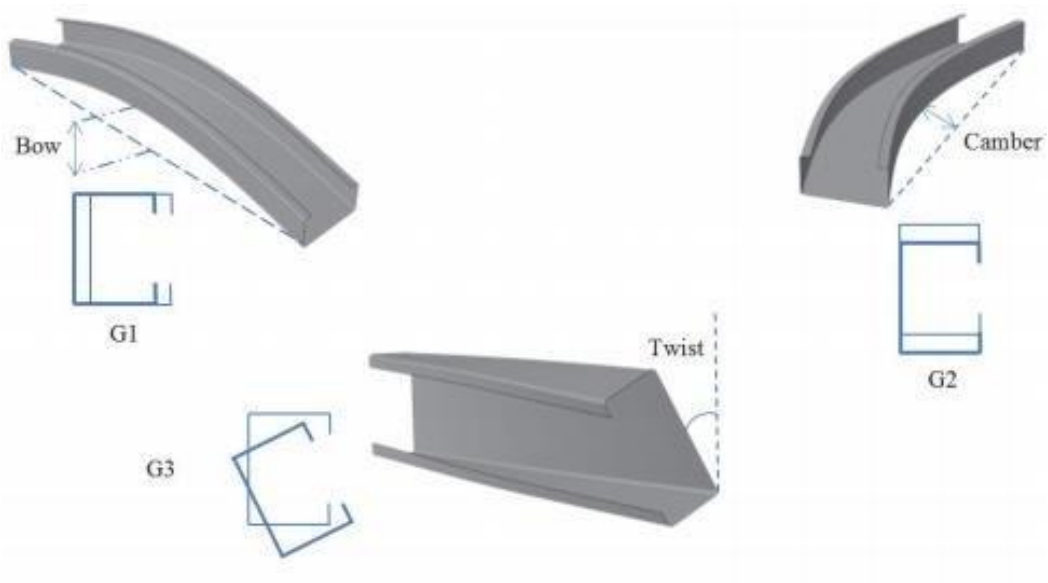

Figure 2.20: Global imperfections types for a C section.

Table 2.3: Measured flexural imperfection for various steel profiles [30].

Authors & references	Profile type	f_0/l
[38]	All profiles	1/800 to 1/1000
[34]	I (camber)	1/1590
	I (bow)	1/1010
	I (camber)	1/2940
	I (bow)	1/4350
[35]	$I_{hot\text{-}rolled}$ (camber)	1/4850
	$I_{hot\text{-}rolled}$, (bow)	1/5430
	I_{welded}, (camber)	1/3060
	I_{welded}, (bow)	1/1190
[36]	L-shape cold formed	1/740
[37]	L-shape cold folded	1/2420
[29]	U and C cold folded	1/2530

Table 2.4: Measured torsional imperfection for various steel profiles (in degree/meter) [30].

Authors & references	Profile type	θ_0/l
[35]	I hot-rolled.	0.12
	I welded	0.30
[34]	I hot-rolled	0.07
[37]	L-shape cold folded	0.53

The measurement of the initial deflection in the longitudinal direction of lipped and unlipped channel sections for multiple configurations was carried out by [29]. This allowed to visualize the imperfections in the two main directions, on the free edges of the sections and on the flange-stiffener connection of the sections. In general, there are two types of deflection; (i) deflection consisted of several half-waves, (ii) deflection in a single half-wave. [28] confirmed this classification by reporting imperfections in simply supported members (Figure 2.21), and we can clearly see, from these observations, that geometric imperfections can be broken down into global and local or distortional types.

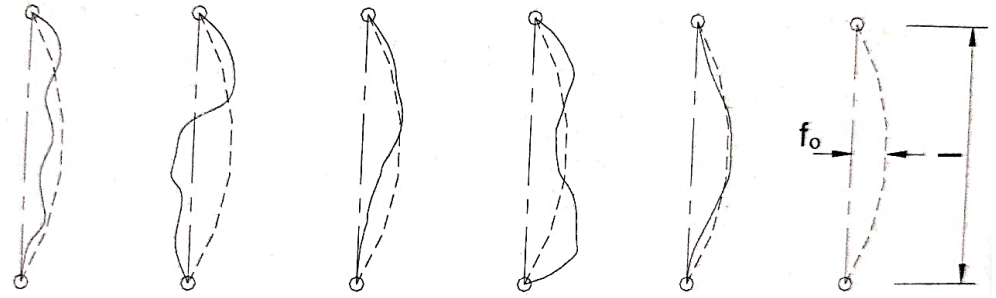

Figure 2.21: Different sinusoidal distribution due to imperfections presence [28].

The sinusoidal form of the global deflection for a simply supported column is written as follows:

$$z = f_0 sin\frac{\pi y}{l} \qquad \text{Eq 2.7}$$

Where y is the longitudinal axis.

2.8 Residual stresses and hardening

Residual stresses are a default property in steel profiles, due to the manufacturing process: hot rolling, welding, torch cutting, in hot-rolled steel, profiling and press-braking in cold formed steel. On another hand, hardening which is generally the phenomenon of increasing the yielding stress and decreasing ductility, is only produced by cold forming. Among the two cold forming process, profiling leads to a significant increase in yielding stress in rounded portions, and less important in flat ones, whereas, press-braking causes a similar increase in rounding, but flat portions are less influenced. Thus, residual stresses and hardening appear in cold formed members, and their intensity maybe important simultaneously at the same location of the cross-section (rounding or flats), this is a reason we chose to present them under the same paragraph. Another more pivotal reason, is that some authors tend to introduce both residual stresses and hardening in the same numerical model, and then compare them with experimental results [30].

Figure 2.22 shows the variations in yielding stress measured in cold-formed sections, while Figure 2.23 shows the influence of cold forming methods on the increase in the elastic limit, as reported by [31].

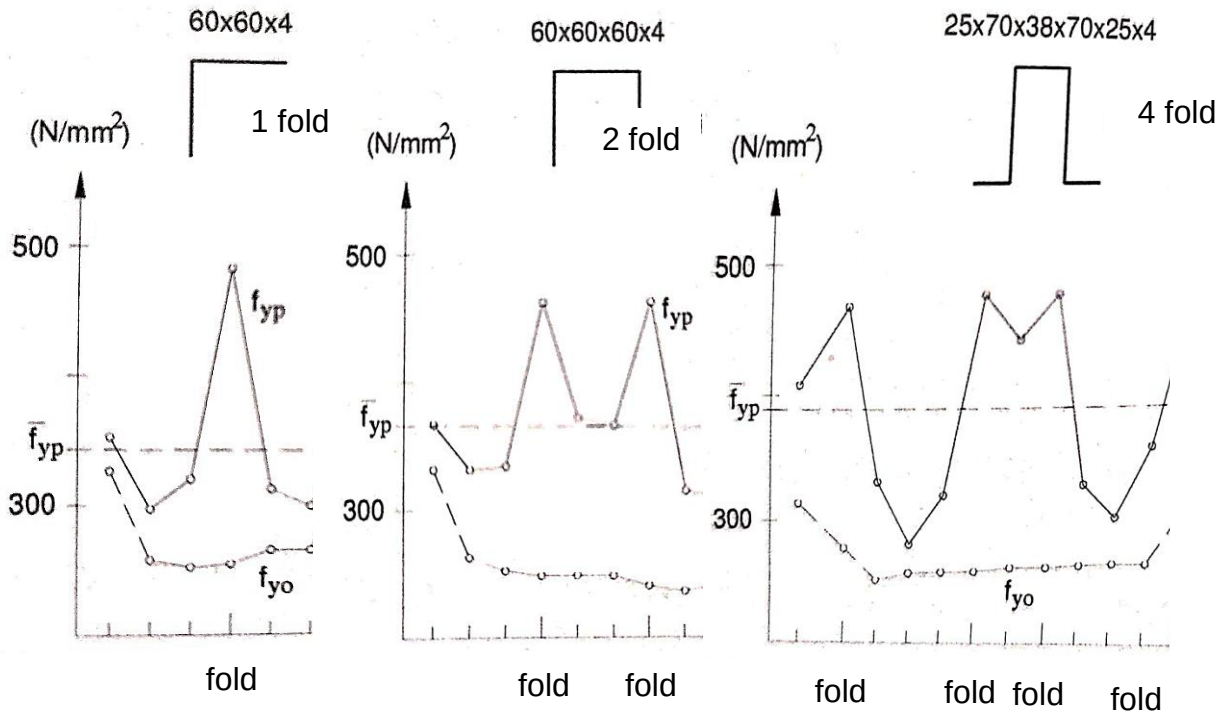

Figure 2.22: Effect of cold forming on yielding stress augmentation [31].

Where f_{y0} is the plate (before cold forming) yielding stress, f_{yp} is the yielding stress of the cross-sectional profile, $\overline{f_{yp}}$ is the average yielding stress on the overall profile's cross-section, from Figure 2.21, it is well illustrated that augmentation of fold numbers, contributed in increasing the average yielding stress $\overline{f_{yp}}$.

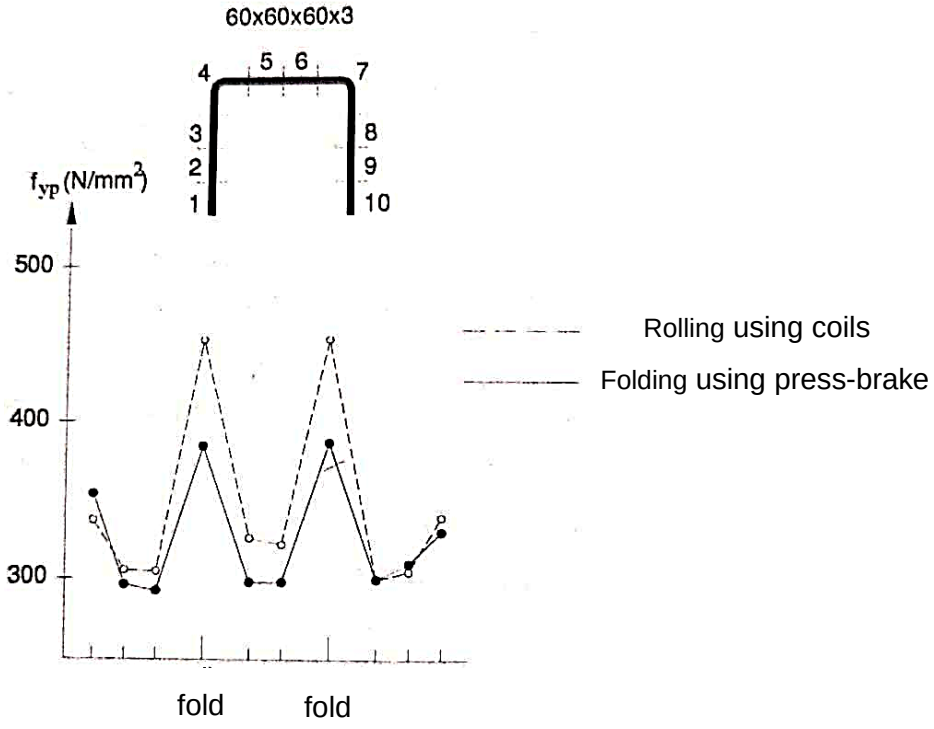

Figure 2.23: Increase of yielding stress due to profiling and folding processes [31].

The longitudinal residual stresses on the cross section of a profile are self-equilibrated and they are idealized as the sum of two types: membrane and bending. The membrane type is essential in hot-rolled profiles, while the flexural type predominates for cold formed profiles. The variation in residual stresses across thickness leads to premature yielding of the faces of cold-formed profiles.

2.8.1 Profiles made from carbon steel

Recommendations for modeling residual stresses were suggested by [21]. The statistical results for the membrane residual stresses are summarized in Table 2.5 where it can be seen that the membrane residual stresses in the roll-formed profiles are higher than in the press-braked profiles, in addition significant residual stresses exist primarily in the roundings. On the other hand, the elastic limit is also high in these corners as shown in Figures 2.22 & 2.23. If large membrane residual stresses are modeled in roundings or other influenced areas by hardening, the yield stress reported

in these regions must also be modeled. Conversely, if the membrane residual stresses are ignored, the increase in the elastic limit should not be included in the simulations.

Table 2.5: Membrane residual stress as $\%f_y$ [21].

	Roll-formed		Press-braked	
Element	Mean	Variance	Mean	Variance
Corners	6.8	1.1	5.2	0.4
Edge stiffened	3.9	1.0	0.9	1.0
Lip	7.9	1.5	0.2	0.3
Stiffened	−1.7	1.2	0.9	0.1

The recommendation for modeling the flexural residual stresses in all elements with an assumption of linear variation through the wall thickness has also been suggested by [21]. Table 2.6 and Figure 2.24, illustrate the measurements of the investigation.

Table 2.6: Flexural residual stress as $\%f_y$ [21].

	Roll-formed		Press-braked	
Element	Mean	Variance	Mean	Variance
Corners	26.8	5.0	32.7	3.3
Edge stiffened	23.5	1.0	8.0	2.5
Lip	6.7	6.4	56.0*	11.6
Stiffened	38.9	6.2	16.9	4.5

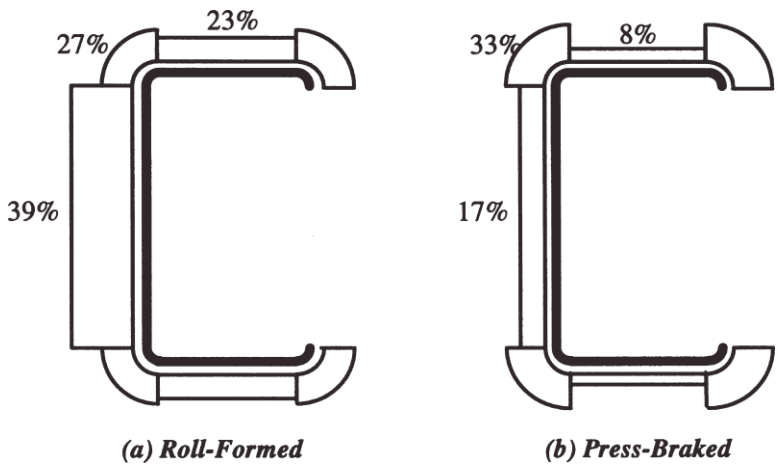

Figure 2.24: Average bending residual stress as %f_y [21].

In cold formed channel section by rolling process [32,33] proposed to divide the cross-section into two zones: rounded zone and flat zone, the rounded zone is extended to $0.5\pi r$ in outside the curved portion (Figure 2.24). The elastic limits of the flat zones are considered uniform and taken equal to the characteristic elastic limit f_y of the steel grade of the section. The elastic limits of the rounded zones f_{ye} has a greater value and the increase of the elastic limit in the rounded zones is taken as follows:

$$\Delta f_y = 0.60\left[\frac{B_c}{(r/t)^m} - 1.0\right] f_y \qquad \text{Eq 2.8}$$

Where:

$$B_c = 3.69\left(\frac{f_u}{f_y}\right) - 0.819\left(\frac{f_u}{f_y}\right)^2 - 1.79$$

$$m = 0.192\left(\frac{f_u}{f_y}\right) - 0.068$$

f_u is the ultimate limit of the base steel; r is the internal radius of the rounding considered. Accepting these elastic limits, each zone is designated an idealized multilinear stress-strain relationship as shown in Figure 2.25.

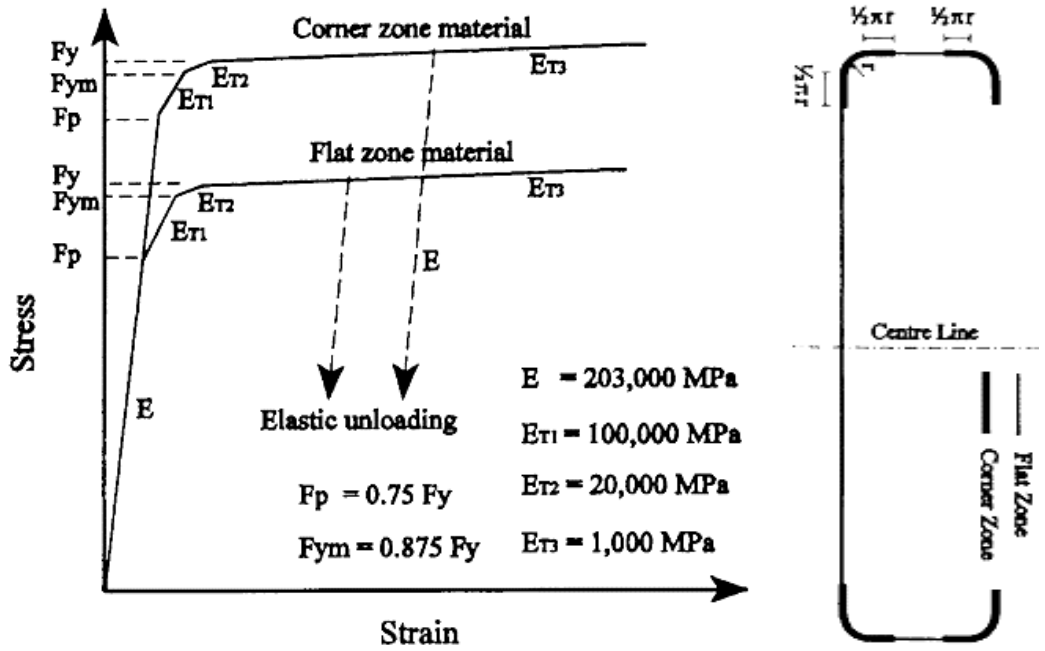

Figure 2.25: Material model for analyzing and defining flat and rounded zones of the cold formed C section [32].

2.9 Non-linear behavior of cold formed steel members

The nonlinear behavior of thin-walled structures can be investigated by laboratory tests, analytical nonlinear analysis or numerical nonlinear analysis. The laboratory testing method is expensive and totally depends on the precision of the measuring instruments. The analytical method, is only feasible in restricted cases where the requirements of equations applicability is fulfilled in the specimen being investigated, and almost impractical because of the mathematical difficulties in more complex cases. The numerical non-linear analysis, is now the most adopted method, it resolves most of the problems encountered and allows parametric study conduction. It is often

verified with replication of a series of laboratory tests to confirm the accuracy of results and the correct model simulation, this method is of a high feasibility and allows the simulation of unlimited number of specimens, if it meets with high computing specifications, hence, this method is the most favorable path for developing modern design codes [30].

The nonlinear behavior of thin-walled structures is expressed by geometric, material and hybrid geometric and material nonlinearities. Buckling stresses resulting from local, distortional and global modes, can be much smaller than the yield strength. In some cases, geometric nonlinear analysis alone can describe the response up to failure. In addition, this nonlinearity presents another supplement and verification of the linear buckling calculation. In case of members experiencing buckling failure before the yielding stress, an apparition of a transitory phase before reaching failure called post-buckling phase is noticed, because thin-walled structures may have a reserve of strength before reaching the failure stress; this is due to the membrane behavior of thin members. When geometric deformation does not play an important role as for structures with relatively thick walls, one can perform the material nonlinear analysis solely without taking into account the displacements of the individual elements of a member. However, in most cases of thin-walled members, mixed, geometric and material non-linear analysis must be carried out. The final objectives of the composite analysis are to determine the failure load that the structure is capable of supporting and to mimic the actual behavior of the structure as closely as possible, hence, in the calculation models, we try to introduce all the inevitable imperfections such as geometric imperfections of local and global types, residual stresses, and changes in the yielding and ultimate stresses. Whereas, the focus will be given to modeling their impact. However, determining imperfections is a difficult task and depends on the manufacturing process and the types of products, additionally, the measurements may be different from an investigation to another. It should be noted that we often seek to model the most unfavorable distribution of imperfections.

2.10 Cold-formed steel calculation methods

In the literature on the subject of thin-walled structures, there is a large amount of research. This area has attracted researchers for a long time. Methods for analyzing thin-walled structures can be classified into the following four main categories:

+ Experimental methods

+ Analytical methods

+ Semi-empirical methods

+ Numerical methods

2.10.1 Experimental methods

Historically, design relying on experimental tests is widely used in thin-walled sections. [39] summarized the experimental works on plates, beams and columns. The experiment obviously gives reliable results, but it is in general only applicable for simple cases and even in these cases the costs are high. Since numerical methods have made progress, laboratory tests have become less frequent. However, they are still necessary for the validation of numerical models, and for special cases such as purlins attached to sheets, members with holes in their walls, composite floors. etc.

2.10.2 Analytical methods

The analytical method with the notion of non-uniform torsion and sectoral coordinates was developed by VLASOV since 1940. He established the differential equations which govern the overall behavior of thin-walled members with open section. His theory was based on the assumptions of small deformations and undeformability of the cross section in its plane. The non-deformability of the cross section can be ensured by the stiffener plates which are welded transversely along the member. The cross section can be warped in the longitudinal direction of the member and the warpage is proportional to the sectoral coordinates of the section, the non-uniform torsional shear stresses are taken canceled at the mean lines of the walls of the section. After

VLASOV study, several authors presented and developed the theories of thin-walled members. [40] explicitly applied this theory in linear buckling problems in several realistic cases. BENSCOTER assumed that the non-uniform torsional shear stresses are not canceled at the wall mean lines for closed thin-walled sections and are taken equal to the uniform torsional shear stresses of SAINT-VENANT. The theories of VLASOV and BENSCOTER are included in [41] book, which gave general formulas to determine the geometric properties of any section and contributed to the development of the calculation of thin-walled members by its theory of spatial mechanisms. [42] dealt exclusively with global buckling phenomena in his book, he deduced that lateral torsional buckling of particular beams can be derived in their deformed states notably if the second moments of inertia in the two main directions of the cross-section are almost equal.

The analytical methods presented above, always consider the hypothesis of the undeformability of the cross section in its plane and they can only describe the behavior at the global level in thin-walled members. Cross-sectional buckling instabilities consisting of local and distortional buckling (presented in section 2.6.2 of this Chapter) must also be considered in the overall deformation of the member, the distorted cross-section in its plane and the interaction between the component plates of the member plays a pivotal role. These local modes can be approximately resolved by VON KARMAN plate theory for local buckling, and the coordination between VLASOV theory and plate theory for distortional buckling. For local buckling case, the component plate is isolated and its supports are idealized [40]; the effect of adjacent plates can be approximately taken into account in simple cases, the rectangular hollow sections for instance [43]. For distortional buckling, a portion of the cross section is isolated and considered to rest on elastic supports to replicate the influence of adjacent plates. [44,45] established explicit formulas to calculate the distortional buckling stress of channel section in the two simple cases of uniform compression and uniform bending.

Classical analytical methods cannot take into account the deformability of the section in its plane and the interaction between buckling modes. An alternative method entitled 'Generalized Beam Theory' (GBT), developed by SCHARDT with his colleagues in Germany [46] and then by [47,48], can take these phenomena into account by adding intermediate nodes at the interval of the component plates of the section. The GBT method can be classified into 'analytical methods' category.

2.10.3 Semi-empirical methods

Semi-empirical methods which are based on the concept of effective widths or effective sections have been common for several years. They make it possible to consider the interaction between buckling modes (local and global modes, distortional and global modes, and local and distortional modes). They are simple to calculate by hand and suitable for engineers. Therefore, semi-empirical methods are generally accepted by most codes and specifications for the design of thin-walled structures around the world.

2.10.3.1 Effective width method

The semi-empirical methods used in codes and specifications which take into account local and distortional buckling phenomena of thin-walled structures are based on the concept of effective widths of stiffened or unstiffened walls which are totally or partially in compression. The effective width method considers the plates making up the cross section in isolation. It was originally proposed by VON KARMAN for insulated plates and modified for cold formed sections based on experiments conducted by WINTER. Imperfections are implicitly incorporated into the semi-empirical expression of WINTER. This expression is adopted in the design codes of several countries. EUROCODE 3, part 1-3 [49] provides the rules for determining effective widths under different stress distributions. The effective widths of the isolated plates are combined to form an effective section and the design of a thin-walled members is then completed by conventional techniques where the AYRTON-PERRY type equation is widely used [50,51]. The effective width method allows the

interaction of buckling modes to be approximately incorporated, and the interaction between buckling and yielding is introduced at the ultimate limit state by replacing the elastic limit in the effective width expression. It also takes into account post-buckling behavior by reducing the widths corresponding to the level of service constraints, in a step-by-step solution.

2.10.3.2 Direct Strength Method (DSM)

As sections become more and more complex, with the addition of end or intermediate stiffeners, the determination of effective widths and effective section properties become more complicated. The consideration of isolated walls is less accurate because each wall does not veil in isolation but interacts with the others. To solve these problems, a new method called 'Direct Strength Method' (DSM) was developed by [52,53] who proposed a design procedure based on elastic buckling solutions for the overall cross-section; in combination with available software using the finite strip method [54] or the 'Generalized Beam Theory' method presented above, to determine the critical loading strength of cold formed steel members. these critical loads are then included in convenient DSM expressions for global, local and distortional buckling. These expressions take the conventional equations for effective widths method and applies them for the full section. However, [55] noticed that DSM can overestimate the ultimate loads for elements subjected simultaneously to an axial load and a bending moment if a shift in the center of gravity causes an additional moment. They have suggested that more studies are needed before DSM is generally applied.

2.10.4 Numerical methods

2.10.4.1 Finite Element Method (FEM)

The finite element method is the most widely used and versatile among numerical methods, capable of simulating virtually any cross-sectional geometry and arbitrary loading and support conditions. The finite element method introduces discretization along the length and cross-section of the member, necessitating a substantial number

of degrees of freedom to ensure precise estimation of the buckling stresses. This causes the generation of a considerable quantity of candidate buckling modes, which the finite element method is incapable of automatically differentiating. Consequently, the responsibility of identifying the buckling modes falls upon the user. Furthermore, it should be noted that the finite element method lacks the capability to compute the critical load directly linked to a pure buckling mode (whether it be local, distortional, or global). This drastically restricts its practicality when it comes to analyzing the stability of thin-walled members [56].

2.10.4.2 Finite Strip method

The semi-analytical finite strip method (FSM) was originally developed by [57]. In the cross-sectional direction, the displacements are interpolated by the polynomial functions and in the longitudinal direction the displacements are interpolated by the harmonic functions deduced from the sinusoidal longitudinal forms of displacements in the vibration problem of bars. The harmonic functions must satisfy the boundary conditions. This method can be considered as the application of FOURRIER series to the numerical analysis of structures and it is also called the semi-analytic finite strip method. It has some advantages over the general finite element method when analyzing thin-walled elements. Particularly, the great reduction in the number of degrees of freedom for a given structure, and a simple conformability of membrane and flexional displacements at the junction of the assembled plates. However, it is difficult to apply for support conditions other than simply supported members and it can only be used for constant section along the member's length.

[58] relied on [57] work to create CUFSM [54], a software intended for the solution of elastic buckling problems in thin-walled members. The buckling modes and the value of the critical stresses depend on the half-wave length and the buckling stresses visualized in signature curves and deformed shapes are provided in the output of the software. The local and distortional instabilities are easily determined on signature curve, and correspond to the minimum points of the curve as presented in

Figures 2.12 & 2.13 (section 2.6.2 of this Chapter). However, FSM is limited to structures subjected either to uniform compression or bending or in combination of the two loads. [59] examined a special case where the compressive stresses vary along the longitudinal axis of channel section member subjected to uniformly distributed lateral loads. In the expression for determining the geometric rigidity matrix, they replaced the constant axial stress by the function describing the longitudinal variation of axial stresses. They were also able to resolve local, distortional and lateral buckling problems in beams under lateral loads. This approach requires prior knowledge of the analytical distribution of axial stresses. In addition, the geometric rigidity matrix is different in the explicit form of symbols, from a loading case to another.

Spline finite strip method

The spline finite strip (FSM's) is a variation of the semi-analytic finite strip method that came later and can effectively overcome most of the restrictions encountered in FSM, while retaining the reduction in the number of degrees of freedom compared to the finite element method. The FSM's consists of replacing the trigonometric longitudinal series by a linear combination of local B3 spline functions while retaining the polynomial transverse interpolations [60]. There are other spline functions valid for different applications. [61] applied a cubic X-spline function by analyzing bending plates with irregular edge conditions. while [62] studied the buckling of oblique plates by applying B-spline functions in the longitudinal and transverse directions. [63] adopted the B3-cubic spline functions, used by [60], in order to study the buckling of plates and thin-walled sections. Different edge conditions such as simple support, fixed support, fixed support with free edge, can be treated by modifying particular local splines adjacent to the edges. Additionally, an intermediate support along a thin-walled member can be incorporated. However, support conditions other than those called ideal cannot be described, and the FSM's is not applicable to structures with elastic supports, and structures composed of elements which are not rectilinear to each other such as portal frames. Therefore, the finite B3-spline strip was extended to

linearly analyze assembled spatial non-prismatic structures composed of flat plates [64]. Unlike previous authors, who used classical theory, [64] used MINDLIN-REISSNER plate theory, but he did not explain how he incorporated rotation in the plane of the plate to ensure compliance of rotations at junctions. spatial dimensions of the plates.

2.11 Conclusion

This chapter provides a comprehensive overview of CFS members, emphasizing their growing importance in modern construction. Cold-formed steel members, distinguished by their manufacturing process and material properties, offer unique advantages such as light weight, high strength, and versatility. Key insights into the material properties and effects of cold working on steel demonstrate the influence of the forming process on mechanical characteristics, such as increased yield strength and reduced ductility. The discussion on geometrical limits underlines the importance of precision and adherence to design guidelines to avoid instability and ensure structural integrity. the chapter also introduces critical behavioral aspects, including warping and various buckling modes (local, distortional, and global), which are fundamental to understanding and optimizing CFS member performance.

Finally, this chapter provides a robust framework for understanding the behavior of CFS members under various loading conditions. it emphasizes the need for advanced modeling and analysis techniques to address the challenges posed by the unique characteristics of CFS, ensuring reliable and efficient structural designs. This foundational understanding serves as a critical step toward developing innovative approaches and improved design standards in the field of cold-formed steel structures.

In summary, Chapter 2 establishes a strong foundation for exploring the design, behavior, and application of cold-formed steel members, highlighting their potential to address the demands of modern construction through innovative and efficient solutions.

Chapter 3
Literature review

3.1 Introduction

The construction industry has recently seen a notable increase in the use of cold-formed steel plates in metal frames construction. The flow direction is influenced by the flexibility provided by the cold-forming technique, enabling the production of various shapes and sizes. These profiles are a practical substitute for conventional hot-rolled steel members in average-important constructions due to their lightweight nature and effortless transport. However, the utilization of thin steel sheets subjected to compression stresses can lead to buckling stability problems, including local, global, and distortional buckling. The current chapter discusses multiple aspects related to cold formed steel built-up members subjected to bending loads, Firstly, it details the importance of the cross-sectional conception of built-up sections and their utilization as flexural members, notably, the adequacy and advantages of using built-up member types as open or closed sections, as well as the impact of integrating different stiffening methods on the flexural strength and buckling modes of such members. Transitioning from the discussion of the cross-sectional conception of built-up sections, the second part focuses on examining different design assumptions used for built-up members. These assumptions play a crucial role in evaluating the effectiveness of current design provisions, particularly the utilization of the Direct Strength Method (DSM). By exploring these assumptions and their implications, valuable insights are made into optimizing the design and performance of built-up members under bending loads. Moreover, this chapter delves into exploring the effect of using fasteners, a unique aspect susceptible to affect the flexural strength of CFS built-up members. Finally, the chapter concludes by addressing the central issue of this study: the conception and design of innovative built-up closed sections subjected

to bending, engineered to efficiently resist local buckling failure. It examines various aspects related to the behavior of these members under bending loads and presents a reliable, generalized design method for built-up beams prone to local buckling.

3.2 Literature review

3.2.1 Built-up sections in bending

3.2.1.1 Built-up open sections

Built-up open sections, also known as back-to-back sections, consist primary of two channel sections connected together to form an I-shaped section. Depending on the presence of stiffeners within the channel sections, the resulting section may be either stiffened or unstiffened. the advantages acquired from this sectional configuration compared to the traditional CFS mono-sections, had influenced researchers to extensively investigate the flexural behavior and performance of this section, particularly in the last decade, therefore, numerous studies had been conducted on experimental, numerical and analytical level [65-70], by altering key parameters such as the geometrical properties, the slenderness and screws spacing, with a goal of understanding the behavior of I-section in capturing different failure modes, the buckling instabilities evidenced from experiments provided a global understanding on built-up I-beams, and served as a validation of the upcoming parametric studies, which delved more into comprehending the behavior of these sections by undergoing extensive numerical analysis.

[65,71] investigated the interaction between local and distortional buckling instabilities on many sectional configurations of back-to-back channel sections in bending (Figure 3.1), lateral bracing of the beams was provided to prevent torsional buckling failure. The study revealed that all the beams investigated failed in the constant moment span by L-D interaction (Figure 3.2). The cross-sectional bending capacities of test results were compared with EN1993-1-3 [49] predictions, which were found to be safe and accurate for the geometries adopted. The current AISI

(2016) [2] DSM equations also yielded safe predictions, suggesting moderate erosion of ultimate capacity due to local-distortional interaction. Alternative DSM formulations based on NDL and NLD curves as prescribed in [2] provided conservative predictions.

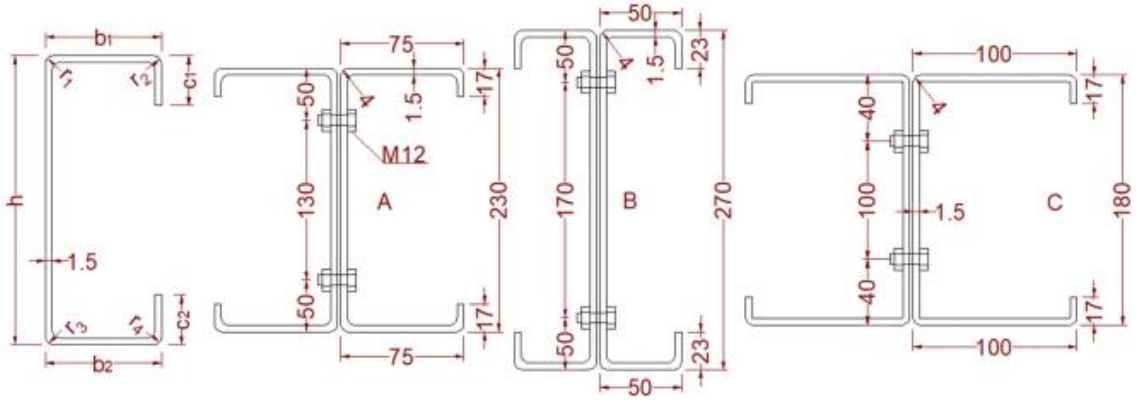

Figure 3.1: Sectional configurations of back to back channels [65].

Figure 3.2: Local distortional buckling interaction in test beam [65].

Recently, [72] investigated the design aspect of built-up back to back sections, by assessing the current design provisions ability in predicting the flexural strength of an unconventional shaped back-to-back section, the particularity in their proposed section was to opt for an unsymmetrical web about the bending axis as presented in Figure 3.3 the study primarily focused on investigating the effect of distortional buckling on 15 specimens, therefore, bracing and stiffeners were provided for both webs and flanges to prevent lateral torsional and local buckling, which enabled the test specimens to fail

by distortional buckling as shown in Figure 3.4. The results of the investigation, concluded that the current DSM predictions were too conservative for low slenderness range ($\lambda_d \leq 0.673$), therefore a new distortional slenderness limit was introduced.

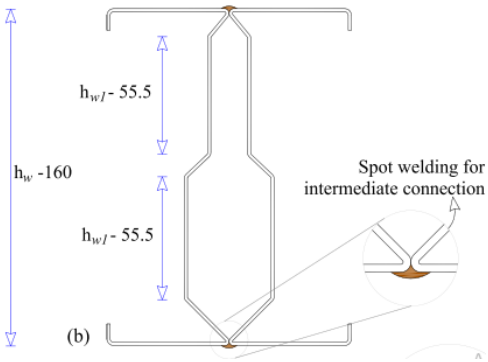

Figure 3.3: Cross-sectional geometry of built-up back-to-back section adopted by [73].

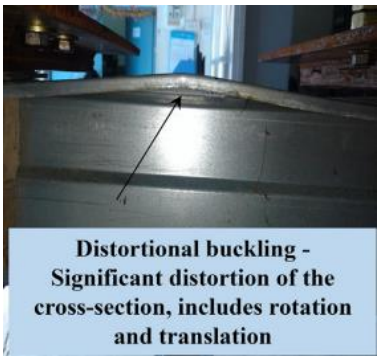

Figure 3.4: Distortional buckling in the upper-lip of built-up open section [73].

At first, experimental tests were conducted to identify the occurred buckling instabilities, [73] conducted a series of tests and FEA on channel and back-to-back I-sections with long beams of 3.6 m length, unrestrained laterally. the results revealed that all specimens I built-up section beams recorded a flexural capacity of 3.5 times higher than normal channel beams as depicted in loading mid-displacement curves of Figure 3.5(a&b). the gained performance is not only explained by the use of double channel sections, but also with the higher torsional rigidity obtained from the symmetrical shape compared with normal channel section.

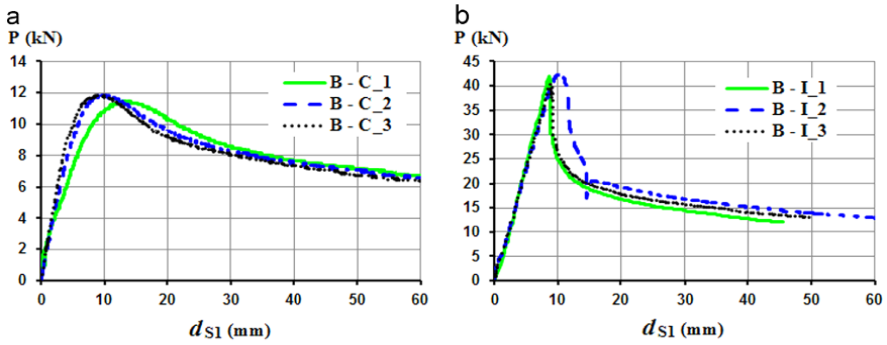

Figure 3.5: Load-mid-displacement curves of; (a): Channel beams (B-C), (b): I beams (B-I) [73].

More investigations on long I-beams revealed that despite the higher torsional rigidity provided by this section, lateral torsional buckling still occurred [67, 68], as evidenced in failure modes depicted in Figure 3.6(a&b).

(a)

(b)

Figure 3.6: Evidence of lateral torsional bucking in three and four-points bending built-up I-beams, (a): [67] study, (b): [68] study.

3.2.1.2 Built-up closed sections

Also knew as built-up face to face sections, the idea behind adopting such sectional configurations was to form a hollow cold-formed steel section, individual sections may either be connected face-to-face to form an embedded box section, or toe-to-toe to create a closed section, where screws and bolts are the convenient fasteners for the first case, and spot welds are more adapted to the later (Figure 3.7). The main advantage of built-up closed sections is their higher torsional rigidity compared to both individual and built-up open sections, [73] was one of the first investigations focusing

on comprehending the impact of lateral torsional buckling on individual C channel and built-up open and closed sections in bending, the studied sections are shown in Figure 3.7. High cross-sectional aspect ratio of 5.8 as well as a length of 3600 mm were adopted to ensure failing in lateral torsional buckling. LVDT's were provided in three cross-sectional positions along the length (S1, S2 & S3) as shown in the schematic test set-up of Figure 3.8(a). In the transversal direction LVDT's were positioned in the direction of the web as illustrated in Figure 3.8(b). this was to capture possible lateral rotation of the beam. Any differences in readings acquired from the LVDT's in the three positions, indicates a higher suceptibility to lateral rotation.

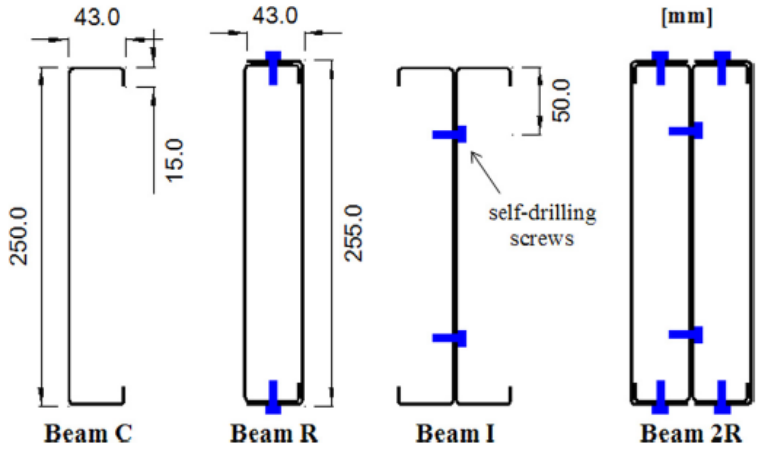

Figure 3.7: Cross-sectional geometry of the four beams investigated [73].

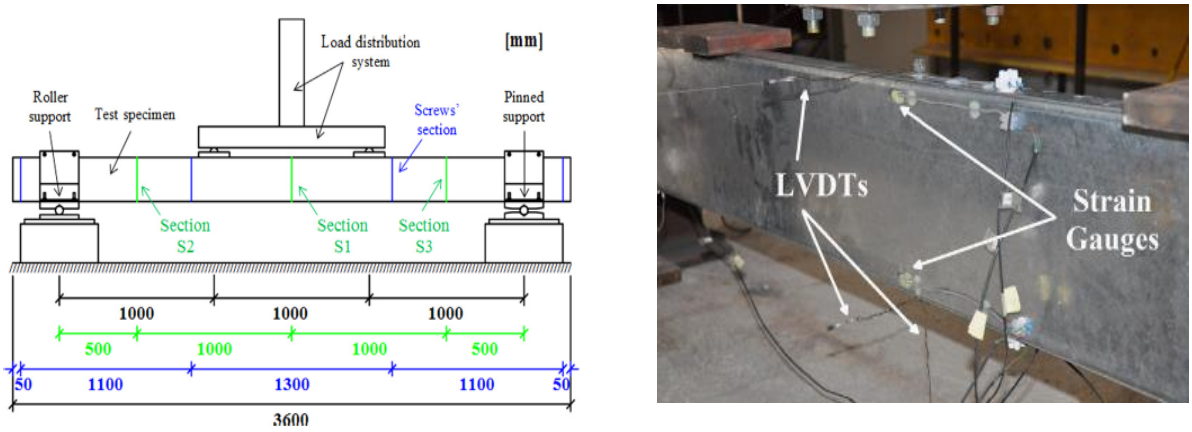

(a) (b)

Figure 3.8: Schematic view of the experimental set-up for bending tests [73].

The results of this investigation are presented in form of loading ratio P/P_{max} against lateral rotation at mid of the length (S1 section) curves, by recording lateral rotation of the specimen with gradual bending load, as depicted in Figure 3.9. it was concluded that built-up closed sections (B-R & B-2R) recorded the highest lateral rotation resistance. Section B-I although having considerably improved the rotational rigidity compared to B-C section, lateral rotation still recorded in the failure of B-I beams. These results prompt towards the higher capacity of built-up closed sections in sustaining lateral torsional buckling.

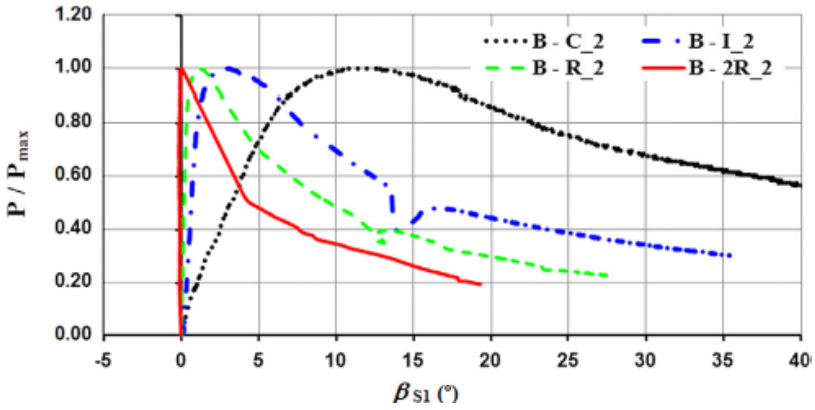

Figure 3.9: P/P_{max} versus lateral rotation at mid-length (S1 section) for specimens (BC_2, B-I_2, B-R_2, B-2R_2) [73].

[74,75] conducted an extensive experimental and numerical analysis on built-up closed sections with different assembling methods and stiffeners, the cross-sections proposed are depicted in Figure 3.10, their studies focused on investigating local and distortional buckling occurrence, therefore, all specimens were laterally restrained at supports and loading points, In addition to investigating novel approaches in assembling closed sections, their research provided a dependable finite element model (FEM) that could reliably predict the flexural strength of built-up sections.

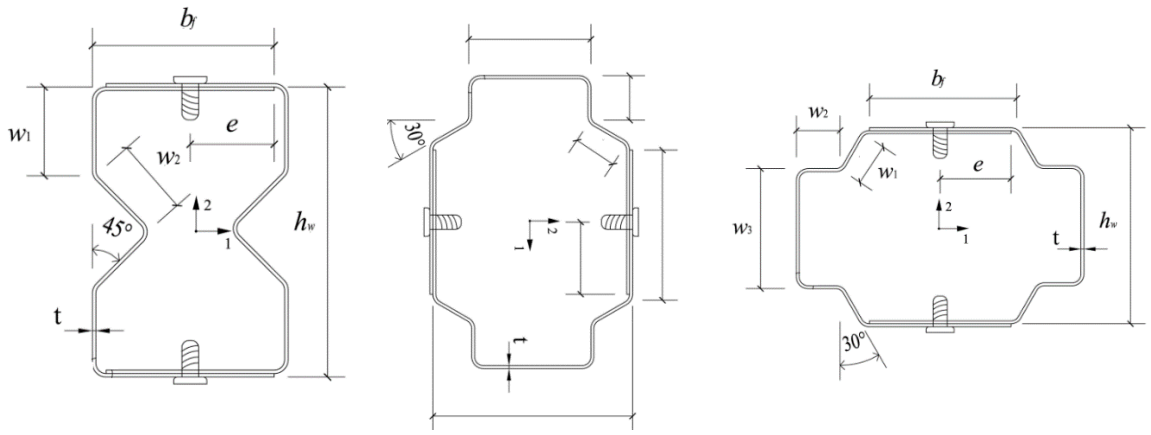

Figure 3.10: Built-up closed sections investigated in [74,75] studies.

In recent studies [76,77] investigated the flexural behavior of built-up toe-to-toe sections assembled using spot welds as presented in Figure 3.11, the buckling instability reported by these sections was the distortional buckling occurred in the upper flange of the cross-sections.

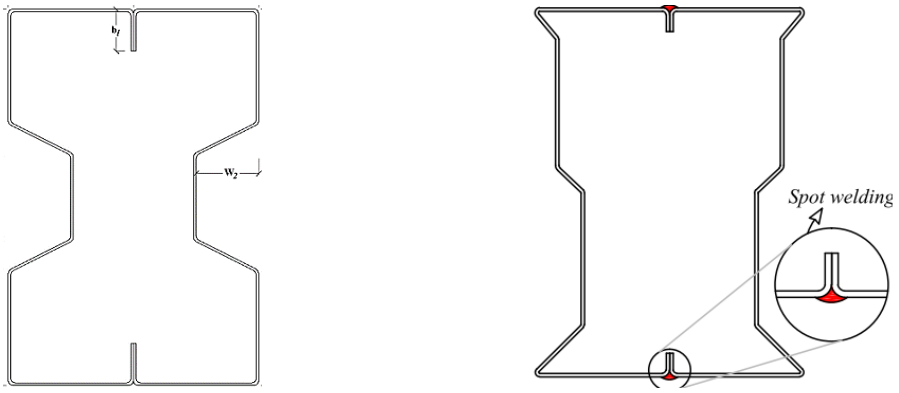

[76] [77]

Figure 3.11: Built-up toe-to-toe sections proposed by [76] & [77].

3.2.2 Stiffening methods used in built-up sections

The stiffening methods adopted in built-up members are categorized into two categories:

3.2.2.1 Stiffeners within built-up section design

The adoption of stiffeners in the cold forming manufacturing process present numerous advantages. Besides the increased strength and minimized buckling effects

provided by stiffeners in ensuring a robust structural integrity for the built-up member, the adoption of stiffeners partially facilities the strength prediction using the present design methods, in comparison with more complex stiffening approaches [78-82].

[74,75] investigated the design flexural strength of built-up back-to-back stiffened sigma section, including stiffeners in both lip and web as shown in Figure 3.12.

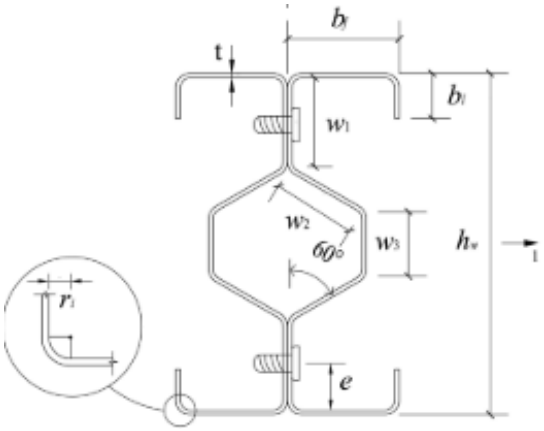

Figure 3.12: Stiffened back-to-back built-up section named as (OI) [74].

Table 3.1 illustrates the outcome of the study by comparing both the maximum bending strength obtained from experiments and FEA, with Direct Strength Method (DSM) predictions, the results revealed that DSM can accurately predict the bending strength of OI section with a mean value of M_{EXP}/M_{DSM} = 1.00, and COV of 8% which is considered as a low variation in results.

The use sigma section was proposed by [77] with a face-to-face configuration in toe-to-toe connection, resulting in a totally closed stiffened section as showed in Figure 3.11. The flexural strength obtained from such a configuration reported failure solely in distortional buckling, Figure 3.13 illustrates the distortional buckling occurrence in test specimen. The adopted stiffeners contributed effectively in avoiding local buckling failure.

Table 3.1: Comparison of flexural Strengths Obtained from test with DSM Predictions for OI Section [74,75].

	Tests or FEA	DSM predictions		Comparison	
Specimens	M_{EXP} or M_{FEA} (kN mm)	Failure mode	λ_l	M_{DSM} (kN mm)	M_{EXP}/M_{DSM} or M_{FEA}/M_{DSM}
29-OI-1.2	7,989	D + F	0.738	7,617	1.05
24-OI-0.75	4,153	D + F	0.924	3,976	1.04
23-OI-0.75	4,201	L + D + F	0.924	4,008	1.05
31-OI-0.6	2,785	L + D + F	0.972	2,513	1.11
25-OI-0.6	2,913	L + F	1.112	2,852	1.02
26-OI-0.6	2,634	L + F	1.115	2,783	0.95
35-OI-0.6	3,378	L + F	1.129	3,859	0.88
34-OI-0.6	3,398	L + F	1.129	3,888	0.87
31-OI-0.48	1,984	L + D + F	1.130	1,819	1.09
32-OI-0.6	5,407	L + D + F	1.141	5,261	1.03
25-OI-0.48	2,180	L + F	1.329	2,021	1.08
27-OI-0.48	1,897	L + F	1.331	1,970	0.96
26-OI-0.48	1,756	L + F	1.332	1,972	0.89
30-OI-0.75	3,830	L + D + F	1.378	3,934	0.97
29-OI-0.6	2,860	L + F	1.402	2,549	1.12
30-OI-0.6	2,815	L + D + F	1.691	2,725	1.03
33-OI-0.6	4,512	L + D + F	2.321	4,716	0.96
OI-0.48-B4	1,880	L + F	1.513	2,079	0.90
Mean (P_m)	—	—	—	—	1.00
COV (V_P)	—	—	—	—	0.080
$\phi_b = 0.8$, reliability index (β_1)	—	—	—	—	2.91
$\phi_b = 0.8$, reliability index (β_2)	—	—	—	—	2.72

Note: D = distortional buckling; F = flexural buckling; L = local buckling.

Figure 3.13: Distortional buckling failure in face-to-face sigma section adopted by [77].

For built-up sections subjected to high loads, more sophisticated and intricate bracing techniques involve the utilization of corrugated webs within the member design [83-86]. These webs exhibit a superior ability to prevent buckling failures when compared to flat webs, Figure 3.14 shows the deformation pattern in a corrugated beam subjected to four-points bending.

Figure 3.14: Deformed shape in corrugated beam subjected to four-points bending [83].

3.2.2.1 External stiffeners for built-up members

Within this stiffening category fall various technics involving the use of external steel plates and elements, or the introduction of composite materials such as concrete [87-89], lightweight materials like GFRP, and high-density polystyrene [90,91], these stiffening materials are disposed along the member's length to reinforce high stressed area and suppress buckling instabilities, particularly local and distortional buckling.

Experimental tests on gradual stiffening approach for built-up beams, meant to increase the flexural strength of 4 specimens with large geometrical imperfections pertaining from a poor manufacturing process was conducted by [92], the evidence for these imperfections is shown in Figure 3.15. Figure 3.16 shows the cross sectional configurations used for the beams in parallel with the gradual stiffening approach adopted for each specimen along the length.

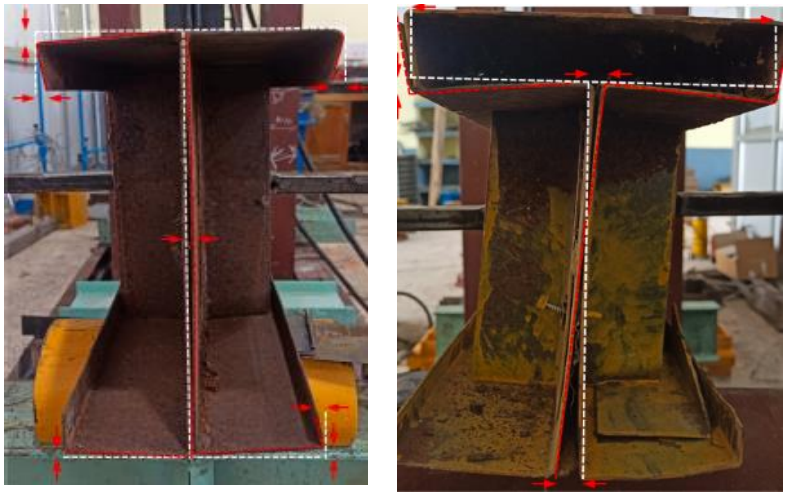

Figure 3.15: Global geometrical imperfections in cross-sectional configuration.

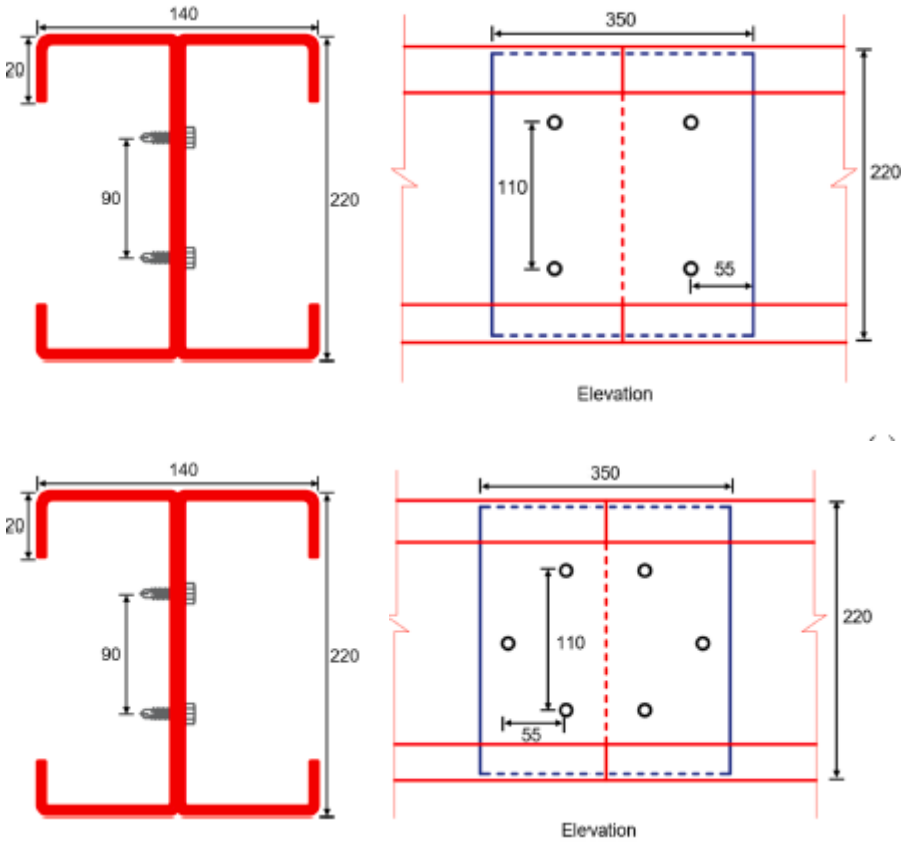

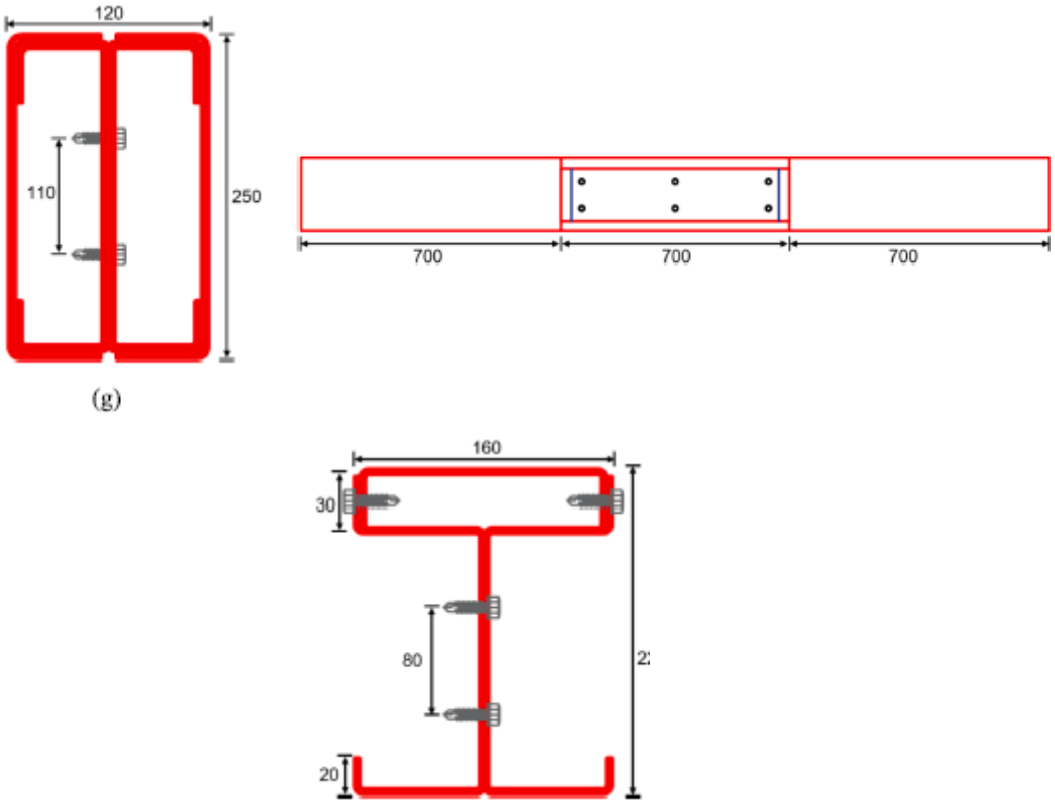

Figure 3.16: Cross-sectional configuration of the investigated specimens with the corresponding gradual stiffening approach [92].

In a similar study on large geometrical imperfections, [93] conducted experimental tests by focusing on built-up I beam, and suggested a stiffening scheme using various stiffeners schemes along the length of the specimens Figure 3.17 show the repartition of the stiffeners adopted in the longitudinal profile. These particular stiffening technics used specifically for beams with large geometrical imperfections, has significantly enhanced the structural efficiency of distressed specimens by over 60%, providing an effective and time-saving solution to realistic structural engineering problems. These experimental investigations present a valuable insight for conducting supplemental numerical investigation on stiffening method, which open the door toward developing design guidelines for these members.

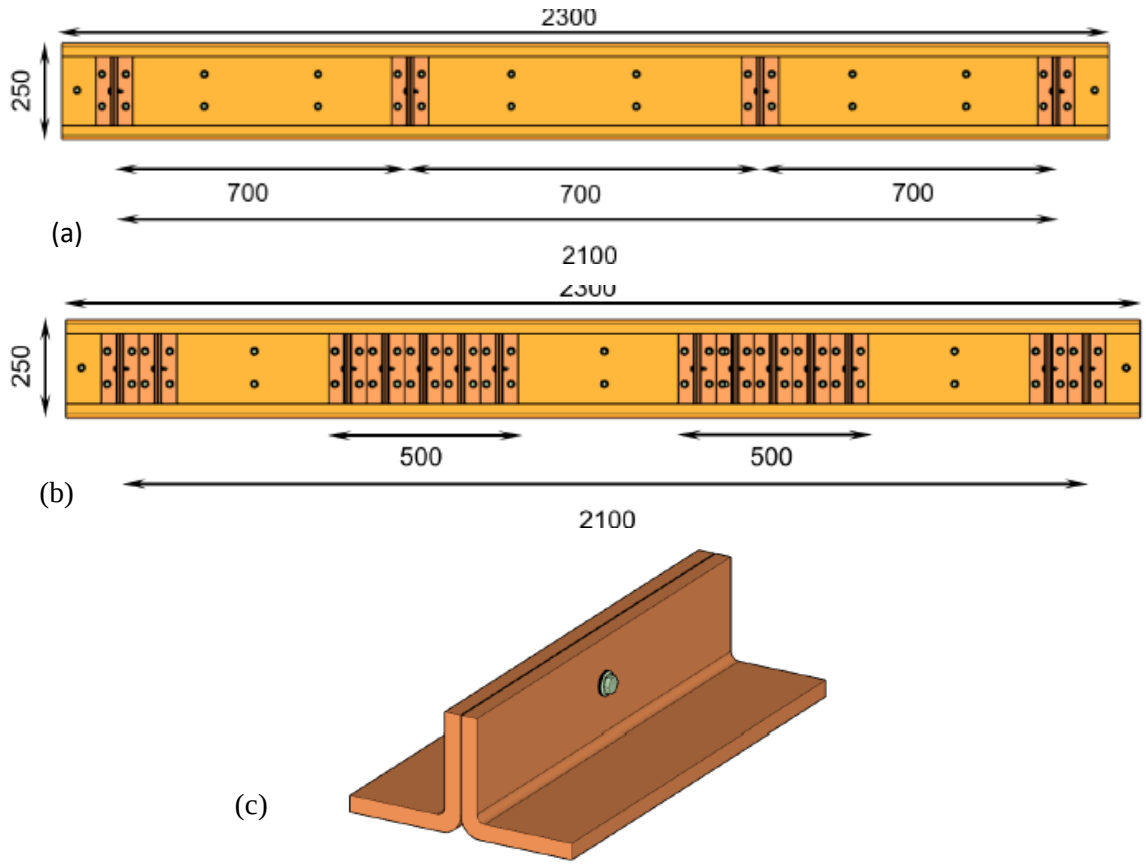

Figure 3.17: Details of the specimens adopted; (a), (b): repartition of stiffeners along the length of the I-beams, (c): built-up stiffener adopted [93].

Recently, [94] conducted a comprehensive test program to examine the flexural behavior of CFS GFRP composite built-up open-section beams. The composite specimens were prepared using intermittently stiffened CFS sections with GFRP planks (as shown in Figure 3.18), the four specimens were subjected to four-point loading. Results were analyzed in terms of peak strength, initial stiffness, load-deformation response, failure modes, and strength-to-weight parameter. all the GFRP built-up sections, were compared with conventional I shaped profiles hot rolled and cold formed.

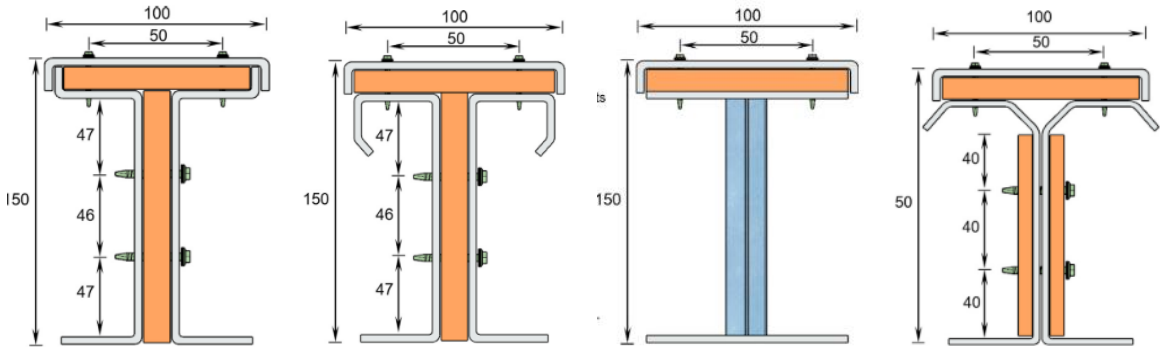

Figure 3.18: cross-sectional component of CFRP CFS built-up section, (a): RGS, (b): CGS, (c): TGS, (d): MGS [94].

This study results revealed that the incorporation of CFRP in built-up beams helped avoiding premature local buckling in the compression flange and web. The best performed configuration among the four specimens in terms of higher flexural strength was the MGS configuration. The inadequate use of stiffeners resulted in instable behavior and separation between component in the rectangular flange, which affected the flexural strength (as it is the case for RGS specimen), and recorded the lowest performance among the specimens. This study also revealed that the incorporation of GFRP planks increased the flexural capacity by about 180% compared to conventional CFS built-up I-beams. On the other side GFRP planks contributed to achieving around 80% of the flexural strength of a hot-rolled steel I-beam, leading to the creation of highly efficient lightweight built-up beams suitable for practical use.

3.2.3 Current state of Direct Strength Method application for built-up sections in bending

Direct Strength Method (DSM) was initially developed to facilitate the computation of more intricate and optimized CFS cross-sections. According to the present state of research, computational elastic stability analysis and DSM can serve as the engine for shape optimization. Furthermore, it has been demonstrated through research that DSM-optimized for CFS cross-sections can utilize fewer families of members with unique shapes and outperform current solutions across a broad spectrum of demands [95], in recognition of the fact that manufacturers produce families of shapes to satisfy market demands. While more advanced CFS cross-sections are widely utilized on a

global scale, North American Specification [2] has been relatively slow to implement these advancements in numerous contexts [96]. Additional efforts are required in the areas of technology transfer, DSM tool development, and DSM training for manufacturers and engineers in order to fully capitalize on the advantages of previously developed innovations and new research. The state of DSM research concerning built-up innovative cross-sections is not an exception, particularly for the calculation of flexural members. The current AISI-S1000 [2] reports the design prediction of only CFS individual sections in bending, and the applicability of such prediction in case of built-up section, is only limited to built-up section with generic shape such as back-to-back I-cross-section, therefore, additional researchs are required for flexural built-up members.

The first attempts for extending the applicability of DSM expressions to built-up sections, was made by [97] for compressed members, where overlapping zones of the built-up section are considered to be double-thickness in order to replicate the effect of screws used in experimental tests assembly. This supposition was further considered in the analytical analysis of numerous built-up sections subjected to compression [98]. In accordance with this presumption [74,75], investigated DSM applicability on a variety of built-up open and closed beams, the outcomes of flexural load experiments were compared to the design strengths determined using DSM [2]. Although the DSM simplifies the process by removing the requirement for complex estimation of the effective widths in the cross-section, the comparison revealed inconsistencies between the test measured strength and the strength predicted by DSM. Efforts were therefore concentrated on modifying DSM equations to extend its predictability, with the exception of situations in which the existing DSM performed well. As a consequence, multiple modified DSM variations were proposed to satisfy the strength prediction of the innovative investigated built-up sections (Figure 3.19), these modifications were consecutively made to the original DSM expressions through trial and errors depending on the reported experimental and numerical data of the

study, with a goal to satisfy the strength calculation of a particular built-up section shape.

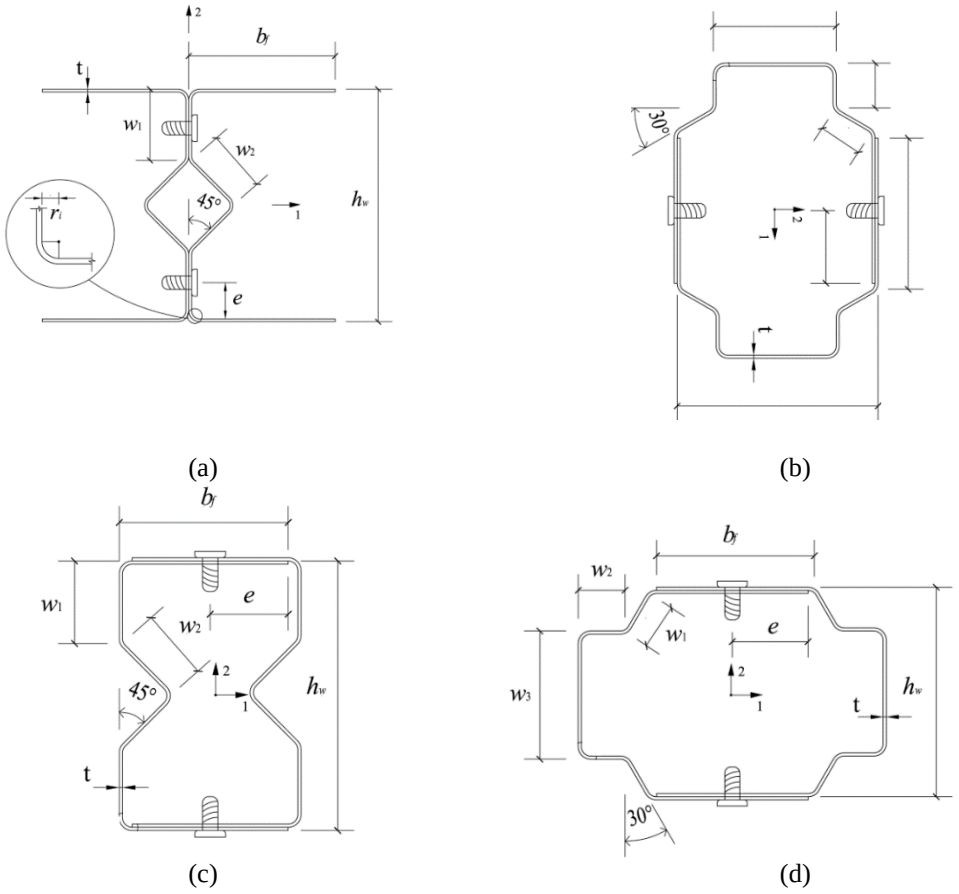

Figure 3.19: Cross-sectional details of specimens studied by [74,75]: (a) OV section; (b) COW section; (c) CV section; (d) COF section.

Recent studies [76,77] examined the accuracy of the existing DSM equations and the modified DSM equations proposed by [74,75] on more advanced built-up members. These studies demonstrated that both the current and modified DSM equations are not effective in predicting bending capacity for closed built-up members made up of sigma sections set up toe-to-toe as showed in Figure 3.11 (see section 3.2.2 of this Chapter). Therefore, new DSM expressions were proposed based on the same assumption followed by [74,75].

This inspired several research to investigate deeper into these cases and formulate unique design equations customized for a variety of unconventional built-up cross-sections, confronting the double thickness approach in particular. However, in certain assessments, individual sectional model approach was utilized in lieu of double thickness, which resulted in accurate predictions. Some investigations considered alternatives to modifying the two times the thickness coefficient (2×t) to other coefficients, as opposed to modifying the DSM equations, however, the individual sectional model assumption was only applied on columns. An increasing quantity of suggested adjustments to the DSM equations seeks to encompass a broad spectrum of innovative built-up sections. Additionally, a multitude of propositions for DSM equations have been published [99].

3.2.4 Effect of fasteners spacing on the flexural behavior of built-up members

One key distinctions can be made for CFS individual sections and built-up sections, with the latter containing connectors. In contrast to individual CFS sections, which generally do not necessitate any imposed fastening between components, built-up sections primarily rely on fasteners. They are critical for ensuring the structural integrity of single-element profiles during connection and must be taken into account during the design process. The absence of design provisions for conventional built-up sections in the existing NAS [2], particularly for the minimum fasteners spacing (except in case of a regular I shaped section) presents a difficulty in ascertaining the convenient number of fasteners in both the longitudinal and cross-sectional directions, notably for unconventional built-up sections. In an attempt to comprehend the effect of screw spacing on deformed shapes, buckling instability and flexural strength of CFS built-up members, limited number of studies have been conducted, to contribute into the development of a minimum fastener's spacing recommendations for assuring the structural integrity of the member.

[100] conducted a study to comprehend the impact of screws spacing variation on built-up open and closed flexural members as presented in Figure 3.20, the screws

spacing variation in this study was only considered in the bending span along the length of the beam, considering the presence of higher stress in this area, Figure 3.21 shows the longitudinal distribution of screws in the beam, many screws configuration were adopted, while intermittently changing cross sectional parameters. The numerical and experimental results of this investigation indicate that the increase in the flexural strength, and alteration of the behavior was particularly significant in closed built-up sections as a result of fasteners being positioned in the upper flange, thereby regulating local buckling occurrence in that area. In case of built-up open section, the screws spacing had no contribution in increasing the flexural strength.

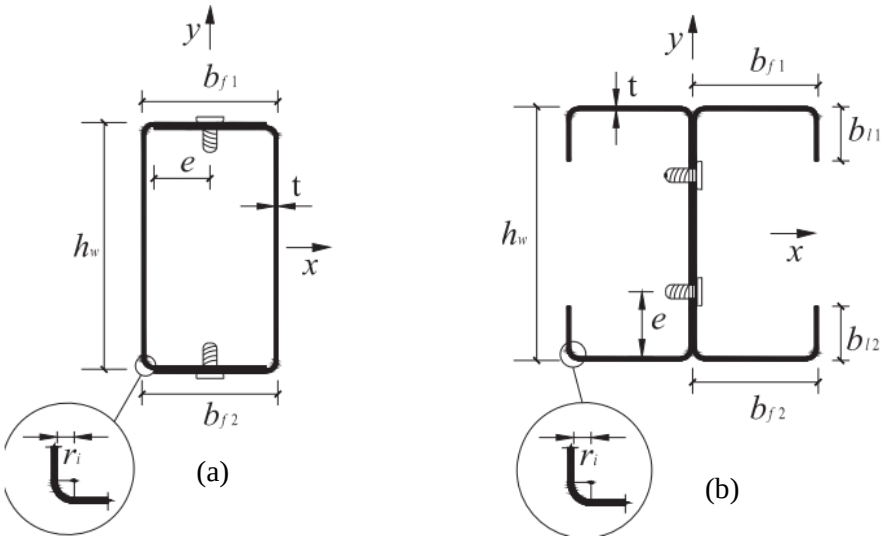

Figure 3.20: Definition of symbols and location of screws in cross section. (a) Built-up closed section. (b) Built-up open section [100].

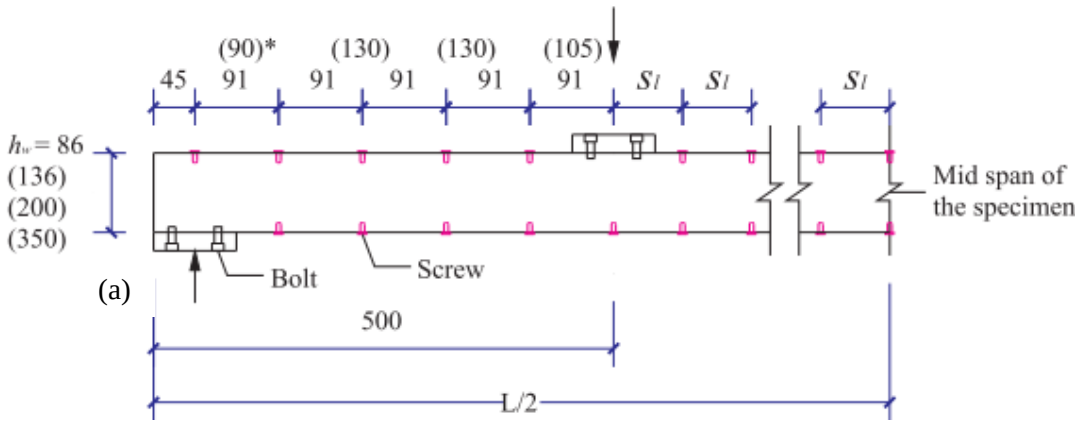

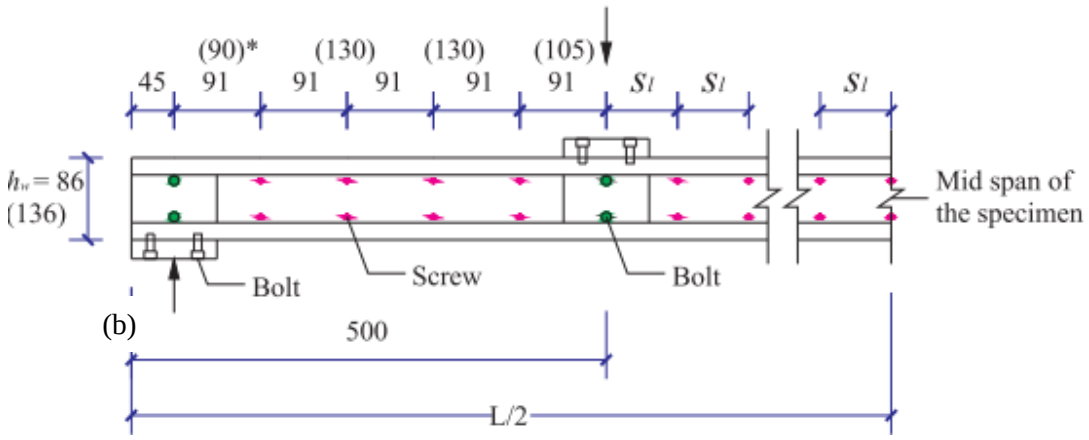

Figure 3.21: Distribution of fasteners along the length of (a): built-up closed section, (b): built-up open section [100].

In order to optimize the flexural strength improvement achieved by fasteners, a minimal fastener spacing is determined in consideration of the built-up section's local buckling half wavelength, as determined by the Finite Strip Analysis software (CUFSM) [101], indeed the minimum spacing recommended in this study must not surpass the buckling half wavelength of the member. As a conclusion, this contributed to the establishment of a limit fasteners interconnection of four times the web depth ($4\times h_w$) [100].

Moreover, there is ongoing inconsistency regarding the appropriateness of utilizing a individual sectional model approach or double-thickness assumption in overlapping regions to ensure precise analytical strength calculation. For the calculation of the elastic buckling stress, the current DSM equations utilize CUFSM; they were devised predominantly for CFS individual members. This emphasizes the constraint of screws modeling in CUFSM and, consequently, the accurateness of DSM in precisely forecasting the flexural strength of built-up flexural members.

A recent study conducted by [102] based on a compound finite strip model approach with the purpose of faithfully simulating fasteners in built-up members. However, this study while being capable to include discrete fasteners within the model design, its applicability was restrained to a conventional built-up I beam.

3.3 Conclusion

This chapter provided a comprehensive literature review on CFS built-up sections, focusing on their behavior under bending loads, their design considerations, and the challenges associated with their structural performance. The chapter explored both open and closed built-up sections, highlighting their strengths, weaknesses, and how different design assumptions and stiffening methods affect their performance.

The stiffening methods employed in built-up sections were a key focus of the literature, with several studies highlighting the benefits of incorporating internal and external stiffeners. Internal stiffeners, such as those added to sigma sections, improved both bending strength and buckling resistance. External stiffeners, including the use of materials like GFRP, offered significant improvements in structural performance, particularly in sections with large geometrical imperfections, thus providing a viable solution for distressed structures.

The chapter concluded with a discussion on the current state of Direct Strength Method (DSM) application for built-up sections. While DSM has proven to be an effective tool for analyzing CFS individual sections, its applicability to built-up sections remains limited. Several modifications to DSM equations were proposed to extend its use to these more complex configurations, with promising results from various studies. Despite these advances, the DSM's ability to predict the strength of innovative built-up sections under bending remains an area for further research.

In summary, the chapter emphasized that while significant progress has been made in understanding the behavior of built-up CFS sections, continued research is necessary to refine design methods, improve the accuracy of strength predictions, and develop more reliable, efficient, and practical solutions for real-world applications.

Chapter 4
Finite element model development and validation study

4.1 Introduction

This chapter details the development of the finite element model (FEM) used in this investigation, carried on finite element analysis software ABAQUS version 6.14, a robust and recognized software for analyzing the behavior of thin and thick shell elements, and accommodated for predicting cold formed steel (CFS) member's behavior. The numerical analysis is used as an alternative tool for the experimental tests in predicting the behavior and strength of (CFS) built-up sections under investigation. The numerical validation of the (FEM) was realized by replicating experimental tests in a controlled laboratory environment, conducted on CFS built-up sections in a literature investigation [74]. To ensure the quality and credibility of the developed finite element model in predicting the true structural behavior of CFS members, three levels of numerical validations were addressed. The first level concerns the generation of moment-displacement curves to assess the compatibility between the numerical and experimental results in terms of flexural rigidity and maximum displacement when reaching the ultimate stress. The second level presents the visualization and comparison of the obtained deformed shapes, this ensures the quality of the numerical model in simulating the true buckling modes and deformed shapes. Finally, a comparison level of numerical and experimental maximum bending strength values is reported. The validation of the FE model on these three levels ensures its robustness in predicting the results and enables its application on more built-up sections, including the ones under investigation.

4.2 Finite Element developing

The application of finite element modeling for cold-formed steel members requires a certain level of intricacy, dealing with thin-walled sections and their potential elastic buckling occurrence prior to strength yielding failure, increases the level of complexity in selecting convenient parameters, meant to contribute in successfully running the analysis, and build reliable model capable of predicting the strength under various conditions, these parameters include the choice of a convenient analysis and finite element type, the precision of mesh discretization, the imposition of boundary conditions, the nature of loading conditions, the incorporation of material properties and the geometric imperfections.

4.2.1 Nonlinear analysis

The complex behavior of cold formed steel members suggests to account for nonlinearity in the numerical model, indeed, nonlinearity arises from different aspects related to the material, therefore, using the nonlinear model in FEA is recommended to accurately predict the strength and simulate the reality in terms of deformed shapes, to achieve this goal ABAQUS software [103] uses two types of nonlinearities, the material and geometrical nonlinearity.

4.2.2 Material Nonlinearity

Material nonlinearity plays a crucial role in determining the true stress-strain relationship, especially when dealing with thin-sheet steel. This is because nonlinear models can accurately represent the inherent behaviors of such materials, allowing plasticity to emerge before reaching the ultimate load.

Incorporating material nonlinearity into the finite element model (FEM) involves using the actual stress-strain relationship extracted from experimental tests. However, due to the unavailability of actual stress-strain curves from tensile tests reported by [74], we had to consider using an approximate model for stress-strain simulation. The selection of a suitable model, one that accurately describes the true tensile test, and thus the behavior of cold-formed steel members, required a review of previous studies,

such as the ones conducted by [76] and [65] which utilized the elastic perfectly plastic model, after conducting a series of comparison tests between the actual tensile test data incorporation into the FE model, and the consideration of an approximate behavioral model. These studies explored the impact on behavior and critical load prediction for built-up beams in [76] and columns in [65]. The results demonstrated that the elastic-plastic model provided an accurate and practical performance in predicting the strength of these members, highlighting its application suitability in built-up CFS members. Figure 4.1 presents a comparison between the actual stress-strain curve and the elastic perfectly plastic model obtained from [65] investigation.

It's also important to note that our current study does not delve into complex material phenomena, such as strain hardening, strain softening, sensitivity to yield stress, load redistribution, or unrealistic plastic strain. In such cases, the material's behavior is significantly affected by these factors, therefore, alternative models may be better suited and adequate. As a result to all these considerations, The current study followed the adoption of the bilinear elastic-plastic model, to present the material behavior.

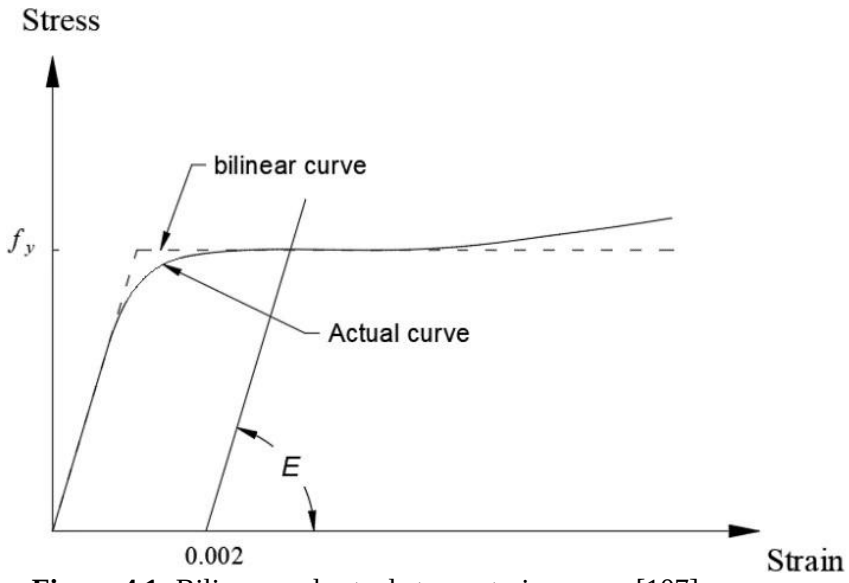

Figure 4.1: Bilinear and actual stress-strain curves [107].

4.2.3 Geometric nonlinearity

Geometric nonlinearity arises when a structure undergoes in-plane deformation, causing changes in the shape and dimensions of its cross-section. In simpler terms, if a structure with geometric nonlinearity deforms, it may no longer behave as if its parts remain perfectly straight or unreformed. This is particularly relevant in the context of cold-formed steel members, which exhibits a certain level of ductility, allowing for significant deformations. In situations of large-strain analysis, geometric nonlinearity is accounted for by including the Newton-Raphson iteration method in the numerical model as available in ABAQUS library, this method consists of linearizing the nonlinear relationship, with tangent stiffness matrix by using linear increments, and iteratively reaching the converged solution for the appropriate number of increments. The basic equation for the Newton-Raphson method involves solving a linear system of equations, often presented by:

$$\Delta u = K^{-1}. R \qquad \text{(Eq 3.1)}$$

Where:

- Δu is the incremental displacement vector.
- K^{-1} is the inverse of the tangent stiffness matrix, which captures the stiffness changes due to deformation.
- R is the residual vector, representing the unbalanced forces at the current solution.

4.2.4 Element type and mesh

The element type chosen for the mesh analysis was the conventional shell element S4R, a general-purpose quadrilateral linear element cornered with four nodes, and based on reduced integration points in its formulation, each node of this element was set free for transition and rotation in the three directions. Its suitability for handling thick-shell element problems stems from the ability to account for transverse shear

deformations. It is also highly effective in analyzing thin-shell elements due to its adherence to the principles of discrete Kirchhoff theory, ensuring that sections normal to the mid-surface of the shell remain straight and undistorted throughout mid-surface deformation. Additionally, this finite element model (FEM) uses finite membrane strain, a formulation suitable for inherent large deformations and rotations problems, making it a befitting option for modelling CFS members. While the S4R element is a computationally less expensive choice, it may sometimes lead to an unreal numerical deformation known as the 'hourglass effect.' This effect typically occurs when elements are discretized with reduced integration points, causing distortion in highly strained areas. In the present investigation, the geometric distortions associated with the 'hourglass effect' were not recorded as shown in Figure 4.2. This suggests that this element is well-suited for predicting the behavior of these sections.

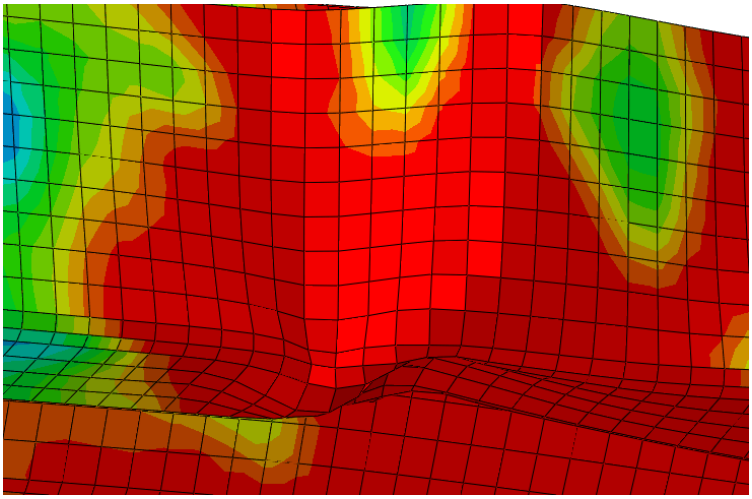

Figure 4.2: Absence of hourglass effect deformation.

S4R element was commonly used for CFS members [75-77], in details it offers six degrees of freedom (three translational and three rotational) for each node with reduced integration, a convergence study was conducted to determine the appropriate size of the finite element, through a mesh sensitivity analysis conducted on three built-up beams, with mesh sizes of 5 and 10 mm. The outcomes of the analysis are illustrated in a comparison between the experimental test results and FE models with the two

mesh sizes adopted, the results are reported in form of moment-displacement curves, as shown in Figure 4.3(a-c). The results show that the mesh size variation influence on COW-1.0-B4 was insignificant, however, for OV-1.0-B4 and CV-1.0-B4 specimens, notable differences compared to the test results have been reported, both in terms of maximum bending strength and flexural rigidity, particularly for OV-1.0-B4 specimen. Based on this sensitivity outcomes, the present study concludes with a mesh size of 5×5 mm.

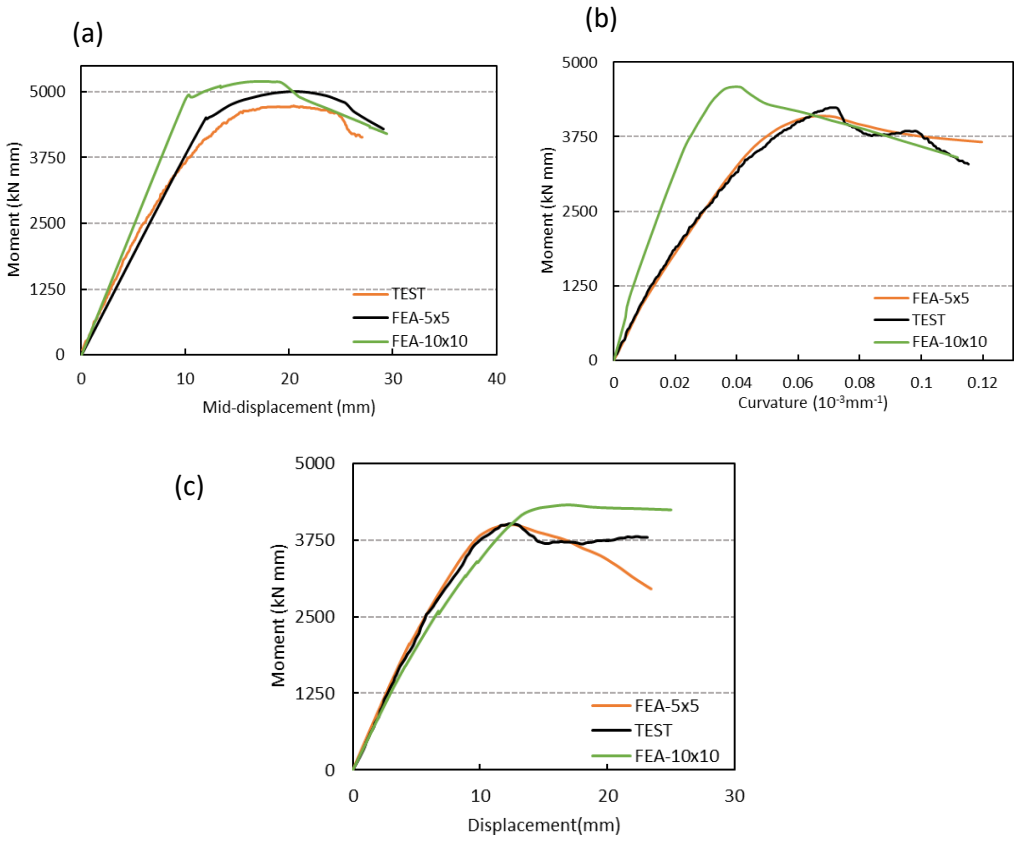

Figure 4.3: Mesh sensitivity analysis for specimens: (a) COW-1.0-B4, (b) OV-1.0-B4 and (c) CV-1.0-B4 [106].

4.2.5 Contact interaction and fasteners

The numerical model encompasses a range of options and procedures to simulate the physical characteristics of cold formed steel members. In the case of built-up sections, where multiple layers interact, the initial step involved establishing contact between master and slave surfaces before the nonlinear analysis, to prevent interpenetration of

layers during the analysis. Figure 4.4 shows the definition of interaction between master-slave surfaces. To ensure the releasement of this contact, a gap equal to the thickness of the built-up section is introduced in the geometrical model between the two surfaces, this adjustment allows for the correct representation of the component layers based on mid-surface assumption. In the contact properties, 'hard contact' setting is defined for normal behavior to prevent any overlap, while 'frictionless' behavior is selected for tangential interactions to avoid resisting sliding. The 'small sliding' approach is preferred over ‘finite sliding’, considering the minimal relative sliding between the two surfaces. This not only reflects the experimental set-up of tests, but also reduces computational time compared to the ‘finite sliding formulation’. In terms of numerical accuracy, the chosen adjustment tolerance slightly exceeds the thickness of the section, this allowance accounts for any potential numerical errors arising from the discretizing finite nature, particularly in nodal coordinates.

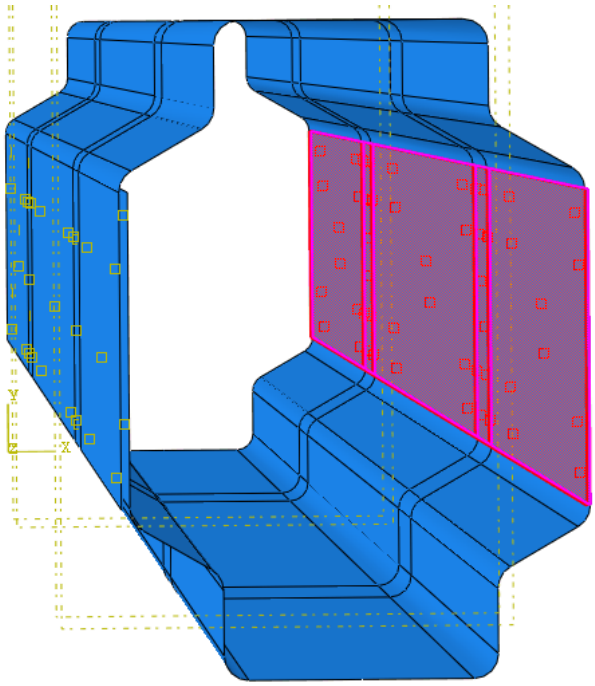

Figure 4.4: Interaction of master-slave surfaces.

The connection between individual parts of the built-up section, was handled using mesh-independent fastener option available in the ABAQUS library. This option used

in the validation tests and later extended to the parametric study, involves the attribution of attachment points in contact areas, used as a set-based points for the application of mesh independent fasteners, this virtual fastener modelling technic emerged as effective compared with physical screws modelling, since there were no screws damages occurring before reaching the specimen yield strength in tests as reported in [74]. Figure 4.5 shows the distribution of fasteners along the length of the beam. Additionally, this approach allows for a smooth alteration of fasteners spacing, leading to a comprehensive investigation of their impact on the structural strength, as it will be further investigated in the parametric study of Chapter 7.

4.2.6 Loading and boundary conditions

Loading and boundary conditions were applied to the finite element (FE) model, using reference points defined in the model's geometry, and positioned at specific locations along the beam. These reference points were then kinematically linked to the adjacent surfaces using ABAQUS Standard Interaction. Figure 4.5 illustrates locations of reference points (RP's) considered. To replicate simply supported beam conditions, RP's were placed at the centroids of the sections at both ends of the beam, all rotational and translational degrees of freedom (dof's) were locked, except for the rotation around the X-axis. This setup allowed the beam to flex as expected under bending loads, while also enabling the simulation of C-clamps to prevent lateral-torsional deformation of the member during the analysis. Moreover, the use of reference points at the centroid ensured that all degrees of freedom were constrained through their connection to adjacent surfaces, as a result, it contributed into preventing web crippling and localized deformation of the beam, caused by loading concentration, and shear forces at the extremities. Loading plates were not physically modeled, instead, it was simplified by using additional reference points above the beam model at loading points locations, and tied with surfaces similar to the plate dimensions, in only transitional dof's, to avoid rotational deformation of these locations during the analysis.

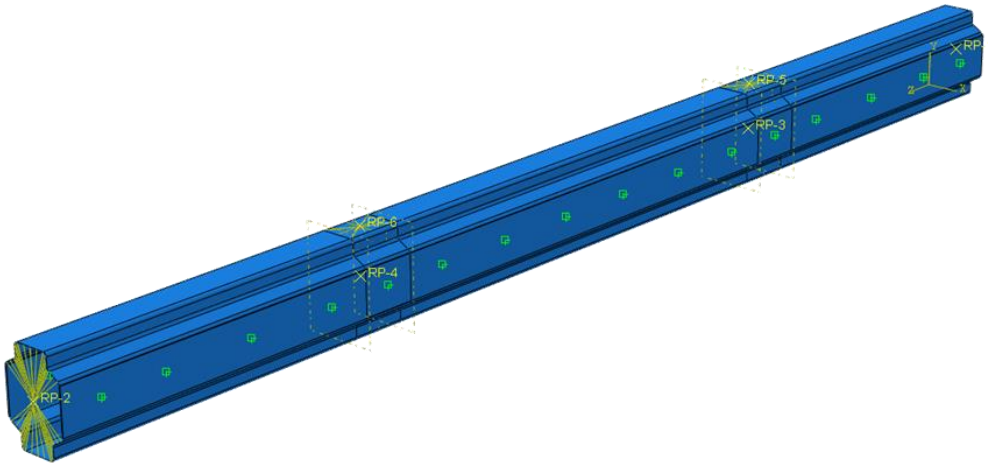

Figure 4.5: Boundary conditions, loading and connector modelling approach.

4.2.7 Geometric Imperfections

Geometrical imperfections are of utmost importance in thin-walled members and should be meticulously incorporated into finite element modeling to ensure accurate and reliable behavior predictions. These imperfections encompass both sectional imperfections (local imperfections) and length-based or global imperfections.

To include both imperfections in the numerical model, a buckling analysis is undertaken to determine the prominent buckling modes that significantly influence the behavior of the investigated beams. These buckling modes were scaled and integrated as eignemodes into the model. Their values corresponded to a geometric imperfection of 0.34×t, as recommended by [21,27], where (t) is the thickness of the section,

Figure 4.6 shows the first critical eigenmode resulted from the buckling analysis, representing local imperfections, for COW-1.0-B4 specimen.

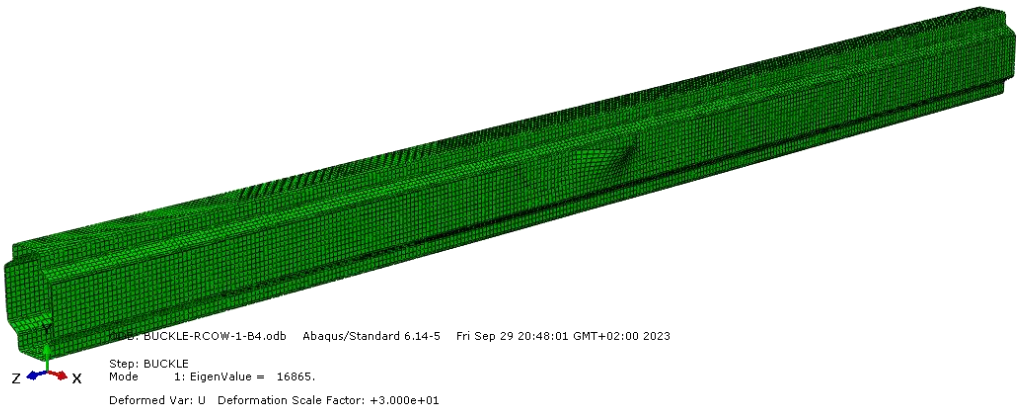

Figure 4.6: First buckling Eigenmode for COW-1.0-B4 specimen.

4.2.8 Automatic stabilization

During the numerical analysis, consideration of the equilibrium criteria was taken into account, through the verification of equilibrium equations for the static case (E-I=0). In case of modeled beams, internal forces (I) heavily rely on stiffness forces (K.u), the absence of damping forces, in addition to the sudden change and loss of stiffness contact gaps and premature buckling failure, hinder the static solver's ability to achieve equilibrium and prematurely terminated the analysis. To attain to these issues, Abaqus recommends the use of automatic stabilization scheme, consisting of attributing fictional damping forces to the nodes located in contact areas where there are discontinuities of the material, to maintain the equilibrium targeted by the absence of stiffness. Nonetheless, these damping forces were cautiously introduced to the model to not cause any alteration in the numerical results or producing unrealistic deformations. To control the amount of damping forces added to the numerical model, the ‘dissipated energy fraction’, which presents the ratio of the energy dissipated due to damping forces, and the total strain energy in the first step, was limited to a value of 0.0002.

4.2.9 Nonlinear solution method

ABAQUS Standard incorporates nonlinearity into the model by considering geometric, material, and boundary conditions. Therefore, relying solely on the Newton-Raphson iteration method for a nonlinear solution is inadequate for achieving convergence. Convergence is greatly influenced by contact options, the type and size of the finite element mesh, as well as the type of the problem, which involves both local and global instabilities. Given these factors, the process of developing a comprehensive FE model that includes all the mentioned components was found to be a challenging undertaking. Hence, numerous convergence problems arose, resulting in the analysis being prematurely terminated prior to achieving the ultimate stress. Furthermore, the investigation necessitated a substantial amount of time to be fully conducted. Nevertheless, these problems were successfully overcome by augmenting the quantity of intervals and integrating artificial damping with a predefined value of 0.0002 in the nonlinear phase. This helped to avoid the loss of stiffness in areas of contact. In addition, a preliminary initial static step was implemented prior to the main step. The purpose of this step was to progressively apply minor displacements to the model, which would help facilitate the development of contact between the different components of the beam. The combination of these improvements effectively resolved convergence concerns and guaranteed the analysis was successfully completed.

4.3 Validation of the FE Model

The validity of the Finite Element Model (FEM) is realized by replicating experimental tests conducted by [74], these tests involved the modelisation of 9 built-up open and closed sections shown in Figure 4.7, with 8 beams undergoing four-point bending and one subjected to three-point bending. Geometric and material properties are detailed in Tables 4.1 & 4.2. Table 4.3 illustrates the validation results of the specimens, showing the good fit between the ultimate bending strength resulted from experimental and numerical analysis, with a mean bending ratio M_{EXP}/M_{FEA} of 1.00.

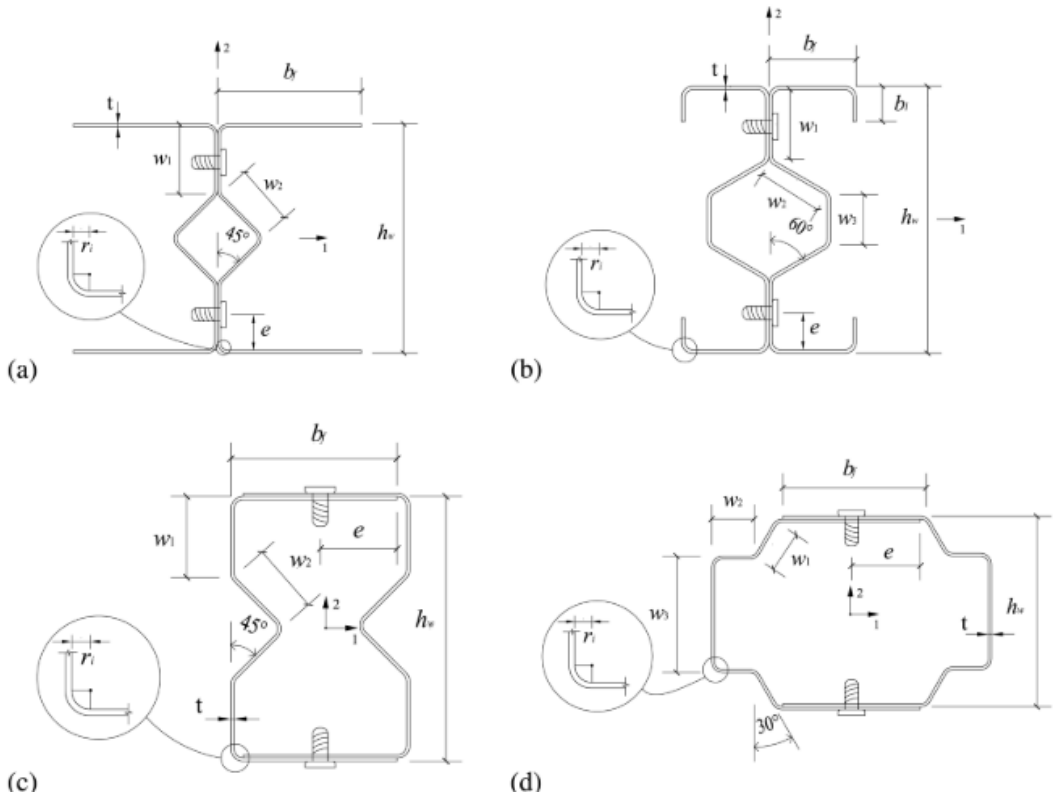

Figure 4.7: Definition of symbols and location of screws in cross section: (a) OV section; (b) OI section; (c) CV section; (d) COF section (bending about Axis 1) and COW section (bending about Axis 2) [74].

Figure 4.8 shows the quality of the numerical model by presenting the obtained buckling modes and comparing them with the experimental tests deformed shapes for specimens, CV-1.0-B4, COW-1.0-B4 and COF-1.0-B4 once the ultimate flexural threshold is reached. An additional graphical evaluation of the FE model's quality, is presented in Figure 4.9 & 4.10, through moment-displacement and moment-curvature curves respectively, for specimens CV-1.0-B4, COW-1.0-B4, CV-1.0-B3 and OV-1.0-B4. Highlighting the compatibility between numerical and experimental curves in terms of flexural rigidity and maximum displacements. Those three validation levels ensure the consistency and reliability of the FE model to be used further in the present investigation.

Table 4.1: Cross-sectional properties of experimental tested beams [74].

Specimen	b_l(mm)	b_f (mm)	h_w(mm)	w_1(mm)	w_2(mm)	w_3(mm)	t	t*(mm)	r(mm)
OV-1.0-B4	-	53.7	85.6	26.5	22.2	-	1.041	1.003	3.5
OI-1.0-B4	14.5	29.9	98.4	25.9	26.7	17.1	1.028	0.986	3.4
CV-1.0-B4	-	52.1	85.6	27.3	22.7	-	1.046	1.008	3.3
CV-0.48-B4	-	53.7	85.7	26.2	24.2	-	0.565	0.475	3.5
COW-1.0-B4R	-	50.2	70.9	15.7	16.7	43.9	1.066	1.020	3.5
COW-0.48-B4	-	50.6	69.4	14.7	15.6	42.8	0.575	0.475	3.8
COF-1.0-B4	-	51.9	70.2	15.0	15.4	44.8	1.065	1.019	3.5
COF-0.48-B4	-	50.6	69.4	14.7	15.6	42.8	0.575	0.475	3.8
COW-1.0-B3	-	50.0	72.1	14.6	16.4	45.5	1.058	1.012	3.5

Table 4.2: Mechanical properties of experimental tested beams [74].

Section [74]	E(Gpa)	$\sigma_{0.2}$ (MPa)	σ_u (MPa)	ε_f (%)
CV-0.48	213	661	690	2.0
OV-1.0/CV-1.0	213	598	599	9.7
COF-0.48/COW-0.48	214	662	707	1.8
COF-1.0/COW-1.0	216	572	583	9.6
OI-1.0	216	592	599	8.6

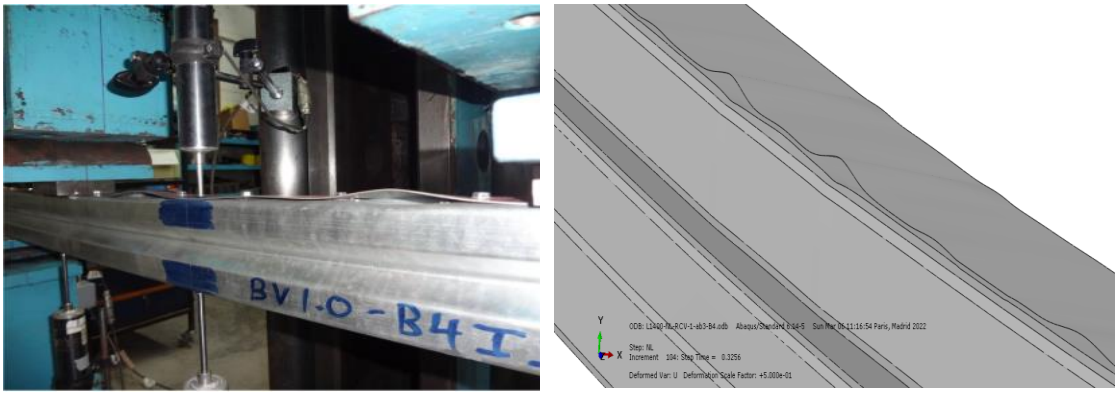

a) For CV-1.0-B4 section

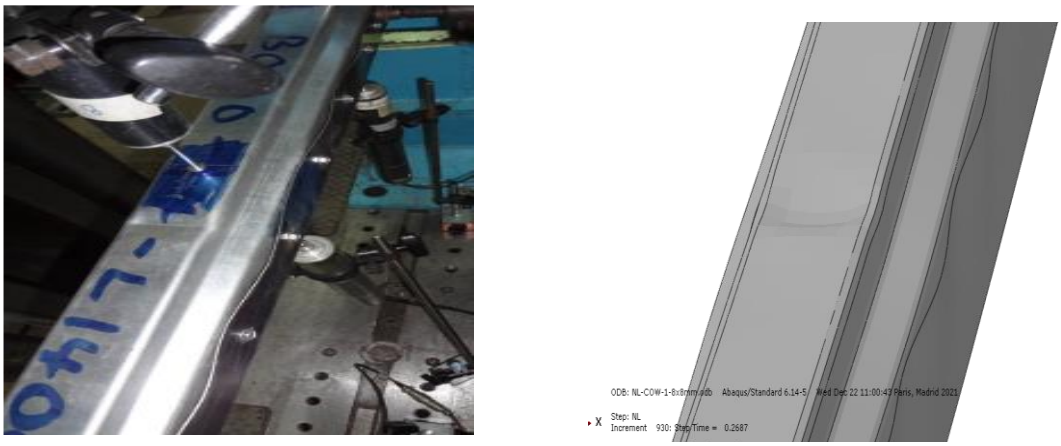

b) For COW-1.0-B4

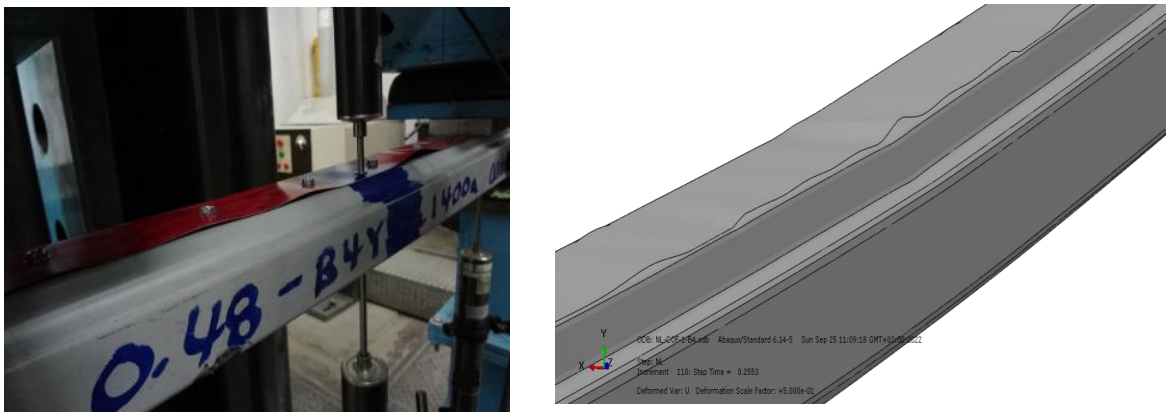

c) For COF-1.0-B4

Figure 4.8: Comparison of failure modes from test and FE modelling [74,106].

Table 4.3: Comparison between maximum flexural strength and collapse deformations from tests and numerical analysis.

Specimens	Tests		FEA		Comparaison
	M_{EXP} (KN.mm)	Failure Modes	M_{FEA} (KN.mm)	Failure Modes	M_{EXP}/M_{FEA}
OV-1.0-B4	4238	L+F	4105	L+F	1,03
OI-1.0-B4	6092	D+F	6037	D+F	1,01
CV-1.0-B4	4088	L+F	3997	L+F	1,02
CV-0.48-B4	1266	L+F	1360	L+F	0,93
COW-1.0-B4	4730	L+F	5002	L+F	0,95
COW-0.48-B4	1699	L+F	1780	L+F	0,95
COF-1.0-B4	3749	L+F	3547	L+F	1,06
COF-0.48-B4	1278	L+F	1168	L+F	1,09
COW-1.0-B3	5181	L+F	5494	L+F	0,94
Mean					1,00

Note : L : Local Buckling ; D : Distortional Buckling; F : Flexural Buckling.

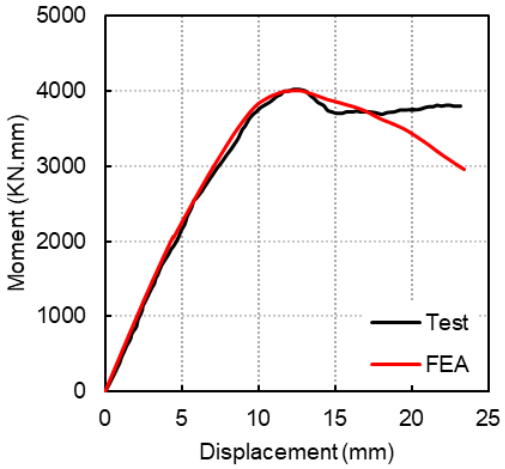

a) For CV-1.0-B4.

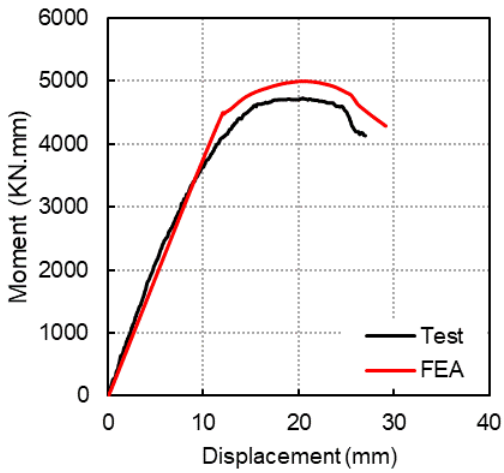

b) For COW-1.0-B4.

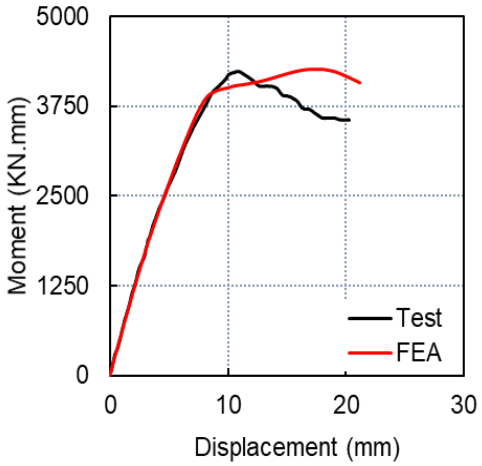

c) For CV-1.0-B3.

Figure 4.9: Comparison of Moment vs Mid-Displacement curves.

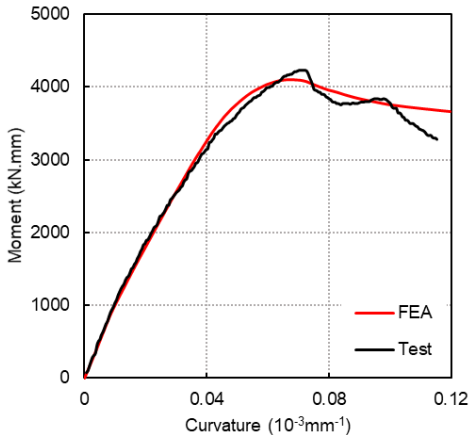

Figure 4.10: Comparison of Moment-Curvature curve for specimen OV-1.0-B4.

4.4 Conclusion

This chapter details the techniques procedures and approaches used to develop the FE model intended to be applicable for the parametric studies detailed in the subsequent chapters, the FE model undergoes a meticulous numerical validation against several CFS built-up open and closed sections selected form literature [74]. the well performed reached a high accuracy level in predicting the flexural strength of the tested specimens, in terms of the maximum bending values, moment-displacement curves and deformed shapes after reaching failure, therefore it has proved its prediction capabilities in forecasting CFS built-up sections strength, with complex and unconventional shapes, prompting for its application in the present study.

Chapter 5

Flexural behavior of efficient CFS built-up section for local buckling

5.1 Introduction

In recent years, the construction industry has witnessed a surge in demand for cold-formed steel (CFS) sections offering increased capacities, the use of such sections primarily focused on mid-rise and low-rise residential and industrial buildings, which has initiated a new trend in the application of CFS members through the formation of "built-up" cross-sections from multiple single sections. Individual sections are typically joined together using fastening devices like screws, bolts, welding, and clinches. The moment capacities of the built-up section are greater than the capacity of an individual section, as a result it offers a composite action. This chapter delve into the investigation of the flexural capacity of innovative built-up section, the new concept attributed to this section proposes to form a closed section by vertically linking two hat sections (instead of using typical individual sections such as C, Z and sigma), and joining them with using screw fasteners. The utilization of such concept resulted in offering a middle web stiffener to the generic closed box section, as presented in Figure 5.1, this concept intermittently offers more stiffening to the section, and serves as screws location, thereby increasing the sectional capacity of the section. The assessment of the new built-up section is realized by performing an understanding comparative study between three built-up closed sections (including the one proposed), thereby, similar parameters were varied and attributed to this three sections, to investigate the potential flexural behavior and buckling failure of such sections, these parameters comprises varying cross-sectional slenderness, geometrical properties and screws spacing. The outcomes of the parametric investigation are

illustrated in tables summarizing the maximum flexural strength values with corresponding buckling instability, and figures representing visual interpretation of deformed shapes.

5.2 Details of the built-up sections used

The built-up closed sections used in this parametric study are divided into two categories; the first is the proposed built-up section named as DH, consists of assembling two individual hats in a way to obtain a partially stiffened section, the second category includes two unstiffened box sections named as DC and DU. The nomenclature associated with the three sections was based on their cross-sectional geometry shapes; egg DH: stands for double (‘D’ letter) hat (‘H’ letter) section (Figure 5.1(a)), DC: consists of a double (‘D’ letter) channel (‘C’ letter) section (Figure 5.1(b)), DU: is a double (‘D’ letter) ‘U’ section (Figure 5.1(c)).

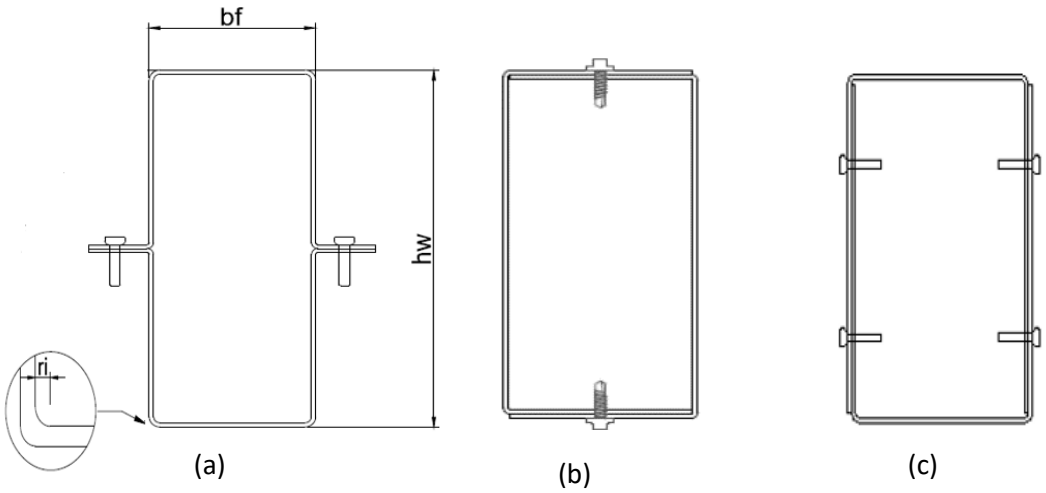

Figure 5.1: Nomenclature of the three closed built-up sections used in the study; (a): DH, (b): DC, (c): DU.

5.3 Details of the parametric study

The main goal of this parametric study is to evaluate the flexural strength and buckling instabilities of the proposed built-up section DH. A total of 15 FE analysis were conducted on beams in four-points bending. To assess the behaviour of this section towards the flexural strength and buckling instabilities, notably sectional buckling

(local and distortional), multiple parameters variations are considered. The choice of two different beam lengths, 1600 mm and 2150 mm, allows us to investigate the effect of slenderness on the flexural strength and buckling instabilities. By altering the length, one can observe any behavioural changes that may occur. Additionally, varying the web depths is important to consider due to the potential occurrence of buckling failure prior reaching the yield stress, therefore, a web high of 86 and 136 are considered. Moreover, the sectional slenderness of the specimens is varied through adopting thicknesses of 0.42, 1.2 and 1.9 mm. An important parameter deemed pivotal to vary during the analysis is the screws spacing, to determine the effect of screws on possible increase in the flexural strength. The spacing between screws was adopted according to the configurations suggested by [100], where the inter-spacing between screws was only changed in the middle span of the beam (span with the maximum flexural strength). This selection is made prior to the lack of specific guidelines for fasteners spacing for closed sections in the current AISI-S100 specification [2]. Figure 5.2 shows the distribution of screws along the length of the beam with the adopted configuration. These parameters variations allow to assess the stability and performance of the section under different structural conditions.

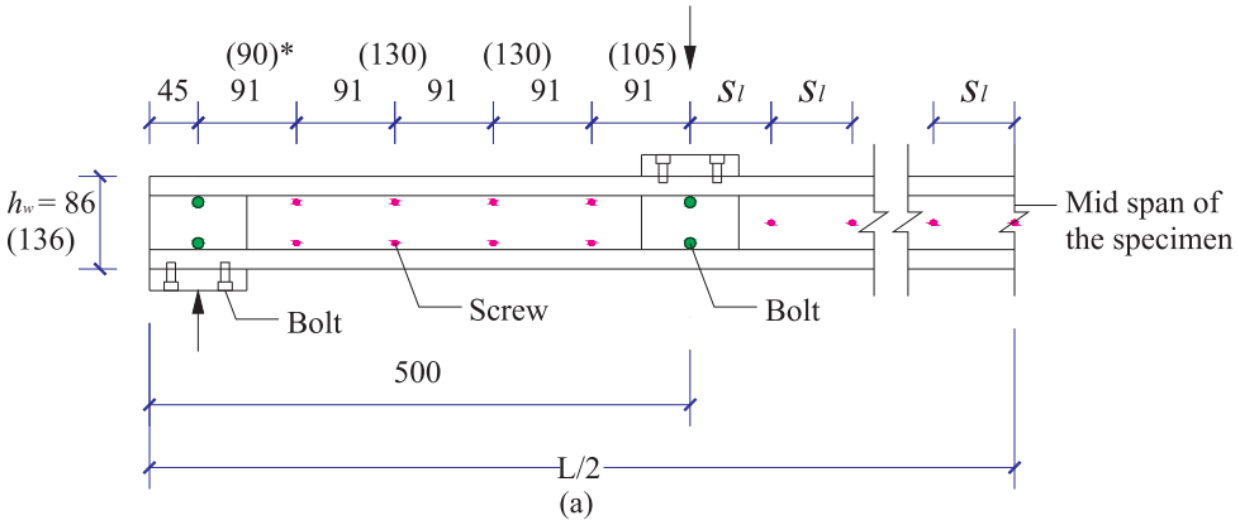

Figure 5.2: Distribution of screws along the length of the beams with web heights of 86 & 136 mm [100].

The validation process of the proposed built-up closed section DH, was not only done on the parametric study level, additionally, a comprehensive comparative study is conducted on the three closed built-up sections, the mechanism of strength for the three sections is assured by different stiffening method. For the proposed section DH, the strength is assured by attributing a stiffener in the middle of the web (Figure 5.1(a)). For DC and DU sections, the strength against buckling and flexural load is assured by overlapped zones (superimposed thickness) in web and flange (Figure 5.1(b&c)). Particularly, the built-up section DC is selected form bending experimental tests conducted by [100]. The parameters varied in the comparative study for the three sections are the same considered in the parametric study conducted on DH section, including the geometrical properties and screws configurations of the sections. The importance of considering different screws configurations for the three sections, was to assess the behavioural changes susceptible to favour a closed cross-section over another, and not primary to select a convenient spacing limit, which will be the focus in the next Chapter. Table 5.1 summarizes the geometrical details of the sections. The nomenclature adopted for the specimens is according to the parameters varied in each beam; egg: DH-0.42-86-S75, stands for, DH section, with 0.42 mm thickness, a web high of 86 mm, and of 75 mm of screws interconnection spacing, specimens with non-mentioned lengths will automatically take a length of 1600 mm. The consideration of these details in conducting a comparative study ensures a reliable and robust understanding of the performances of closed sections.

5.4 Results of the parametric study

5.4.1 Flexural strength and deformed shapes of DH section

Flexural Strength of DH section:

Table 5.2 reports the critical bending moment and the corresponding failure modes for the 15 DH specimens investigated in the parametric study, all the parameters varied through the study, influenced the flexural strength of the specimens.

Table 5.1: Geometrical properties for the three built-up closed sections.

Specimens ID	Geometrical properties				
	Web high (h_w) (mm)	Flange width (b_f) (mm)	Thickness (t) (mm)	radius (r_i) (mm)	Screw spacing (mm)
DH/DC/DU-86-L1600	86	53	0.42 - 1.9	0.75 - 1.25	75 150 130
DH/DC/DU-86-L2150	86	53	0.42 - -	0.75 - -	345 575 1150
DH/DC/DU-136-L1600	136	53	- 1.2 1.9	- 1.00 1.25	150 300 600

The web high played a pivotal role in thick specimens, indeed, specimens with web high of 136 and 1.2 mm thickness recorded higher flexural strength compared to specimens with web high of 86 and thickness of 1.9 mm, as reported in Table 5.2 for specimens DH-1.2-136 and DH-1.2-86, this indicates that the consideration of the web high is more important than the wall thickness in capturing the best performance of DH section. The effect of screws spacing on the flexural strength was more meaningful for specimens with 0.42 mm thickness, thick specimens did not report any increase in the flexural strength in regards to the screws spacing variation. this indicated that most of DH specimens reached the required performance without need on focusing on screws interconnection.

Deformed shapes of DH section:

The governed buckling mode was the local buckling occurred in both flange and compressed portion of the web, this mode was particularly pronounced for specimens with 0.42 mm thickness. Distortional buckling mode was only observed for specimens with large screws interconnection S600, S575 and S1150, this mode effected the cross-section by causing a slip between its individual components, particularly in moment

span distance, Figure 5.3(a&b) shows a comparison between specimens DH-0.42-S600 with no screws in the moment span, and DH-0.42-S75 with screws in the moment span. Additionally, distortional buckling had a similar impact on DH-1.2-136-S600 specimen.

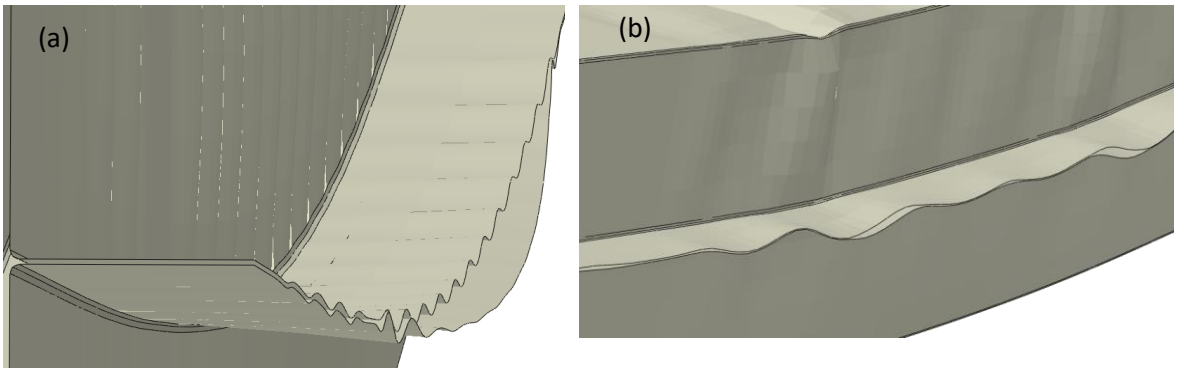

Figure 5.3: Effect of sectional buckling failure on specimens , (a) DH-0.42-S600, (b) DH-0.42-S75.

5.4.2 Comparison between DH and DC built-up sections

Table 5.2 reports the maximum bending strength for DC specimens, as well as a comparison between the flexural strength of DH and DC sections, the comparison of the obtained results will be held based on the thickness of specimens as follows:

DH and DC specimens with 0.42 mm thickness:

At this range of thickness, specimens of the two sections experienced different behaviours towards the flexural strength, in overall, DH specimens recorded the highest flexural strength by reaching a maximum mean bending ratio M_{DH}/M_{DC}=1.64 (64%), particularly for specimen DH-0.42-86-S75 in comparison to DC-0.42-86-S75 specimen. Figure 5.4 shows a comparison of local buckling propagation in both specimens. For specimens with a length of 2150 the flexural strength only increased by 21 %. This discrepancy in results stem from the length of the specimens. Shorter beams (1600 mm) exhibited a significant increase in flexural strength due to their susceptibility to local buckling failure before reaching yield stress. Moreover, the DH section's design, featuring double-edge stiffened flange in addition to the stiffened web (Figure 5.1(a)), enhanced its overall capacity to withstand local buckling compared to

DC built-up section, which consists of individual channels stiffened only at one flange edge (Figure 5.2(b)). In contrast, the increase in specimens with a length of 2150 mm was less significant due to the reduced impact of local buckling. This led to a greater tendency for beams to fail at yield stress or exhibit an interaction between local buckling and yielding stress.

The consideration of screws spacing in the comparison between DH and DC specimens, recorded a maximum increase of 8% for the two sections, as illustrated in Table 5.2.

DH and DC specimens with 1.2 mm thickness:

Similarities in the flexural behaviour of the two sections has been reported for this thickness range, this extends as well for the failure modes observed, where all specimens recorded failing in local buckling. the mean bending ratio for these specimens M_{DH}/M_{DC}=1.01. At this range of thickness local buckling is less pronounced than 0.42 mm specimens, and similar deformed shapes are reported for both sections.

DH and DC specimens with 1.9 mm thickness:

For 1.9 mm thickness specimens, DC section recorded the highest flexural strength, DH specimens with 86 mm and 136 mm web high, experienced a decrease in flexural strength of 19% and 14% respectively compared to DC specimens. At this range of thickness yield stress becomes the dominant failure in DH beams as shown for specimen DH-1.9-86-S300 (Figure 5.5), and Table 5.2 results, this is explained by the overlapped flanges provided by the sectional configuration of DC section resulting in higher flexural strength for DC specimens compared to DH specimens.

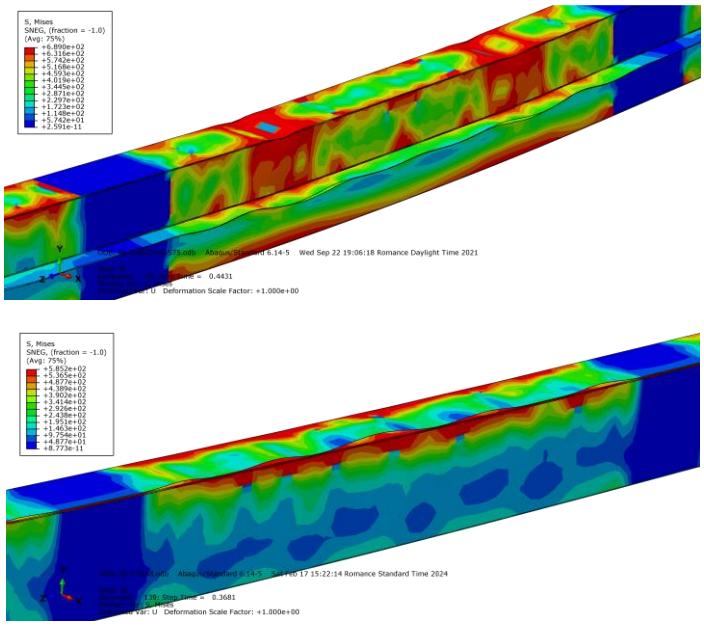

Figure 5.4: Local buckling propagation in specimens DH-0.42-86-S75 & DC-0.42-86-S75.

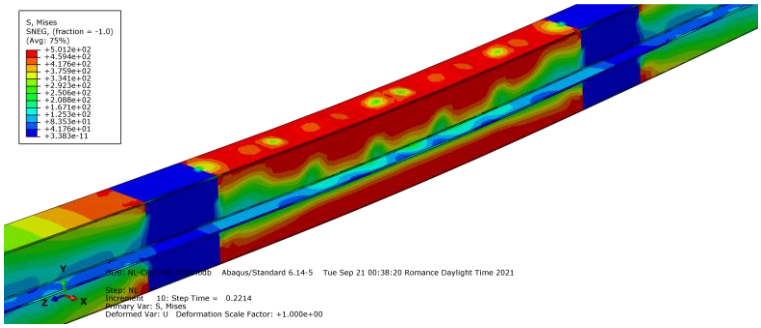

Figure 5.5: Governance of yielding failure over buckling for specimen DH1.9-86-S300.

Table 5.2: Comparison of maximum bending resistance and failure shapes of DH & DC built-up sections.

Specimens	Tests		Specimens	FEA	
	$M_{EXP/FEA}$ (KN.mm)	Failure mode		M_{FEA} (KN.mm)	Failure mode
DH-0.42-86-S75	1278	L+Y	DC-0.42-86-S75	796	L
DH-0.42-86-S150	1265	L+Y	DC-0.42-86-S150	796	L
DH-0.42-86-S300	1222	L+Y	DC-0.42-86-S300	735	L
DH-0.42-86-S345-L2150	1075	L	DC-0.42-86-S345-L2150	902	L+LTB
DH-0.42-86-S575-L2150	1106	L+D	DC-0.42-86-S575-L2150	865	L+LTB
DH-0.42-86-S1150-L2150	996	L+D	DC-0.42-86-S1150-L2150	858	L+LTB
DH-1.2-136-S150	7445	L+Y	DC-1.2-136-S150	7553	L
DH-1.2-136-S300	7495	L+Y	DC-1.2-136-S300	7348	L
DH-1.2-136-S600	7271	L+D+Y	DC-1.2-136-S600	7053	L
DH-1.9-86-S75	6953	Y+L	DC-1.9-86-S75	8509	L
DH-1.9-86-S150	6935	Y+L	DC-1.9-86-S150	8167	L
DH-1.9-86-S300	6927	Y+L	DC-1.9-86-S300	7803	L
DH-1.9-136-S150	12237	Y+L	DC-1.9-136-S150	14,151	L
DH-1.9-136-S300	12454	Y+L	DC-1.9-136-S300	14,060	L
DH-1.9-136-S600	11969	Y+L	DC-1.9-136-S600	12,535	L

5.4.3 Comparison between DH and DU built-up sections

The maximum bending strength of DU specimens are presented in Table 5.3. The comparison between the flexural strength and failure shapes of DH and DU is also reported. The subsequent comparisons of results will be conducted according to the thickness of the specimens (as presented in section 5.4.2):

DH and DU specimens with 0.42 mm thickness:

Within this thickness range, the flexural strength of specimens from the two sections exhibited distinct behavior. On the whole, specimens from DH section demonstrated

the highest flexural strength, as evidenced by the maximum mean bending ratio M_{DH}/M_{DU}=1.40 (40%). DH-0.42-L1600 specimens in particular exhibited this superiority over DU-0.42-L1600 specimen. The flexural strength of specimens measuring 2150 mm in length was only increased by 21%. Therefore, the same discussion could be made as for when comparing DH to DC built-up section, it should be also mentioned that DU section exhibited higher flexural strength than DC.

DH and DU specimens with 1.2 & 1.9 mm thickness:

In this thickness range DU specimens recorded the highest flexural strength, with an increase of 19% and 40% for 1.2 mm and 1.9 mm thickness, when compared to DH specimens, additionally, the effect of screws spacing was meaningful for DU specimens, with an increase of 21% in strength for DU-1.2-136-S150 compared to DU-1.2-136-S600 specimen. These results enumerate the high performance of DU section in sustaining failure caused by yielding and distortional buckling interaction, Figure 5.6 shows the deformed shape for specimen DU-1.9-136-S150. The design concept of DU section provides an overlapped thickness along the web height, which effectively increases the bending capacity of the section compared to other built-up sectional configurations.

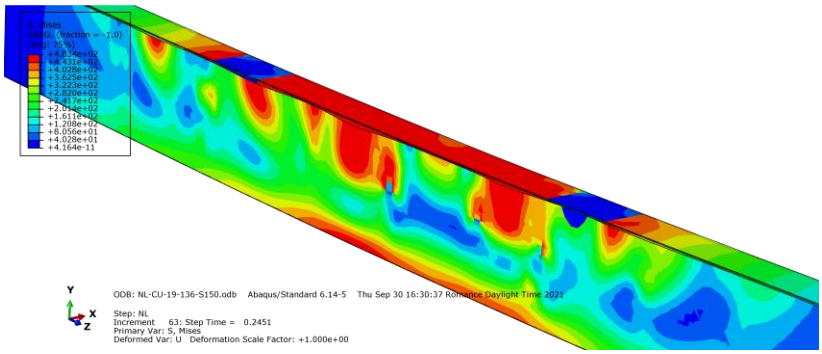

Figure 5.6: Interaction of yielding and distortional buckling for specimens DU-1.9-136-S150.

Table 5.3: Comparison of maximum flexural strength and deformed shapes of DH & DU built-up sections.

Specimen ID	Tests		Specimens	FEA	
	$M_{EXP/FEA}$ (KN.mm)	Failure mode		M_{FEA} (KN.mm)	Failure mode
DH-0.42-86-S75	1278	L	DU-0.42-86-S75	909	L+D
DH-0.42-86-S150	1265	L	DU-0.42-86-S150	890	L+D
DH-0.42-86-S300	1222	L	DU-0.42-86-S300	895	L+D
DH-0.42-86-S345-L2150	1075	L	DU-0.42-86-S345-L2150	903	L+D
DH-0.42-86-S575-L2150	1106	L+D	DU-0.42-86-S575-L2150	858	L+D
DH-0.42-86-S1150-L2150	996	L+D	DU-0.42-86-S1150-L2150	848	L+D
DH-1.2-136-S150	7495	L+Y	DU-1.2-136-S150	9990	L+D+Y
DH-1.2-136-S300	7445	L+Y	DU-1.2-136-S300	8409	D+L+Y
DH-1.2-136-S600	7271	L+D+Y	DU-1.2-136-S600	8235	D+L+Y
DH-1.9-86-S75	6953	Y+L	DU-1.9-86-S75	9693	Y+D
DH-1.9-86-S150	6935	Y+L	DU-1.9-86-S150	9530	Y+D
DH-1.9-86-S300	6927	Y+L	DU-1.9-86-S300	9254	Y+D
DH-1.9-136-S150	12237	Y+L	DU-1.9-136-S150	17895	Y+D
DH-1.9-136-S300	12454	Y+L	DU-1.9-136-S300	16684	Y+D
DH-1.9-136-S600	11969	Y+L	DU-1.9-136-S600	16521	Y+D

*L: Local buckling, D: Distortional buckling, Y: Yielding, LTB: Lateral torsional bucking.

5.5 Conclusion

This chapter presented the flexural behavior of innovative built-up box section named as DH, this section presented a new concept for assembling built-up closed section by intermittently using fasteners location as stiffeners, a numerical analysis on a total of 45 specimens was conducted, the first part of the study included an investigation focused on predicting the flexural failure of DH section as well as the resulted buckling modes of 15 beams, whereas, numerous parameters has been varied. The second part of the study concerns a conduction of a comparison study between three different built-up box sections (DH, DC and DU sections), the investigation involved a comparison between 45 specimens in bending under various parameters variation, the overall study concludes with the following points:

- DH section recorded the highest flexural strength compared to DC and DU sections, in thin built-up beams with 0.42 mm thickness. This suggests that DH section has a greater capacity to withstand local buckling failure compared to the other sections, due to the great stiffening ability provided by this section, consisting of a double-edge stiffened flange as well as a stiffened web. where other closed sections consist only of one-edged stiffened element flange (in DC section case) or web (in DU section case).
- DU section recorded the maximum flexural strength compared to DH and DC sections, in case of thick built-up beams ($t > 1.2$ mm), this was due to its higher ability in managing flexural failure caused by yielding, indeed, this built-up section surpasses other sectional configuration in terms of geometrical properties, particularly for the moment of inertia which is proportionally related to the flexural strength. Hence, the adoption of DU configuration is more suitable for thick CFS built-up sections.
- Average suitability was reported for DC built-up section compared to DH and DU sections, although this section showed higher performances in case of thick specimens ($t=1.9$ mm) compared to DH section, DU built-up section was more effective at this range of thickness, the noticeably thing about DC section is that it failed only with buckling failure and no yielding failure was reported.

Chapter 6
Effect of fasteners on the behavior of cold formed steel built-up sections

6.1 Introduction

Cold-formed steel built-up members typically have thinner steel plates compared to hot-rolled steel sections. As a result, the failure mechanisms of these members often involve a combination of local and distortional buckling, along with overall buckling. Hence, the structural characteristics of cold-formed steel built-up section members may vary from those of conventional hot-rolled steel sections. In addition, the built-up sections are only joined at specific points throughout the length of the member, resulting in a more intricate structural behavior compared to cold-formed single section sections. Doubly symmetric built-up open sections and built-up closed sections can be fabricated by joining two channel sections using different types of fasteners [74-77]. The totality of the conducted studies on built-up sections have mostly focused on compression members. therefore, more studies need to be carried out on built-up sections in bending. It should be noted that the primary focus of our study is not to study the effect of shear or tension load on fasteners, nor is it to carry out a study for selecting the most convenient type of fastener for built-up sections, instead, the goal is to study the impact of fasteners on the behavior of unconventionally shaped built-up sections. The developed sections don't adhere to generic cold-formed shapes such as C, Z, or sigma. These generic sections produce regular-shaped built-up sections such as I or closed box sections, where the impact of fasteners on their behavior has been investigated in previous studies; therefore, the unique behavior of the present sections must be investigated by taking into consideration the effect of fasteners on the flexural strength and buckling modes. To attain this goal, a numerical analysis is

conducted using the finite element model (FEM) developed in Chapter 4. The study encompasses a total of 54 beams investigated under three screw spacing configurations. The innovative built-up sections investigated in this study undergo multiple parameters variations, considered for capturing distinctive behavior of the beams. These parameters consist of varying geometrical properties of the cross-sections, thickness of the wall, and loading types. The results obtained are illustrated in Tables summarizing the values of the maximum bending moment along with the buckling instability observed, moment-displacement curves, and numerical visualization of deformed shapes.

6.2 Details of the built-up sections under investigation

The developed Finite element model used in predicting the strength and performance of diverse built-up sections reported in literature tests as demonstrated in Chapter 4, was used to investigate the behavior of three innovative built-up sections, the design concept for the new sections consist of using non-conventional cold formed steel shapes, in a way such as the overlapped zones are used as stiffeners and screws location intermittently. The nomenclate given to the sections is based on the shape of the individual sections used; egg: DH: refers to assembling two hat (referring to H letter) individual sections (Figure 6.1(a)), DO: consists of assembling two Omega (referring to O letter) individual sections (Figure 6.1(b)), DOS: this section is similar to DO section, with adding a middle stiffener (S refers to stiffener) in the flanges (Figure 6.1(c)), the key differences between the three sectional configurations adopted is the stiffening degree, where DH and DO are partially stiffened sections, while DOS is a fully stiffened section. It should be noted that the term fastener is a general term, that includes different fastening method, the convenient fasteners type for assembling the built-up sections under investigation, can either be screws or bolts, hence, the term fasteners will be replaced by screws, as shown in Figure 6.1. The method used for modelling fasteners was detailed in the development of FE model (Chapter 4).

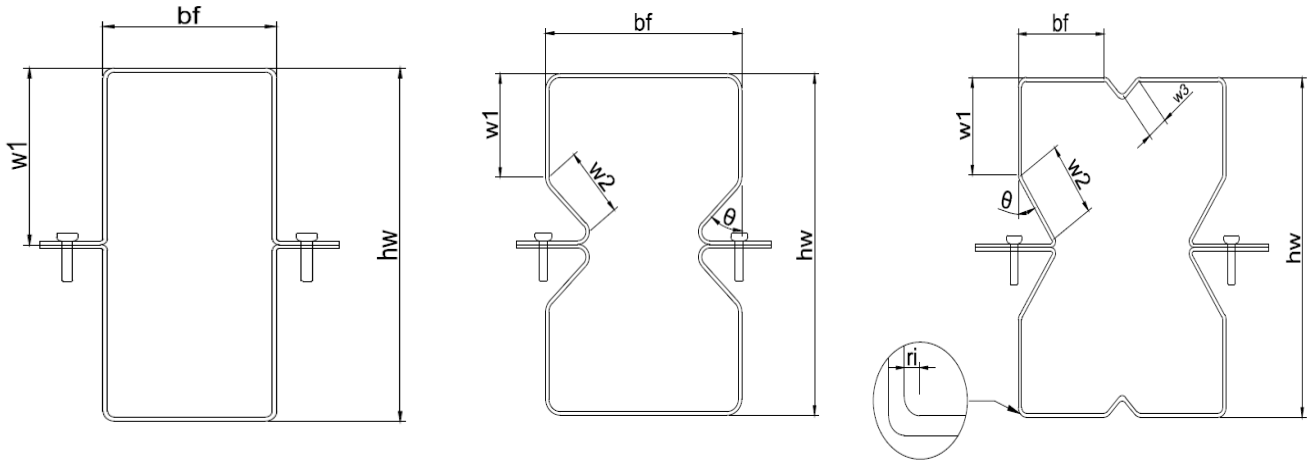

Figure 6.1: Details of Dimensional properties of built-up sections; (a): DH, (b): DO, (c): DOS.

6.3 Details of the parametric study

The main parameter targeted in this investigation is the screws spacing variation, to study its impact on the flexural strength and buckling failure, to achieve this goal, a numerical analysis was conducted on a total of 54 simply supported beams, under various conditions susceptible to influence the flexural behavior and deformed shapes of the beams in presence of fasteners spacing alteration, such as the loading type where 27 specimens undergo three-points bending condition, and 27 specimens were used for four-points bending condition, and the sectional slenderness of the beams achieved by adopting thicknesses of 0.5, 1.0 and 1.6 mm.

An overall of three screws configuration were adopted, the first configuration named as (C1) was in accordance with [100] investigation, which consists of adopting a spacing of 90 mm for the four-points bending specimens along the beam length, and 100 mm for the three-points bending specimens along the beam length, in general, this configuration is based on an approximatively spacing equal to the depth of the web of the built-up section. For the second configuration (C2), the screws were only placed at supports and loading points to avoid separation of the individual sections due to excessive loading concentration. The third configuration consists of investigating the theoretical necessity of screws in designing these built-up sections, hence a

configuration with no screws called (C0) was used. It is important to mention that this study is not meant to precisely determine and attain a minimum threshold spacing distribution of screws, this is because due to the challenging behavior of built-up members in regards of buckling failure instabilities as pointed out in previous studies [77,100], instead, this study focuses on comprehending the true contribution of screws in enhancing the flexural strength, or minimizing elastic buckling failure of these innovative sections. Figure 6.1 along with Tables 6.1-6.3 summarizes the geometrical details of the cross-sections. The symbols used for referring to the specimens consist of attributing the mentioned parameters to the nomenclature; egg: DO-1.0-C1-B4. Where DO the name of the section, 1.0 is the thickness, C1 is the screws configuration, and B4 is the loading type. A constant length of 1400 mm was adopted for all specimens with no alteration in the loading-supports distance.

6.4 Results and discussions

Tables 6.1-6.3 reports the maximum bending capacity at the mid-span of the 54 investigated beams, and the correspondent buckling failure mode when reaching this threshold, in parallel, Figures 6.2&6.3 reports the deformed shapes and the correspondent moment-displacement curves for the four-points and three-points bending specimens respectively. these curves illustrate a comparison between the three screws configurations in case of 1.00 mm thickness specimens.

6.4.1 Influence of sectional configurations on the bending strength and failure shapes

DH built-up cross-section

Figures 6.2 & 6.3 along with Tables 6.1-6.3 results, indicate that screw spacing configurations significantly impact the flexural strength and buckling failure of the three cross sections. Specifically, the partially stiffened section DH, characterized by less geometrical complexity and presence of stiffeners, this section exhibited a notable increase in flexural strength, up to 16%, when using C1 configuration. Analysis of DH specimens failure shapes revealed susceptibility to local, distortional, and lateral

torsional buckling. Consequently, employing this configuration helped mitigate the impact of these buckling failure modes, and systematically enhanced the strength. In more details, this configuration notably prevented lateral torsional buckling observed in DH-1.6-C2-B3 & DH-1.6-C0-B3 specimens, Figure 6.4(a&b) shows a comparison between DH-1.6-C1-B3 & DH-1.6-C0-B3, emphasizing the importance of screws in preventing (LTB) and implying a gain of 16% in the flexural strength. This buckling mode was specifically observed in the three-point bending specimens at this particular thickness, indicating a higher vulnerability to torsional deformation in this loading configuration compared to the four-points bending case, additionally, the C1 configuration contributed into minimizing the intensity of local buckling in specimen DH-1.0-C1-B4 as observed in Figure 6.5(a&b). The shorter fastening distance in C1 configuration also managed to prevent distortional buckling, by maintaining cohesion between individual components, as observed in specimens DH-1.0-C2-B4 and DH-1.0-C0-B3.

DO built-up cross-section

In contrast to DH specimens, the DO specimens experienced failure solely due to local buckling and yielding. Separation between individual components was observed only in C0 configuration specimens, indicating that screws placed only in load concentration areas (C2 configuration) were sufficient to prevent separation of the individual components, however, in terms of flexural strength enhancement, C1 configuration played a major role, resulting in a maximum strength augmentation of 19%.

DOS built-up cross-section

For the fully stiffened configuration presented by DOS section, the screws spacing variations resulted in a diverse impact on the specimens, for the four-points bending specimens, the screws did not contribute in any alteration in the flexural strength, or deformed shapes, in contrast, it has highly impacted the three-points bending

specimens resulting in a maximum strength enhancement of 24%, the governed buckling failure experienced by theses specimens was the distortional buckling mode occurred mainly in the upper flange of the cross-section, with an additional distortion of the web in C2 and C0 specimens.

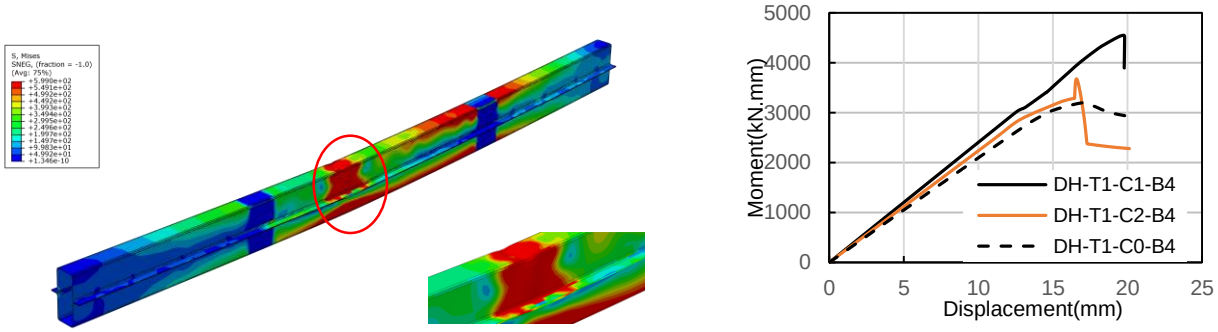

(a): For DH-1.0-B4 beams.

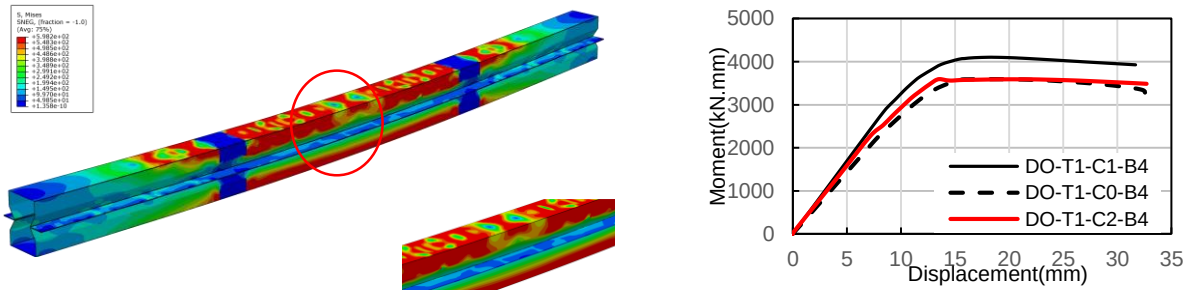

(b): For DO-1.0-B4 beams.

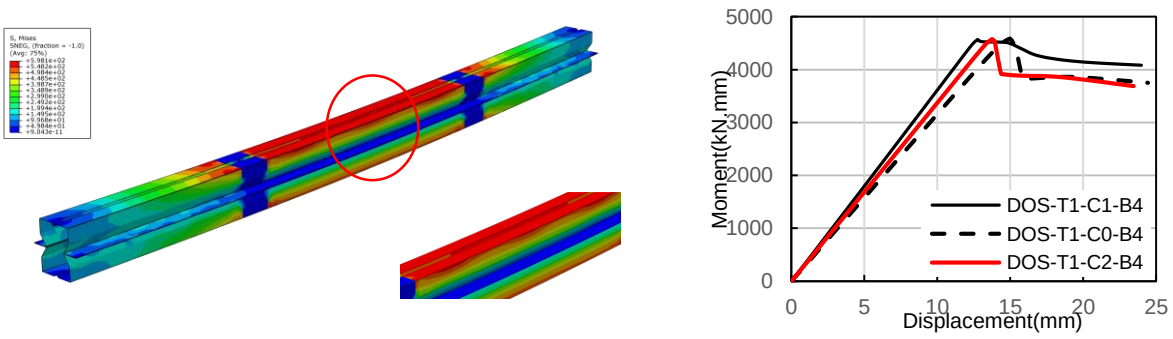

(c): For DOS-1.0-B4 beams.

Figure 6.2: Moment vs Mid-Displacement curve in four-point bending for each configuration with the appropriate deformed shape.

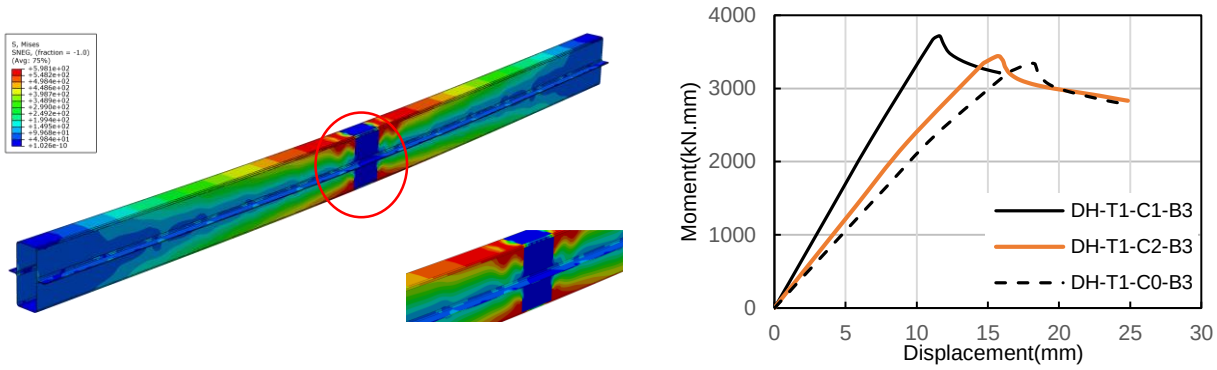

(a): For DH-1.0-B3 beams.

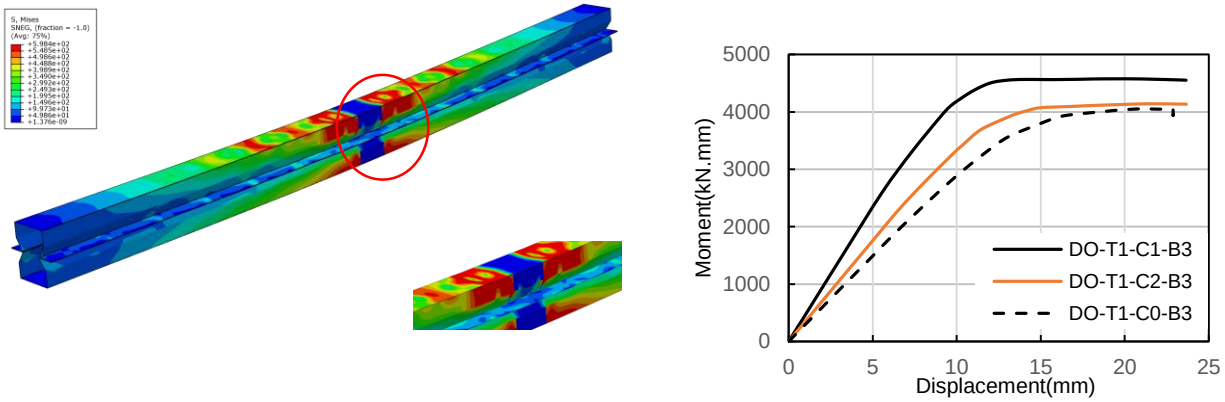

(b): For DO-1.0-B3 beams.

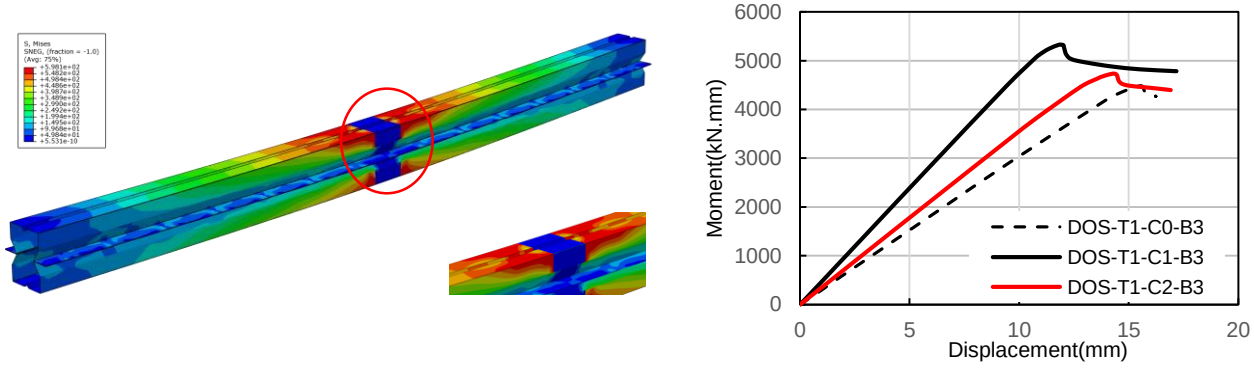

(c): For DOS-1.0-B3 beams.

Figure 6.3: Moment vs Mid-Displacement curve in three-point bending for each configuration with the appropriate deformed shape.

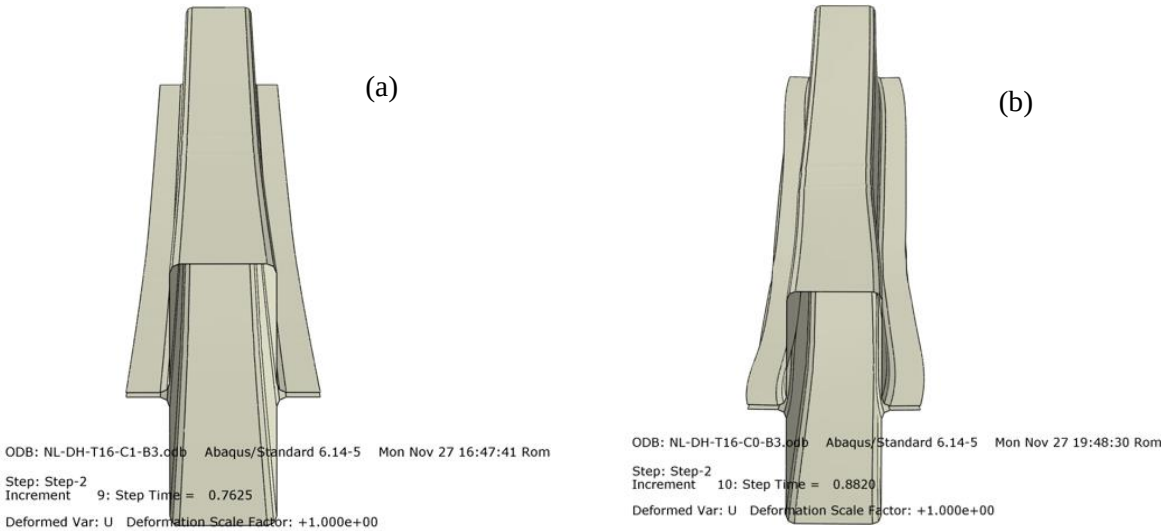

Figure 6.4: Comparison of failure modes between specimens: (a): DH-1.6-C1-B3 & (b): DH-1.6-C0-B3.

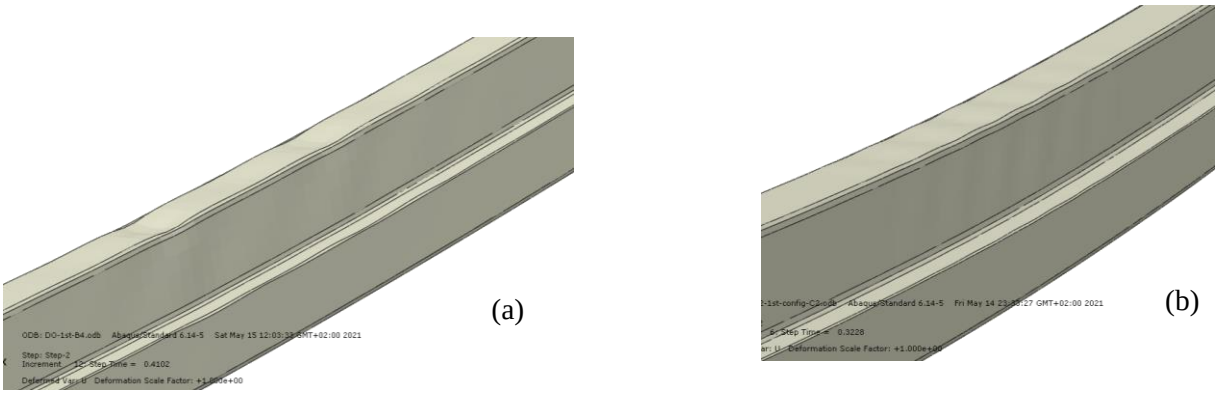

Figure 6.5: Comparison of local buckling intensity between specimens (a): DH-1.0-C1-B4 & (b): DH-1.0-C2-B4.

6.4.2 Influence of loading type on the flexural strength and failure shapes

The choice of loading type significantly influences how beams respond to stress, particularly when considering variations in screw configurations. This investigation reveals notable behavioral differences among the loading types. Figures 6.2&6.3 reports a visual comparison illustrating the differences in the propagation of yielding among specimens with 1.00 mm thickness, observed under four and three-points loading. Respectively, when analyzing the results reported in Tables 6.1-6.3, the alteration of screw spacing increased the strength in three and four-points bending for all sectional configurations, with exception to DOS-B4 specimens which reported no changes in the flexural strength. Figure 6.6 visually emphasizes this observation, depicting strength loss curves corresponding to different screw configurations for both loading types.

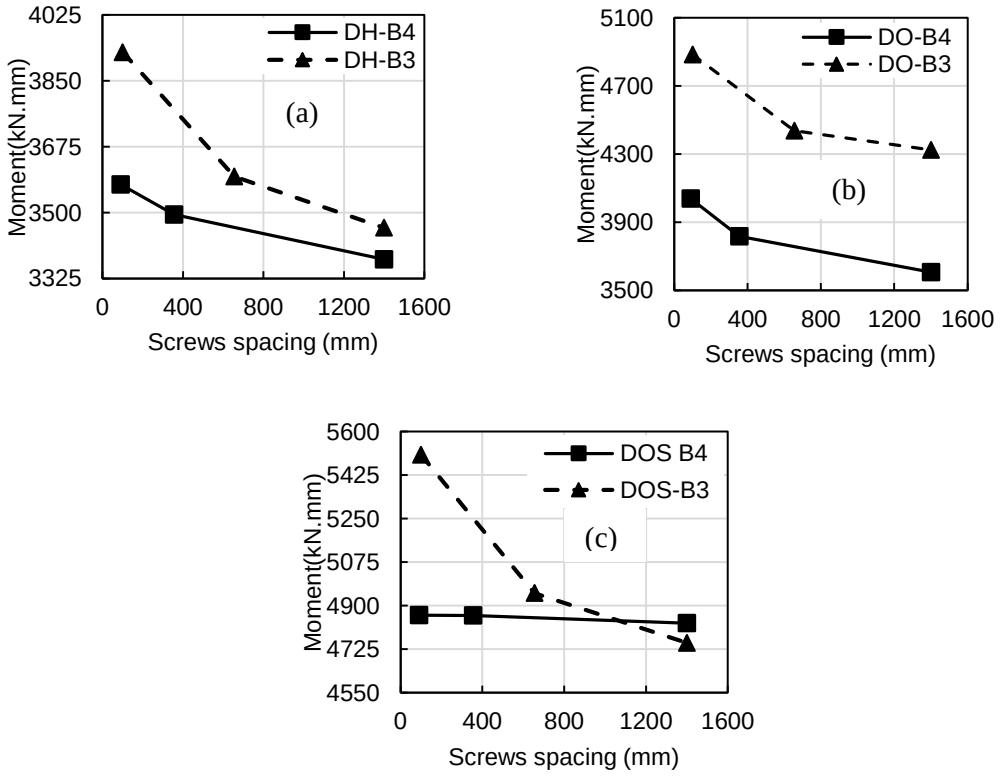

Figure 6.6: Loading types impact on the flexural strength vs screws configurations. (a): DH section, (b): DO section, (C): DOS section.

6.4.3 Influence of thickness on the flexural strength and failure shapes

The decision to vary the cross-sectional slenderness aims to explore different deformed shapes and buckling modes. This allows for analyzing how the three sections respond to variations in screw spacing. Tables 6.1-6.3 highlights the influence of thickness alterations on deformed shapes for both four and three-points loading types respectively. The impact of the C1 configuration on strength enhancement varied across different thicknesses and sectional configurations, directly influencing the observed elastic buckling failures. Specifically, for DH section, the beams behavior was significantly influenced by the thickness value, at a thickness of 1.6 mm, the DH-1.6-C0/C2-B3 specimens distinctly exhibited lateral torsional buckling (LTB), this buckling mode was only observed at this specific thickness. In similar, the impact of thickness on the fully stiffened section DOS reported the occurrence and apparition of distortional buckling at the upper flange for only DOS-1.6-B3 & DOS-0.5-B4 specimens, as depicted in Figure 6.7(a&b).

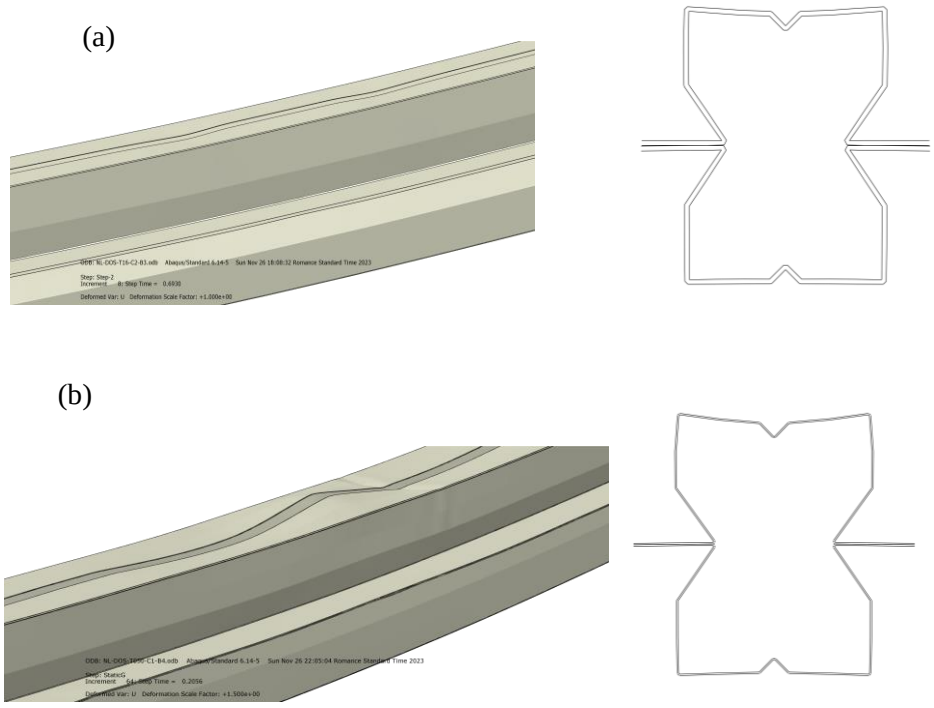

Figure 6.7: Distortional buckling occurrence in the upper flange, for specimens; (a): DOS-1.6-C2-B3, (b): DOS-0.5-C1-B4.

Tables 6.1-6.3 report the mean value of M_{C1}/M_{C0} and the correspondent coefficient of variation (COV) for each sectional configuration, allowing for a statistical assessment of how the three sections respond to variations in cross-sectional slenderness. In average, an increase of 10% in flexural strength (M_{C1}/M_{C0} =1.10) was observed across all specimens. The DO configuration demonstrated the lowest COV (2.92%) among the three cross sections, suggesting minimal variation in the M_{C1}/M_{C0} ratio, and indicating that DO section experienced the least changes in the elastic buckling failure due to thickness variation, whereas it could be interpreted by the governance and uniqueness of local buckling to all specimens of this sectional configuration. In contrary the other sectional configurations (DH and DOS) recorded high COV for M_{C1}/M_{C0} ratio, with values of 8.49% and 9.95%, which is asserted on the distinctive deformed shapes reported in each case. In summary, these results highlight the important role of how sectional slenderness impact the structural behavior of these sections in presence of different screws spacing configurations.

Table 6.1: Dimensional properties, critical buckling moment, and failure mode for DH section.

Specimen ID	Section dimensions					Critical buckling moment		
	h_w (mm)	b_f (mm)	w_1 (mm)	w_2 (mm)	w_3 (mm)	M_{cr} (kN.mm)	M_{C1}/M_{C0}	Failure modes
DH-1.6-C0-B4	91.04	39	45.52	-	-	5833		Y+SP+D
DH-1.6-C1-B4	91.04	39	45.52	-	-	5998	1.03	Y+L
DH-1.6-C2-B4	91.04	39	45.52	-	-	5867		Y+SP
DH-1.0-C0-B4	91.04	39	45.52	-	-	3200		Y+SP+D
DH-1.0-C1-B4	91.04	39	45.52	-	-	3721	1.16	L+Y
DH-1.0-C2-B4	91.04	39	45.52	-	-	3682		L+Y+D
DH-0.5-C0-B4	91.04	39	45.52	-	-	1095		L+Y+D+SP
DH-0.5-C1-B4	91.04	39	45.52	-	-	1006	0.92	L+D
DH-0.5-C2-B4	91.04	39	45.52	-	-	935		L+D+SP
DH-1.6-C0-B3	91.04	39	45.52	-	-	5931		LTB+Y+D
DH-1.6-C1-B3	91.04	39	45.52	-	-	6859	1.16	Y+L

DH-1.6-C2-B3	91.04	39	45.52	-	-	6236		LTB+Y
DH-1.0-C0-B3	91.04	39	45.52	-	-	3343		Y+D+L+SP
DH-1.0-C1-B3	91.04	39	45.52	-	-	3716	1.11	Y+L
DH-1.0-C2-B3	91.04	39	45.52	-	-	3445		Y+L+LTB
DH-0.5-C0-B3	91.04	39	45.52	-	-	1107		L+D+SP
DH-0.5-C1-B3	91.04	39	45.52	-	-	1201	1.08	L+Y+D
DH-0.5-C2-B3	91.04	39	45.52	-	-	1107		L+D+SP
						Mean	1.08	
						(COV) %	8.49	

L: Local buckling, Y: Yielding, D: Distortional buckling, LTB: Lateral torsional buckling, SP: Section separation.

Table 6.2: Dimensional properties, critical buckling moment, and failure mode for DO section.

Specimen ID	Section dimensions						Critical buckling moment		
	h_w (mm)	b_f (mm)	w_1 (mm)	w_2 (mm)	w_3 (mm)	θ(°)	M_{cr} (kN.mm)	M_{C1}/M_{C0}	Failure modes
DO-1.6-C0-B4	88.85	56.3	26.84	17.7	-	45	5994		Y+L+SP
DO-1.6-C1-B4	88.85	56.3	26.84	17.7	-	45	6663	1.11	Y+L
DO-1.6-C2-B4	88.85	56.3	26.84	17.7	-	45	6554		Y+L
DO-1.0-C0-B4	88.85	56.3	26.84	17.7	-	45	3597		L+Y
DO-1.0-C1-B4	88.85	56.3	26.84	17.7	-	45	4102	1.14	L+Y
DO-1.0-C2-B4	88.85	56.3	26.84	17.7	-	45	3598		L+Y
DO-0.5-C0-B4	88.85	56.3	26.84	17.7	-	45	1238		L+Y+SP
DO-0.5-C1-B4	88.85	56.3	26.84	17.7	-	45	1348	1.09	L+Y
DO-0.5-C2-B4	88.85	56.3	26.84	17.7	-	45	1295		L+Y
DO-1.6-C0-B3	88.85	56.3	26.84	17.7	-	45	7299		L+Y+SP
DO-1.6-C1-B3	88.85	56.3	26.84	17.7	-	45	8146	1.12	L+Y
DO-1.6-C2-B3	88.85	56.3	26.84	17.7	-	45	7522		L+Y
DO-1.0-C0-B3	88.85	56.3	26.84	17.7	-	45	4051		L+SP+Y
DO-1.0-C1-B3	88.85	56.3	26.84	17.7	-	45	4578	1.13	L+Y
DO-1.0-C2-B3	88.85	56.3	26.84	17.7	-	45	4140		L+Y

DO-0.5-C0-B3	88.85	56.3	26.84	17.7	-	45	1623		L+Y+SP
DO-0.5-C1-B3	88.85	56.3	26.84	17.7	-	45	1928	1.19	L
DO-0.5-C2-B3	88.85	56.3	26.84	17.7	-	45	1649		L+Y
							Mean	1.13	
							(COV) %	2.92	

L: Local buckling, Y: Yielding, LTB: Lateral torsional buckling, SP: Section separation.

Table 6.3: Dimensional properties, critical buckling moment, and failure mode for DOS section.

Section details	Section dimensions						Critical buckling moment		
	h_w (mm)	b_f (mm)	w_1 (mm)	w_2 (mm)	w_3 (mm)	θ(°)	M_{cr} (kN.mm)	M_{C1}/M_{C0}	Failure mode
DOS-1.6-C0-B4	86.90	28.20	25.65	20.24	6.41	34	7858		Y
DOS-1.6-C1-B4	86.90	28.20	25.65	20.24	6.41	34	8018	1.02	Y+D
DOS-1.6-C2-B4	86.90	28.20	25.65	20.24	6.41	34	7918		Y
DOS-1.0-C0-B4	86.90	28.20	25.65	20.24	6.41	34	4587		Y
DOS-1.0-C1-B4	86.90	28.20	25.65	20.24	6.41	34	4569	1.00	Y
DOS-1.0-C2-B4	86.90	28.20	25.65	20.24	6.41	34	4575		Y
DOS-0.5-C0-B4	86.90	28.20	25.65	20.24	6.41	34	2041		D
DOS-0.5-C1-B4	86.90	28.20	25.65	20.24	6.41	34	2000	0.98	D+L
DOS-0.5-C2-B4	86.90	28.20	25.65	20.24	6.41	34	2090		D
DOS-1.6-C0-B3	86.90	28.20	25.65	20.24	6.41	34	8127		Y+D+L+SP
DOS-1.6-C1-B3	86.90	28.20	25.65	20.24	6.41	34	9158	1.13	Y+D+L
DOS-1.6-C2-B3	86.90	28.20	25.65	20.24	6.41	34	8420		Y+D+L
DOS-1.0-C0-B3	86.90	28.20	25.65	20.24	6.41	34	4482		SP+L+Y
DOS-1.0-C1-B3	86.90	28.20	25.65	20.24	6.41	34	5322	1.19	Y
DOS-1.0-C2-B3	86.90	28.20	25.65	20.24	6.41	34	4728		L+Y
DOS-0.5-C0-B3	86.90	28.20	25.65	20.24	6.41	34	1641		L+D
DOS-0.5-C1-B3	86.90	28.20	25.65	20.24	6.41	34	2040	1.24	L
DOS-0.5-C2-B3	86.90	28.20	25.65	20.24	6.41	34	1701		L
							Mean	1.09	
							COV(%)	9.95	

6.5 Conclusion

This chapter aimed to investigate the effect of screw spacing on the moment capacity and failure shapes of innovative partially (DH and DO) and fully stiffened (DOS) sections. The investigation encompassed a parametric study involving 54 beams. The idea behind developing these unconventional built-up sections, resides in their design of considering web stiffeners as screws location intermittently. The primary focus was to analyze how altering screw spacing, with considering loading types (three and four-point loadings), and varying sectional slenderness (thicknesses of 0.5, 1.00, and 1.6 mm) impact the flexural strength and elastic buckling modes of these three sections.

This study underscores the nuanced relationship between sectional shapes, screw configurations, and resultant failure behaviors, revealing that the alteration of screws spacing yielded substantial influence, across the three cross sections, in the partially stiffened DH section, adopting the C1 configuration yielded a maximum strength augmentation of 16 % and as a result, mitigated various buckling modes, in contrast, the DO section predominantly experienced failures related to local buckling and yielding, with a maximum strength augmentation of 19 % using the C1 configuration, which particularly contributed in enhancing the performance of these specimens toward this particular mode.

In the fully stiffened DOS section, screw spacing showed diverse impacts, notably influencing the flexural strength in distinct loading types. Specifically, this section exhibited significant strength enhancements, notably reaching a maximum strength augmentation of 25% in three-points loading. However, alterations in screw spacing did not affect the flexural strength in four-points bending within this section.

This investigation also highlights how loading types significantly affect beam stress responses, especially when combined with screw configuration variations. The results consistently show that alteration in screw spacing, enhances the strength in both loading types across the sectional configurations, except for DOS-B4 specimens which are not affected by screws spacing variations.

Variation in sectional slenderness, played a major role in determining the true contribution of screws in enhancing the strength, by allowing the analysis of multiple elastic buckling modes, and hence providing a robust decision making regarding the importance and suitability of the convenient screws configuration.

Chapter 7
Development of generalized direct strength method for CFS built-up sections failing in local buckling

7.1 Introduction

This chapter details the development of a novel design method for predicting the flexural strength of cold-formed steel (CFS) built-up members. It explains the motivations and hypotheses, details the development process, and validates the applicability of the new method baptized 'Generalized Direct Strength Method' (DSM-G). This method serves as an expansion of the original Direct Strength Method (DSM) used for predicting the strength of CFS members, by broadening its applicability to various CFS built-up sections, this was done by addressing the limitations inherent in its current equations.

The method's core development is divided into two sections. The first section involves a numerical investigation through a parametric study conducted on two innovative built-up sections referred to as DM and DOW, and characterized with their unconventional CFS shapes. The subsequent section focuses on the analytical aspect of the method development, comprising two parts. The first part applies the Direct Strength Method (DSM) to these built-up sections to comprehensively evaluate the ability of the method in determining the flexural strength of these new sections. This evaluation involves comparing both numerical (M_{FEA}) and analytical (M_{DSM}) bending moments. Towards the end of this section, a comprehensive relationship is established between the numerical and analytical predictions by examining the comparison analysis of the two bending moments. This comparison process led to the development of predictive mathematical model for the (DSM-G) method. This model undergoes meticulous statistical analysis to affirm its suitability in presenting FE analysis results.

Subsequently, the validated method undergoes assessment against six distinct built-up cross-sectional profiles issued from literature [74,75], comparing both the new predicted (M_{DSM-G}) and (test/numerical) ($M_{EXP/FEA}$) bending moments.

7.2 Numerical part of DSM-G development

The numerical part of the method development includes two general sections, the first discusses the effect of screws interconnection on bending strength and failure shapes, considering that fasteners contributes an important part in predicting the behavioral response of CFS built-up sections, implying meticulously comprehending their impact, and how the present design provisions (DSM) accounts for their contribution, Particularly, in considering the double thickness assumption when designing built-up members, this section is discussed under the title ‘First parametric study’, and comprise a total of 56 specimens in four and three points bending.

The second section of the investigation, treats the FE data acquisition for the development side of DSM-G method, and presented under ‘Second parametric study’, all the parameters varied in this section, mainly including the geometrical properties and the sectional slenderness of the built-up sections, were meant to assess the DSM ability in predicting the flexural capacity of DM and DOW sections, by conducting a comparison between the critical flexural moment of both design and (FEA), this section comprises a total of 52 specimens in four-points bending.

7.2.1 Details of the numerical study

Figure 7.1 & Table 7.1 provides the geometrical properties of DM and DOW built-up members used in this investigation, offering a global overview of the sectional properties under investigation, four and three-points bending analysis has been conducted on those sections, resulting in a total of 108 beams investigated. The names given to these new cross-sections were based on their unique forms. More precisely, the abbreviation "DM" stands for Double 'M' sections, as shown in Figure 7.1(a). On the other hand, "DOW" is used to indicate Double sections that form a closed 'O' shape, with stiffeners formed like the letter 'W', as depicted in Figure 7.1(b). The

material properties used for all specimens were obtained from the mechanical properties described in reference [74], specifically according to COF-1.0/COW-1.0 sections as shown in Table 4.2 (section 4.3 of Chapter 4). The specimens were labeled according to the section name, the thickness, and the length of the beam. In the case of studying the influence of screw spacing on flexural strength, the screw spacing was added to the label. For example, a specimen labeled as 15-DM-S600-1.0-L1400 would have a section label of 15-DM, a thickness of 1.0, a screw spacing of S600 in the bending moment span, and a length of 1400 mm. It is important to note that the parametric study's FE model does not include any imperfections.

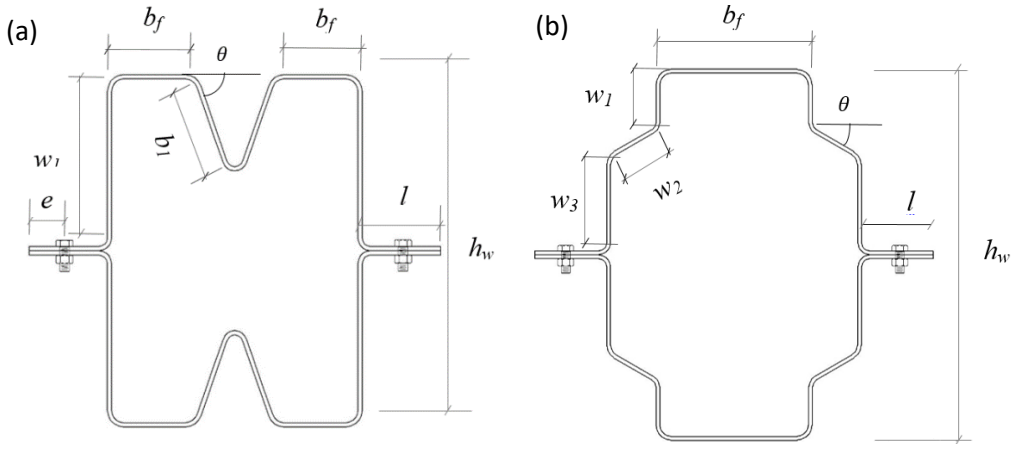

Figure 7.1: Cross-sectional properties of: a) DM et b) DOW sections [106].

Table 7.1: Dimensional properties of DM and DOW sections [106].

Specimens	h_w	b_f	b_1	w_1	w_2	w_3	l	θ(°)	e
DM	82.00	40.72	23.25	39.42	-	-	19.51	70	8.50
15-DM	83.00	37.20	14.22	39.92	-	-	19.51	30	8.50
17-DM	122.00	42.28	23.29	59.41	-	-	19.50	70	8.50
DOW	98.29	41.52	-	15.25	14.68	24.86	19.50	30	8.50
15-DOW	84.95	41.00	-	15.43	11.24	24.72	19.5	0	8.50
17-DOW	126.04	41.00	-	15.72	25.94	23.16	19.5	60	8.50

7.2.2 First parametric study (Screws arrangements)

In general, investigations have generally focused on investigating the impact of fasteners interconnection on resistance and deformation of built-up sections, regardless of the beam analytical design. It is important to acknowledge that the design standards for built-up elements are based on certain assumptions about the areas where screws are put. Hence, it is crucial to take into account the influence of fasteners interconnection when deciding on the appropriate method, whether it is using the double thickness approach in overlapped areas or calculating the combined resistance of two separate sections in a built-up member. In addition, a recent work conducted by [102] presented a technique to incorporate the stiffness of discrete fasteners into the overall stiffness matrix of the beam in Finite Strip Analysis, allowing for direct modeling. To get a more thorough and precise evaluation of the performance of built-up members, it is important to account for the spacing of screws in the decision-making process.

For the present specifications described in AISI-S100 provisions [2] the screws interconnection limits were given only for open built-up flexural members with an allowable longitudinal spacing of (L/6) along the length, while for built-up closed sections assiduous attempts for fasteners interconnection arrangement were conducted, the maximum spacing was fixed at four times the web high, by only varying the spacing in the moment bending span (constant spacing in outer parts). Tables 7.2&7.3 summaries the interconnection details of DM and DOW sections, listing a total of 56 specimens, investigated under the effect of screws spacing variation in four and three-points flexural moment, taking into account the following aspects, (i) in specimen preceded by S, the interconnection was changed only in the moment-span, (ii) in other specimens, the spacing was changed along the beam's length, and spacing of L/2, L/4, L/8 and L/20 were adopted. This was to englobe the screws interconnection impact on the resistance and deformation of the beams, (iii) a

variability of lengths has been investigated, from short to long beams, and the following lengths has been adopted, 900, 1400, 2500, and 3500 mm.

7.2.2.1 Effect of screws spacing on the bending strength

Tables 7.2&7.3 summarize respectively, the FEA results of the influence of screws interconnection on the maximum flexural strength, and the elastic buckling deformations of the beams, for DM and DOW sections respectively, the results show that the two sections recorded similar behavior towards screws spacing impact, in overall, the screws spacing didn't influence the flexural capacity or the deformed shapes, except to thin-walled beams having S1000 in screws interconnection, in these cases the overlapped zone experienced separation of the individual parts, Figure 7.2(a&b), showcases of specimens 17-DM-S1000-L2500-0.38-B4 and 17-DOW-S1000-L2500-0.48-B4 experiencing this separation, additionally, ultra-thin sections had more meaningful increase of the strength when it comes to screws arrangements, due to their sensitive nature toward buckling failures. For all specimens local buckling was the dominant failure mode, while for specimens under 1.0 mm thickness, interactive sectional buckling is reported. Specimens subjected to three-points bending recorded similar behavior to four-points bending specimens toward screws spacing influence. In general, these results indicate a minor effect of fasteners on the strength, however, a minimum number of screws is required particularly in the bending span, to avoid separation between the individual sections.

The local buckling half wavelength acquired from the CUFSM Software [101], as reported in Figure 7.3(a&b) is not accounted for, since the interconnection between screw cannot contribute in preventing local buckling, this can be attributed to the minimal impact of screws interconnection on the bending capacity. Subsequently, this results favors the adequacy of the double thickness assumption, in addition to considering its simplicity in designing built-up sections. Furthermore, this study cannot make use of the single section model assumption because the individual sections are asymmetric about their bending axis, as depicted in Figure 7.1.a&b. This

lack of symmetry makes it inappropriate to consider the capacity of the built-up section as the combination of the individual sections strength.

The results and discussions strongly support the utilization of double thickness assumptions over the other discussed approaches to design fasteners within DM and DOW cross-sections. Therefore, this assumption will be considered further in the design part.

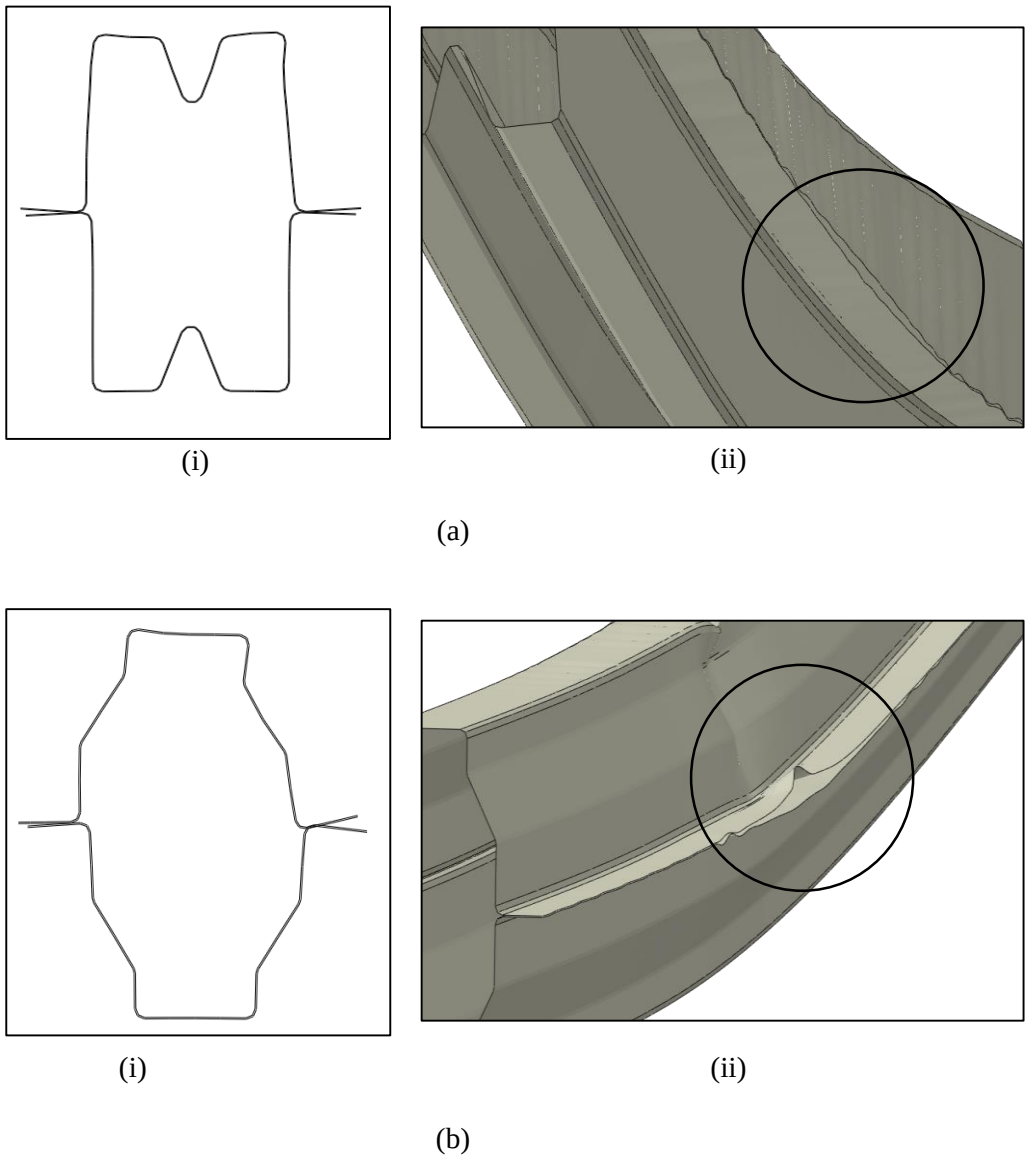

Figure 7.2: Collapse deformation for (a) 17-DM-S1000-L2500-0.38-B4, (b) 17-DOW-S1000-L2500-0.48-B4 specimens. (i): cross section, (ii): longitudinal profile.

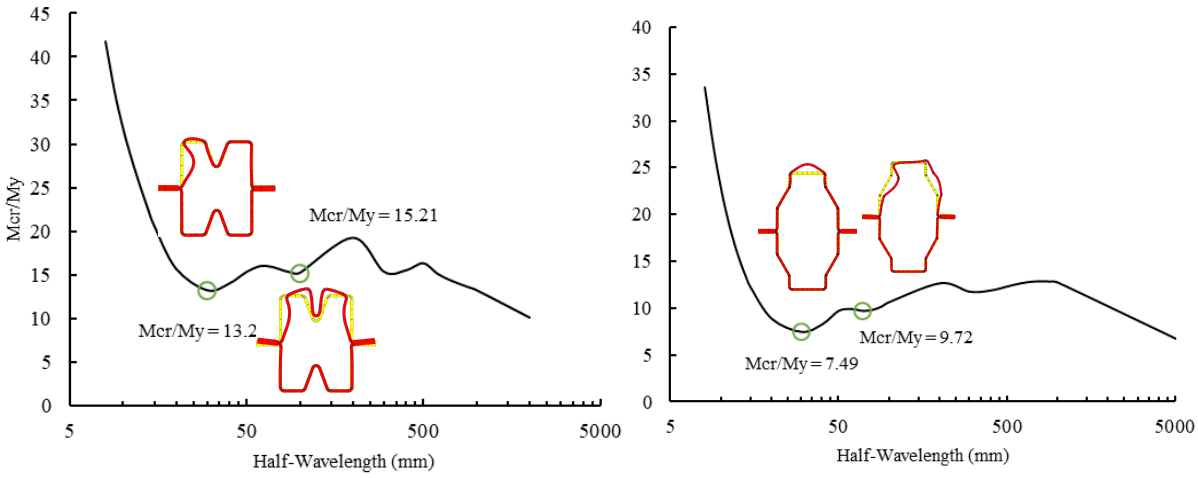

a) DM-2.4. b) 17-DOW-2.4.

Figure 7.3: Signature Curve using FSA CUFSM software for:

a) DM-2.4, b) 17-DOW-2.4 sections [106].

Table 7.2: Effect of fasteners interconnection on the bending strength and failure shapes of DM sections.

Specimens	M_{FEA} (kN.mm)	Failure mode	Specimens	M_{FEA} (kN.mm)	Failure mode
17-DM-S125-L2500-1-B4	7989	L+Y	15-DM-L/2-L1400-0.30-B4	873	L+D+Y
17-DM- S338-L2500-1-B4	7927	L+Y	15-DM-S90-L1400-1-B4	4282	Y
17-DM-S1000-L2500-1-B4	7924	L+Y	15-DM-S300-L1400-1-B4	4235	Y
17-DM-L/20-L2500-1-B4	8028	L+Y	15-DM-S600-L1400-1-B4	4224	Y
17-DM-L/2-L2500-1-B4	7966	L+Y	15-DM-L/20-L1400-1-B4	4267	Y
17-DM-S125-L2500-0.38-B4	2145	L+D+Y	15-DM-L/8-L1400-1-B4	4267	Y
17-DM-S338-L2500-0.38-B4	2069	L+D+Y	15-DM-L/2-L1400-1-B4	4245	Y
17-DM-S1000-L2500-0.38-B4	1282	L+D+SP+Y	DM-S90-L1400-0.48-B4	1897	L
17-DM-L/20-L2500-0.38-B4	2200	L+D+Y	DM-S300-L1400-0.48-B4	1832	L+D
17-DM-L/8-L2500-0.38-B4	2111	L+Y	DM-S600-L1400-0.48-B4	1769	L+D
17-DM-L/2-L2500-0.38-B4	1942	L+Y	DM-L/20-L1400-0.48-B4	1948	L+Y
15-DM-S90-L1400-0.3-B4	1203	L+D+Y	DM-L/8-L1400-0.48-B4	1937	L+Y
15-DM-S300-L1400-0.3-B4	977	L+D+Y	DM-L/2-L1400-0.48-B4	1813	L+Y
15-DM-S600-L1400-0.3-B4	920	D+L+Y	17-DM-S100-L3500-1-B3	8620	Y+L
15-DM-L/20-L1400-0.30-B4	1071	L+D+Y	17-DM-S425-L3500-1-B3	8638	L+Y
15-DM-L/8-L1400-0.30-B4	1006	D+L+Y	17-DM-S1137-L3500-1-B3	8651	L+Y

Note : L : Local Buckling ; D : Distortional Buckling; Y: Yielding; SP: Individual sections separation

Table 7.3: Effect of fasteners interconnection on the bending strength and failure shapes of DOW sections.

Specimens	M_{FEA} (kN.mm)	Failure mode	Specimens	M_{FEA} (kN.mm)	Failure mode
17-DOW-S1000-L2500-1-B4	5262	D+Y	15-DOW-S1000-L2500-1-B4	3818	D+Y
17-DOW-S134-L2500-0.48-B4	3137	L+D+Y	15-DOW-S90-L1400-1-B4	4053	Y
17-DOW-S333-L2500-0.48-B4	2469	L+D+Y	15-DOW-S600-L1400-1-B4	3978	Y
17-DOW-S1000-L2500-0.48-B4	2855	L+D+SP+Y	17-DOW-S90-L2500-1-B3	6411	L+Y
17-DOW-L/20-L2500-0.48-B4	2960	D+L+Y	DOW-S90-L1400-0.30-B4	1076	L+D+Y
17-DOW-L/8-L2500-0.48-B4	2886	L+D+Y	DOW-S600-L1400-0.30-B4	1065	L+D+Y
17-DOW-L/2-L2500-0.48-B4	2509	L+D+Y	DOW-L/2-L1400-0.30-B4	1068	L+Y
15-DOW-S82.5-L900-1-B4	4064	Y	17-DOW-S430-L2500-1-B3	6205	L+Y
15-DOW-S400-L900-1-B4	4076	Y	17-DOW-S1100-L2500-1-B3	6113	L+Y
15-DOW-S82.5-L900-0.3-B4	1305	L+Y	17-DOW-S90-L2500-0.48-B3	2658	L+Y
15-DOW-S400-L900-0.3-B4	1021	L+Y	17-DOW-S430-L2500-0.48-B3	2474	L+Y
15-DOW-S125-L2500-1-B4	3984	Y+D	17-DOW-S1100-L2500-0.48-B3	2406	L+Y

Note : L : Local Buckling ; D : Distortional Buckling; Y: Yielding; SP: Individual sections separation.

7.2.3 Second parametric study

The validated FE model was used in a parametric study to investigate the behavior of 52 beams in four-point bending (27 for DM and 25 for DOW sections), Figure 7.1(a&b) show the cross-section geometry of DM and DOW sections respectively, the new design concept used for these sections, consists of using overlapped areas, situated at the web, as both stiffeners and assembling points simultaneously, to obtain a fully-stiffened composed sections. To understand the structural behavior of these sections, two lengths were investigated, 1400 mm, and 2500 mm, the variation in length was intended to affect the behavior of the beams by increasing the moment bending span distance. In addition, varying the length can potentially affect the sections toward local buckling failure occurrence.

The analysis centered on analyzing the bending strength and deformed shapes of six sectional configurations, comprising three configurations for DM and three for DOW. The thickness of each section varied between 0.30 and 2.4 mm. The minimum thickness used in this study met the guidelines and limits specified in Table B4.1-1 of the AISI specification [2]. According to the specification, the maximum ratio of flat-width to thickness (w/t) should be less than 500 for cases where stiffened flanges are

joined to stiffened webs through edge stiffeners. Furthermore, it was confirmed that the ratio of height to thickness (h/t) should be less than 300 in order to avoid excessive deformation when subjected to the specific design loads. Tables 7.4 and 7.5 display the maximum bending capacity results and the corresponding failure shapes.

7.3 Analytical part of DSM-G development

7.3.1 Direct strength method in present design provisions

Researchers initially utilized the Effective Width Method (EWM), which was originally created for designing individual CFS members, to establish design rules for built-up CFS sections. However, the intricate nature of shapes, particularly for stiffened sections, along with the time-consuming process of applying the EWM, prompted the consideration of the Direct Strength Method (DSM). This method serves as an alternative in various studies and aims to directly calculate the expected strength of the sections. It suggests potential failure due to elastic buckling under flexural loading, specifically identifying nominal buckling moments for local (M_{crl}), distortion (M_{crd}), and global buckling (M_{cre}). The advantage of DSM is that it eliminates the need to individually analyze each element of the section, as required in EWM. The equations presented in DSM are formulated using empirical data, Generalized Beam Theory, and signature curves obtained from buckling analysis conducted with the Finite Strip software CUFSM. The minimum points on these curves represent the essential buckling load that leads to local, distortional, or global buckling. In this study, the built-up sections were considered to be fully braced in order to prevent lateral torsional buckling. As a result, the nominal flexural strength M_{ne} for lateral-torsional buckling is equal to M_y. The focus of the study was on examining the behavior of the beams in relation to potential failure in local or distortional buckling. The predicted DSM flexural buckling strengths align with section F3.2 & F4.1 of the North American Specifications (NAS) [2], and can be summarized as follows:

$$M_{nl} = \begin{cases} M_y + \left(1 - 1/C_{yl}^2\right)\left(M_p - M_y\right) & for\ \lambda_l \le 0.776 \\ \left[1 - 0.15\left(\frac{M_{crl}}{M_y}\right)^{0.4}\right]\left(\frac{M_{crl}}{M_y}\right)^{0.4} M_y & for\ \lambda_l > 0.776 \end{cases} \quad \text{Eq 6.1}$$

$$M_{nd} = \begin{cases} M_y + \left(1 - 1/C_{yl}^2\right)\left(M_p - M_y\right) & for\ \lambda_l \le 0.673 \\ \left[1 - 0.22\left(\frac{M_{crl}}{M_y}\right)^{0.5}\right]\left(\frac{M_{crl}}{M_y}\right)^{0.5} M_y & for\ \lambda_l > 0.673 \end{cases} \quad \text{Eq 6.2}$$

Where $\lambda_l = \sqrt{M_y/M_{crl}}$; $C_{yl} = \sqrt{0.776/\lambda_l} \le 3$; $M_y = S_d S_f$; $M_p = Z_f f_y$

S_f = gross section modulus referenced to the extreme fiber at first yield; Z_f= plastic section modulus ; f_y= yield stress, which is the 0.2% proof stress ($\sigma_{0.2}$) obtained from tensile coupon tests in this study; M_{crl}= critical elastic buckling moment obtained from CUFSM signature curve, $\lambda_d = \sqrt{M_y/M_{crd}}$; $C_{yd} = \sqrt{0.673/\lambda_d} \le 3$; and

M_{crd}= critical elastic distortional buckling moment obtained from CUFSM signature curve.

M_{DSM} is regarded as the minimum of nominal flexural strength for local M_{nl} and distortional buckling M_{nd} :

$$M_{DSM} = min(M_{nl}; M_{nd}) \quad \text{Eq 6.3}$$

Reliability Analysis

To gauge the adequacy of a design criterion, reliability analysis can be undertaken. When the computed reliability index (β) surpasses the specified target reliability index β_0, the design rule is deemed probabilistically secure. In Load and Resistance Factor

Design (LRFD), it is recommended to have a goal reliability index of 2.5 for structural elements. This is stated in Section (K.2.1.1) [2]. In line with Section A1.2 (c), a resistance factor (ϕ_b) of 0.8 was used in the study. The load combinations utilized were (1.2 times the dead load plus 1.6 times the live load) as specified in reference [104], and (1.25 times the dead load plus 1.5 times the live load) as described in reference [105]. Here, DL represents the dead load and LL represents the live weight. A ratio of 1/5 between the dead load and live load was applied, as stated in section (K.2.1.1). The statistical parameters used to measure the bending strength of beams were obtained from Table (K.2.1.1-1) [2]. The mean values for the material factor and fabrication factor (M_m = 1.10, F_m = 1.00), as well as the coefficients of variation (VM = 0.10, V_F = 0.05), were included. Additionally, the statistical parameters P_m and V_P were added. A correction factor (C_P) was incorporated into the reliability evaluation to account for the impact of a limited dataset, as stated in equation K2.1.1-4 from the same source. The calculation of the reliability index (β_1) used a load combination of 1.2 times the dead load (DL) plus 1.6 times the live load (LL), whereas the reliability index (β_2) utilized a load combination of 1.25 times the dead load (DL) plus 1.5 times the live load (LL).

7.3.1.1 Predicted flexural strength using DSM equations

The performance of the DSM design Eq 6.1 & 6.2 in predicting the bending capacity of DM and DOW sections is illustrated in These findings suggest that the existing DSM equations underestimate the bending strength of the built-up sections, resulting in an excessively cautious estimation of the flexural strength. The underestimation of results may be attributed to the non-traditional shapes of the proposed sections, which differ from conventional built-up sections that are connected using channel or sigma sections. Instead, the proposed sections are based on alternative forms such as the double M section (DM). Furthermore, the assumption of double thickness may also pose a limitation in accurately predicting the strength and deformation of the sections.

However, the analysis of screw spacing revealed that it has a minimal impact on the strength.

Tables 7.4&7.5 report the comparison of the maximum flexural strength M_{FEA} to the nominal flexural strength capacity M_{DSM}. The mean value of the bending strength ratio M_{FEA}/M_{DSM} is 1.34 and 1.51, and a coefficient of variation (COV) of 18 % and 24 % for DM and DOW beams respectively. These findings suggest that the existing DSM equations underestimate the bending strength of the built-up sections, resulting in an excessively cautious estimation of the flexural strength. The underestimation of results may be attributed to the non-traditional shapes of the proposed sections, which differ from conventional built-up sections that are connected using channel or sigma sections. Instead, the proposed sections are based on alternative forms such as the double M section (DM). Furthermore, the assumption of double thickness may also pose a limitation in accurately predicting the strength and deformation of the sections. However, the analysis of screw spacing revealed that it has a minimal impact on the strength.

Table 7.4: Comparison between maximum bending strength obtained from FE analysis and DSM equations, for DM sections.

S.No	Specimen	M_{FEA} (kN.mm)	λ_l	λ_d	M_{nl} (kN.mm)	M_{nd} (kN.mm)	M_{FEA}/M_{DSM}
1	DM-2.4	12434	0.28	0.26	11355	11280	1.10
2	DM-1.5	7517	0.43	0.32	6681	6808	1.13
3	DM-1.0	4881	0.64	0.40	4202	4450	1.16
4	DM-0.7	3094	0.89	0.47	2631	3101	1.18
5	DM-0.6	2452	1.04	0.51	2050	2622	1.20
6	DM-0.5	1935	1.23	0.56	1524	2061	1.27
7	DM-0.48	1904	1.28	0.57	1398	2017	1.36
8	DM-0.40	1544	1.51	0.46	1061	1787	1.46
9	DM-0.3	977	1.96	0.73	651	1174	1.50
10	15-DM-2.4	11101	0.34	0.26	10049	10163	1.10
11	15-DM-1.5	6688	0.45	0.44	6145	6053	1.09
12	15-DM-1.0	4282	0.64	0.79	3913	2000	1.09
13	15-DM-0.7	2805	0.90	0.99	2427	1634	1.16
14	15-DM-0.6	2248	1.05	0.89	1882	1182	1.19
15	15-DM-0.5	1759	1.23	0.54	1409	1984	1.25
16	15-DM-0.48	1740	1.28	0.55	1317	1898	1.32
17	15-DM-0.40	1491	1.52	0.47	973	1618	1.53
18	15-DM-0.30	1203	2.00	0.68	602	1142	2.00
19	17-DM-2.4	22230	0.40	0.37	19621	19461	1.14
20	17-DM-1.5	13296	0.63	0.42	11515	12051	1.15
21	17-DM-1.0	8253	0.94	0.40	6533	8151	1.26
22	17-DM-0.7	4903	1.32	0.60	3643	5330	1.35
23	17-DM-0.6	4259	1.54	0.51	2810	4716	1.52
24	17-DM-0.5	3577	1.86	0.46	2054	4012	1.74
25	17-DM-0.48	3017	1.92	0.57	1922	3695	1.57
26	17-DM-0.40	2379[2]	2.29	0.63	1412	3022	1.69
27	17-DM-0.38	2250	2.43	0.73	1288	2279	1.75
Mean	—	—	—	—	—	—	1.34
COV	—	—	—	—	—	—	0.18
Reliability index β_1		—	—	—	—	—	3.58
Reliability index β_2		—	—	—	—	—	3.75

Table 7.5: Comparison between flexural strength obtain from FE analysis and DSM equations, for DOW sections.

S.No	Specimen	M_{FEA} (kN.mm)	λ_l	λ_d	M_{nl} (kN.mm)	M_{nd} (kN.mm)	M_{FEA}/M_{DSM}
1	DOW-2.4	12662	0.37	0.25	11094	11379	1.14
2	DOW-1.5	7714	0.58	0.43	6525	6717	1.18
3	DOW-1.0	4544	0.86	0.55	3818	4301	1.19
4	DOW-0.7	2565	1.22	0.48	2138	3104	1.20
5	DOW-0.6	2160	1.43	0.69	1647	2786	1.31
6	DOW-0.5	1995	1.69	0.43	1219	2257	1.64
7	DOW-0.48	2094	1.77	0.79	1135	1813	1.85
8	DOW-0.40	1312	2.09	0.62	840	1685	1.56
9	DOW-0.3	1046	2.77	0.98	511	983	2.05
10	15-DOW-2.4	10596	0.36	0.76	9336	7513	1.41
11	15-DOW-1.5	6421	0.57	3.02	6248	5029	1.28
12	15-DOW-1.0	4053	0.30	0.65	4024	3472	1.17
13	15-DOW-0.7	2242	1.40	0.60	1643	2496	1.36
14	15-DOW-0.6	2152	1.67	1.37	1247	1274	1.73
15	15-DOW-0.5	1522	2.13	0.81	871	1564	1.75
16	15-DOW-0.4	1263	3.16	0.63	660	1763	1.91
17	15-DOW-0.3	948	2.24	2.67	506	359	2.64
18	17-DOW-2.4	16139	0.37	0.32	11991	12004	1.35
19	17-DOW-1.5	9797	0.58	0.41	9008	9340	1.09
20	17-DOW-1.0	5997	0.86	0.44	5264	6180	1.14
21	17-DOW-0.7	3595	1.21	0.68	2949	3941	1.22
22	17-DOW-0.6	3001	1.41	0.56	2276	3551	1.32
23	17-DOW-0.5	2730	1.67	0.49	1690	3046	1.62
24	17-DOW-0.4	2238	2.09	0.44	1152	2486	1.94
25	17-DOW-0.3	1158	2.67	0.73	721	1631	1.61
Mean		—	—	—	—	—	1.51
COV		—	—	—	—	—	0.24
Reliability index β_1		—	—	—	—	—	3.42
Reliability index β_2		—	—	—	—	—	3.58

7.3.2 Discussion on modified DSM equations for built-up sections

As it is well-known, the current specifications lack of design-specific guideline for addressing built-up sections, which leads to limitations in the applicability of DSM on built-up members. The innovation and creativity in assembling built-up sections to meet specific structural requirement, made it difficult to capture the complexity of their behavior, and accurately predicting the strength by using the original DSM equations. This fact has motivated researchers to made assiduous attempts in providing a reliable design for built-up members notably in bending, by inducing modification

to the original DSM equations (Eq 6.1&6.2), or by relying on simplified approaches that accommodates the analytical analysis of built-up members. Consecutively, Numerous attempts to modify DSM equations have been suggested in an effort to represent the intricate behavior of built-up members in cases where DSM failed, however, these modifications were specific to limited buckling instabilities, and limited in their applications to a restricted number of built-up sections [75-77]. Here are some instances of the modified DSM equations that are used for built-up flexural members:

The flexural strength of built-up closed sections CV, COF and COW which experienced local buckling failure, was determined using Eq. 6.4 and 6.5. proposed by [75]:

$$M_{nl} = \begin{cases} M_y & for\ \lambda_l \leq 0.320 \\ \left[1 - 0.18\left(\frac{M_{crl}}{4M_y}\right)^{0.3}\right]\left(\frac{M_{crl}}{4M_y}\right)^{0.3} M_y & for\ \lambda_l > 0.320 \end{cases} \quad \text{Eq 6.4}$$

$$M_{nl} = \begin{cases} \left[1 + (\eta - 1)\left(1 - 1/C_{yl}^2\right)M_y\right] & for\ \lambda_l \leq 0.949 \\ \left[1 - 0.03\left(\frac{M_{crl}}{M_y}\right)^{0.3}\right]\left(\frac{M_{crl}}{M_y}\right)^{0.3} M_y & for\ \lambda_l \leq 0.949 \end{cases} \quad \text{Eq 6.5}$$

- [75] also proposed another DSM modification to handle the case of built-up open section named as OV:

$$M_{nl} = \begin{cases} \left[1 + (\eta - 1)\left(1 - 1/C_{yl}^2\right)M_y\right] & for\ \lambda_l \leq 0.980 \\ \left[1 - 0.01\left(\frac{M_{crl}}{M_y}\right)^{0.25}\right]\left(\frac{M_{crl}}{M_y}\right)^{0.25} M_y & for\ \lambda_l \leq 0.980 \end{cases} \quad \text{Eq 6.6}$$

- Furthermore, [76] proposed a revised DSM equation for the double sigma face to face section:

$$M_{nl} = \begin{cases} M_y & for\ \lambda_l \leq 0.5 \\ \left[1 - 0.2\left(\frac{M_{crl}}{1.5M_y}\right)^{0.33}\right]\left(\frac{M_{crl}}{1.5M_y}\right)^{0.33} M_y & for\ \lambda_l > 0.5 \end{cases} \quad \text{Eq 6.7}$$

- [77] presented the subsequent equation for face to face hollow section:

$$M_{nl} = \left[1 - 0.15\left(\frac{M_{crl}}{M_y}\right)^{0.25}\right]\left(\frac{M_{crl}}{M_y}\right)^{0.25} M_{ne} \quad for\ \lambda_l \leq 0.776 \quad \text{Eq 6.8}$$

These equations have been modified by adjusting both the constant parameters and the local slenderness thresholds. Furthermore, these alterations have a substantial effect on the assessment of the inelastic reserves for built-up sections, as the existing limit for slenderness ($\lambda_l \leq 0.776$) does not adequately represent the real slenderness values determined from slenderness curves. Furthermore, when considering a single local slenderness limit, it is important to note that this approach does not take into account the variations in behavior that can arise from different methods and approaches used to assemble built-up sections, regardless of the shape of the cross-section. This limitation becomes evident when analyzing data sets from individual CFS sections. Nevertheless, implementing the proposed approach of addressing the distinctiveness of slenderness on a section-by-section basis, through the adoption of a revised local slenderness threshold and adjustments to the constant equation parameters, would conflict with the current methodology of offering comprehensive DSM equations for built-up sections.

It is important to acknowledge that the DSM for calculating the bending capacity of CFS members indirectly takes into account the influence of thickness through the notion of effective width, which is connected to the width-to-thickness ratio (b/t). This is because DSM is primarily based on EWM. Nevertheless, the equation for determining local slenderness ($\lambda_l = \sqrt{M_y/M_{crl}}$) as specified in (NAS) [2], does not specifically include the thickness. Given the substantial impact of thickness on the

local slenderness of thin-walled members, it is essential to explicitly include thickness when assessing their behavior, especially in scenarios where local buckling is expected to occur.

In order to address these constraints in achieving a precise and reliable design approach, a thorough examination is necessary to create a comprehensive DSM that can forecast the flexural strength of various built-up members. Alternatively, a specific set of equations could be formulated to accommodate built-up closed and open sections. The objective is to build a cohesive methodology that can effectively manage the broad range of scenarios encountered in real-world situations.

This chapter presents an earnest attempt to address the current limitations and present a more effective design method for built-up sections, by suggesting a generalized concept for the current DSM, to extend its applicability on built-up flexural members subjected to cross-sectional buckling, particularly local buckling failure.

7.3.3 Generalized Direct Strength Method for Cold Formed Steel Built-up sections failing in local buckling

Drawing insight from the previously discussed aspects pertaining to the design rules for built-up sections and the predicted outcomes of the DSM for DM and DOW sections, the Generalized Direct Strength Method (DSM-G) may be introduced by making the following modifications to the original DSM equation Eq 6.1 [106]:

- For DSM over-conservative flexural strength predictions $M_{FEA}/M_{DSM} > 1.00$ (underestimation of the bending capacity):

$$M_{DSM-G} = \frac{\eta}{0.1565t^3 - 0.774t^2 + 1.2178t + 0.2732} \begin{Bmatrix} [M_y + (1 - 1/C_{yl}^2)(M_p - M_y)] & \lambda_{lf} \leq 0.776 \\ \left[1 - 0.15\left(\frac{M_{crl}}{M_y}\right)^{0.4}\right]\left(\frac{M_{crl}}{M_y}\right)^{0.4} M_y & \lambda_{lf} > 0.776 \end{Bmatrix} \quad \text{Eq 6.9}$$

- For DSM unconservative flexural strength predictions $M_{FEA}/M_{DSM} < 1.00$ (overestimation of the bending capacity):

$$M_{DSM-G} = \eta.(0.1565t^3 - 0.774t^2 + 1.2178t + 0.2732)\begin{Bmatrix} [M_y + (1 - 1/C_{yl}^2)(M_p - M_y)] & \lambda_{lf} \leq 0.776 \\ \left[1 - 0.15\left(\frac{M_{crl}}{M_y}\right)^{0.4}\right]\left(\frac{M_{crl}}{M_y}\right)^{0.4} M_y & \lambda_{lf} > 0.776 \end{Bmatrix} \quad \text{Eq 6.10}$$

Eq. 6.9 and 6.10 were proposed based on the following assumptions, both of which illustrate observable constraints when utilizing the DSM equation for built-up sections:

1. Thinner sections frequently exhibit distinct failure behavior and in comparison to thick sections. The original DSM, obtained mostly from data of thicker members, confront an extra problem in adequately capturing the distinctive behaviors of thinner members, such as local buckling, distortional buckling, and other instability phenomena. Consequently, their suitability for use on thinner components is restricted. this hypothesis allows for a relation establishment between thick and thin members.
2. The fictive slenderness $\lambda_{lf} \leq 0.776$ is used since a true slenderness does not accurately represent the real slenderness of the built-up sections, as previously discussed. The suggested equations do not provide information on the slenderness limits of the sections. Instead, they compute the modified flexural strength M_{DSM-G}. The actual slenderness and inelastic reserve of the sections will be established using slenderness curves. Indeed, this method effectively prohibits any modifications to the original DSM (Eq. 6.1) and provides a robust way for addressing built-up sections.

7.3.4 Development of DSM-G equations

7.3.4.1 Regression analysis

The process of developing the new equation consists of performing a nonlinear regression analysis to model and analyze the relationship between the dependent variable M_{DSM}/M_{FEA}, and the independent variable presented by the thickness of the section, to find the accurate function that describes the relationship between the two

variables, and thus, proceeding from data sets reported in Tables 7.4&7.5 conducted on DM and DOW with their six sectional configurations presented in Figure 7.4.

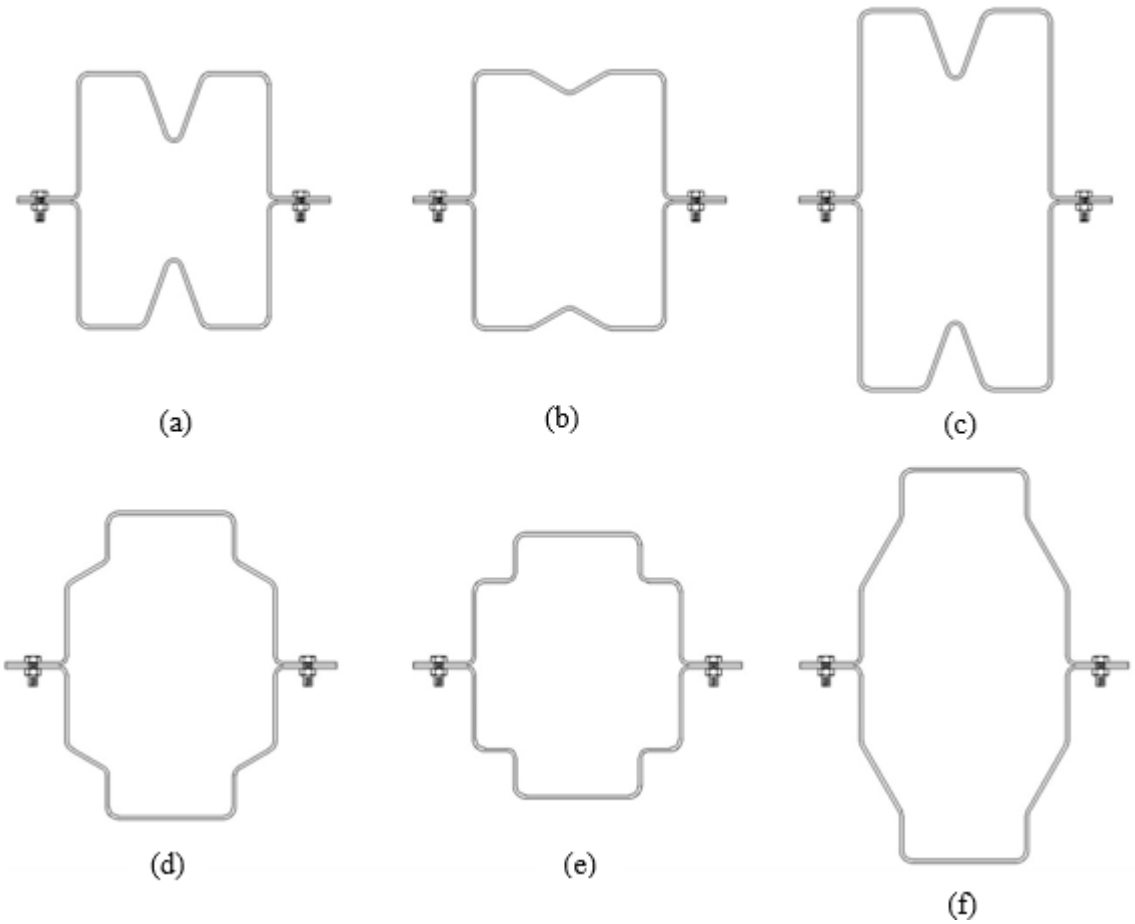

Figure 7.4: Geometrical shapes of: (a): DM, (b): 15-DM, (c): 17-DM, (d): DOW, (e): 15-DOW, (f): 17-DOW sections.

By examining the findings, a significant trend was identified, suggesting that changes in thickness had a strong influence on the level of conservatism. Specifically, as the section thickness decreased, the deviation from the exact solution increased, resulting in an M_{FEA}/M_{DSM} ratio much greater than 1.00. The curves shown in Figure 7.5(a&b) depict the relationship between the M_{DSM}/M_{FEA} ratio and the thickness variation for both DM and DOW sections, based on the observed pattern. Due to the resemblance in shape of the two curves, it is possible to represent this variation using cubic

equations. These equations have been found to accurately match the data points in the given mathematical model:

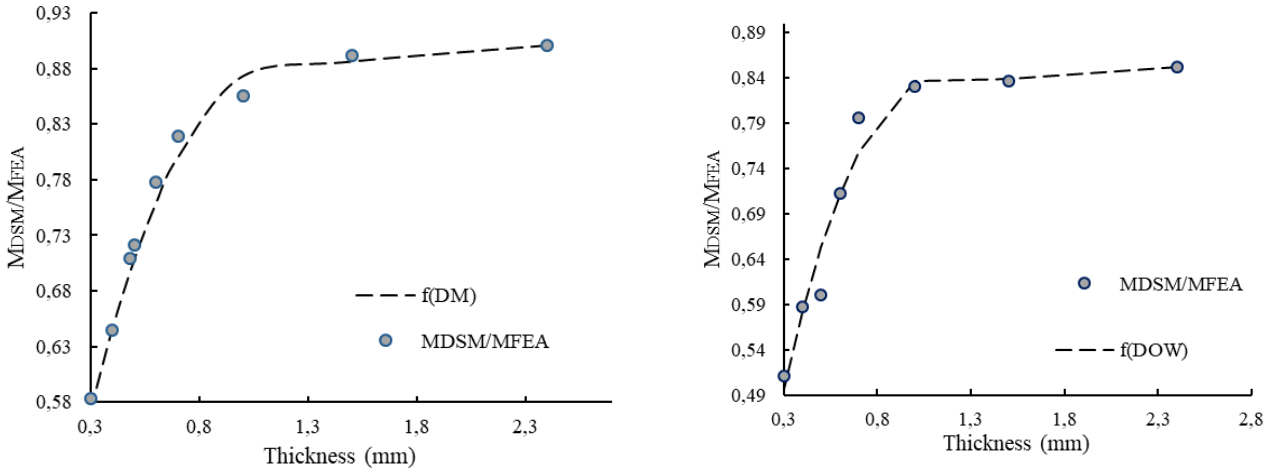

(a) (b)

Figure 7.5: Mathematical model presentation of M_{DSM}/M_{FEA} ratio data for: a) DM, b) DOW sections.

$$\frac{M_{DSM}}{M_{FEA}} = f_{DM}(t) = 0.1565t^3 - 0.774t^2 + 1.2178t + 0.2732 \quad \text{For DM section.} \qquad \text{Eq 6.11}$$

$$\frac{M_{DSM}}{M_{FEA}} = f_{DOW}(t) = 0.193t^3 - 0.9399t^2 + 1.4389t + 0.1444 \quad \text{For DOW section.} \qquad \text{Eq 6.12}$$

The accuracy of the mathematical model in predicting the rational relationship between thickness and M_{DSM}/M_{FEA} ratio, additionally to the reliability establishment of its predictions, is assessed through a statistical analysis, involving convenient metrics for capturing the nonlinear relationship between the two variables.

In order to assess the model's capacity to predict the variation of the relationship, the coefficient of determination (R^2) was computed. The results indicate that the model successfully accounts for 72% of the variability within DOW section and 59% within DM section, as shown in Table 7.6.
The Mean Square Prediction Error (MSPE) coefficient is another important parameter used to assess the dependability of the model. This metric is used to measure the closeness between the expected results and the boundaries of the established model.

The MSPE coefficient for the DOW section is 0.00156, while for the DM section it is 0.000168. These findings indicate a strong agreement between the prediction model and the data points presented in Table 7.6. Additionally, the model's appropriateness is evaluated by doing residual analysis. The results of this study are depicted in Figure 7.6. By calculating the residuals between the data sets and the model's prediction, we can visually assess the model's ability to capture the link between the thickness and the M_{DSM}/M_{FEA} ratio. Ultimately, these values can be categorized as varying from satisfactory to commendable. Due to the novel nature of this approach, which lacks any established standards, these results become even more significant as a helpful reference point for future investigations.

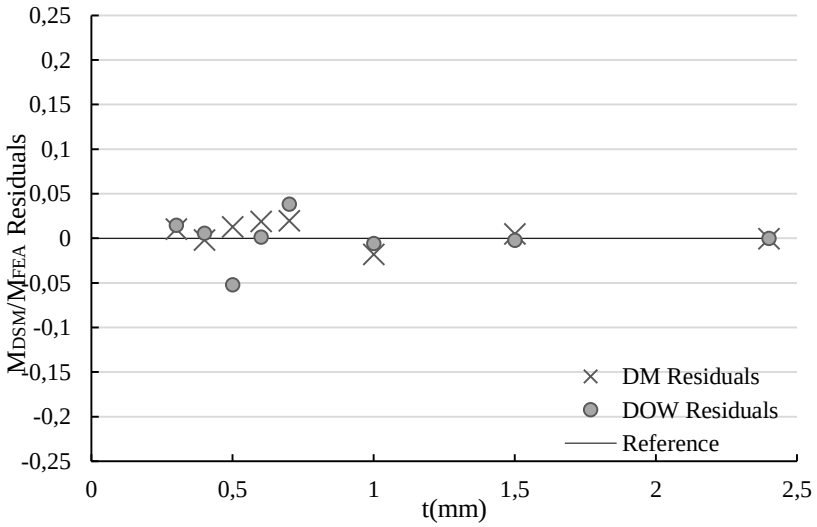

Figure 7.6: Mathematical models residual analysis for DM and DOW sections.

7.3.4.2 Shape Coefficient

In order to consider the impact of the cross-sectional shape of built-up members on their bending capacity, a proportionality coefficient was established between the two curves. This coefficient, also referred to as the shape coefficient, reflects the relationship between the two curves based on the data provided in Table 7.6. For DM sectional configurations (Figure 7.4(a-c)), the shape coefficient is equal to 1, as

equations 6.9 and 6.10 are based on DM section results. However, for DOW sectional configurations, the shape coefficient has a mean value of 1.08, which is calculated by dividing f_{DM} (t)/f_{DOW} (t) at each point, as shown in Table 7.6. The coefficient of variation (COV) for these values is 3.27%, indicating that the values are closely clustered around the mean. It should be emphasized that the coefficient may vary depending on the lead equation. Notable discrepancies may arise if the (DSM-G) equations are derived from Eq 6.12 instead of Eq 6.11, resulting in different predicted values for flexural strength. However, the overall precision and effectiveness of the obtained equation will remain unchanged.

Table 7.6: Benchmarks and form coefficients η determination.

t(mm)	M_{DSM}/M_{FEA}(DM)	M_{DSM}/M_{FEA}(DOW)	$\eta = f_{DM}(t)/f_{DOW}(t)$
2.40	0.901136	0.851968	1.06
1.50	0.8865875	0.839350	1.06
1.00	0.8735	0.836400	1.04
0.70	0.8000795	0.757278	1.06
0.60	0.759044	0.711064	1.07
0.50	0.7081625	0.653000	1.08
0.48	—	0.639863	—
0.40	0.646496	0.581928	1.11
0.30	0.5731055	0.496690	1.15
Mean	—	—	1.08
COV	—	—	0.032
R^2 (COD)	72%	59 %	—
MSPE	0.000168	0.00156	—

The concept of a shape coefficient was introduced before the assertion that built-up sections have a similar polynomial distribution in terms of thickness variation. Therefore, it is possible to determine this coefficient through experimentation in order to obtain the appropriate coefficient for the specific built-up section being studied.

7.3.4.3 Generalized Direct Strength Method equations

The application and introduction of the mathematical model, and shape coefficient into the original DSM (Eq 6.1), will highly depends on the conservativeness degree, determined when applying this equation on a built-up section, indeed, if the predicted

flexural strength results are over-conservative in comparison to FE analysis and experimental solution, the expression $\eta/(0.1565t^3 - 0.774t^2 + 1.2178t + 0.2732)$, will be multiplied to Eq 6.1, to obtain Eq 6.9. In contrast, if the predicted flexural strength results were unconservative, the expression $\eta.(0.1565t^3 - 0.774t^2 + 1.2178t + 0.2732)$ will be multiplied to Eq 6.1, to obtain Eq 6.10, it is important to highlight that this equation in contrast to Eq 6.9, didn't undergo regression analysis, this was due to its reliance to the first hypothesis assumption, claiming that all built-up members, calculated with DSM Eq 6.1, will have the same variation in strength when changing the thickness, as a results, the conduction of a supplemental regression analysis deemed unnecessary.

7.4 Flexural strength predictions using DSM-G method

7.4.1 DSM-G application on DM and DOW built-up sections

In the process of validating DSM-G equations, the new flexural design strength method was used to calculate the bending strength of DM and DOW with a total of 52 beams, to evaluate the precision of the new approach. Table 7.7&7.8 subsequently presents the results of the flexural strength M_{DSM-G}, determined using Eq 6.9, the choice of Eq 6.9 was due to over-conservative results estimations, obtained using the original DSM (Eq 6.1) as discussed in section 6.3.4.1, the comparison of the results with FE Analysis flexural strength M_{FEA} has been carried. Remarkably, M_{DSM-G} design moment was accurately able to predict the flexural strength of the two sections, with a mean value of M_{FEA}/M_{DSM-G}=1.00 for DM section, and 0.99 for DOW section, additionally, the alteration degree in results with reference to the mean value, is determined by the coefficient of variation (COV), with an obtained value of 9.4 % for DM and 8.0 % for DOW, these findings indicate a low degree of alteration. Additionally, the reliability of the new design is evaluated using reliability index β_1 and β_2 calculations, which resulted in exceeding the goal reliability value β_0 = 2.5. This ensures the reliability of the new design equation.

Table 7.7: Comparison between DSM and Generalized DSM equation in bending strength determination for DM sections.

S.No	Specimen	M_{FEA} (kN.mm)	M_{DSM} (kN.mm)	M_{DSM-G} (kN.mm)	M_{FEA}/M_{DSM}	M_{FEA}/M_{DSM-G}
1	DM-2.4	12434	11355	12601	1.10	0.99
2	DM-1.5	7517	6681	7536	1.13	1.00
3	DM-1.0	4881	4202	4811	1.16	1.01
4	DM-0.7	3094	2631	3288	1.18	0.94
5	DM-0.6	2452	2050	2701	1.20	0.91
6	DM-0.5	1935	1524	2152	1.27	0.90
7	DM-0.48	1904	1398	2007	1.36	0.95
8	DM-0.4	1544	1061	1641	1.46	0.94
9	DM-0.3	977	651	1136	1.50	0.86
10	15-DM-2.4	11101	10049	11151	1.10	1.00
11	15-DM-1.5	6688	6145	6931	1.09	0.96
12	15-DM-1.0	4282	3913	4480	1.09	0.96
13	15-DM-0.7	2805	2427	3033	1.16	0.92
14	15-DM-0.6	2248	1882	2479	1.19	0.91
15	15-DM-0.5	1759	1409	1990	1.25	0.88
16	15-DM-0.48	1740	1317	1890	1.32	0.92
17	15-DM-0.4	1491	973	1505	1.53	0.99
18	15-DM-0.30	1203	602	1050	2.00	1.15
19	17-DM-2.4	22230	19621	21774	1.13	1.02
20	17-DM-1.5	13296	11515	12988	1.15	1.02
21	17-DM-1.0	8253	6533	7479	1.26	1.10
22	17-DM-0.7	4903	3643	4553	1.35	1.08
23	17-DM-0.6	4259	2810	3702	1.52	1.15
24	17-DM-0.5	3577	2054	2900	1.74	1.23
25	17-DM-0.48	3017	1922	2758	1.57	1.09
26	17-DM-0.4	2379	1412	2184	1.68	1.09
27	17-DM-0.38	2250	1288	2035	1.75	1.11
				Mean	1.34	1.00
				COV	0.18	0.094
			Reliability index β_1		3.58	3.04
			Reliability index β_2		3.75	3.24

Table 7.8: Comparison between DSM and Generalized DSM equation in bending strength determination for DOW sections.

S.No	Specimen	M_{FEA} (kN.mm)	M_{DSM} (kN.mm)	M_{DSM-G} (kN.mm)	M_{FEA}/M_{DSM}	M_{FEA}/M_{DSM-G}
1	DOW-2.4	12662	11094	13296	1.14	0.95
2	DOW-1.5	7697	6525	8096	1.18	0.95
3	DOW-1.0	4791	3818	4808	1.25	1.00
4	DOW-0.7	2565	2138	2939	1.20	0.87
5	DOW-0.6	2281	1646	2385	1.39	0.96
6	DOW-0.5	1995	1219	1893	1.64	1.05
7	DOW-0.48	2094	1135	1791	1.85	1.17
8	DOW-0.4	1312	840	1429	1.56	0.92
9	DOW-0.3	1046	511	982	2.05	1.07
10	15-DOW-2.4	10596	8526	10408	1.24	1.02
11	15-DOW-1.5	6425	5260	6526	1.22	0.98
12	15-DOW-1.0	4053	3311	4170	1.22	0.97
13	15-DOW-0.7	2242	1643	2259	1.36	0.99
14	15-DOW-0.6	1898	1247	1807	1.52	1.05
15	15-DOW-0.5	1522	871	1353	1.75	1.12
16	15-DOW-0.4	1263	767	1305	1.65	0.97
17	15-DOW-0.3	948	506	971	1.87	0.98
18	17-DOW-2.4	17667	15439	18846	1.14	0.94
19	17-DOW-1.5	10666	9008	11176	1.18	0.95
20	17-DOW-1.0	5997	5264	6629	1.14	0.90
21	17-DOW-0.7	3595	2949	4054	1.22	0.89
22	17-DOW-0.6	3001	2276	3298	1.32	0.91
23	17-DOW-0.5	2730	1690	2625	1.62	1.04
24	17-DOW-0.4	2238	1152	1960	1.94	1.14
25	17-DOW-0.38	1649	1059	1841	1.56	0.90
				Mean	1.45	0.99
				COV	0.32	0.080
			Reliability index β_1		3.42	2.66
			Reliability index β_2		3.58	2.86

7.4.1.1 Local buckling design curves of DM and DOW sections

Figure 7.7 shows design curves for local buckling of DM and DOW sections. Local slenderness curves were provided for both design (DSM, DSM-G) and finite element analysis (FEA) for each section configuration. The distribution of M/M_y was plotted by varying the local slenderness ratio (λ_l) over a wide range of thicknesses [0.3-2.4]. The local slenderness ratio's limitations were found using graphical analysis, specifically by identifying the point at which the curve changes from being linear to experiencing a rapid loss in flexural strength, represented by M/M_y. In 17-DOW

configuration, the local buckling failure of the specimens begins at a critical slenderness ratio λ_l = 0.580, which corresponds to a thickness t =1.5 mm. This is seen in Figure 7.7.d, along with the deformed shape displayed in Figure 7.8.b. Local buckling in DM section was observed at a slenderness ratio λ_l = 0.636, which corresponds to a thickness t = 1 mm. Figure 7.8.a illustrates that local buckling (LB) has a lesser effect on the overall strength of DM section. This matches with the slenderness curves shown in Figure 7.7.a, showing that DM section has higher performance in avoiding local buckling compared to the other sectional configurations.

In general, LC-G slenderness curves have a strong correlation with FEA, in contrast to LC-DSM curves. The local slenderness limit for sections to fail in local buckling is defined by the condition $M_{DSM\text{-}G}/M_y$ >1, rather than M_{DSM}/M_y =1. The discrepancy can be attributed to the modifications included in the original DSM Eq 6.1. The purpose of this slenderness threshold is to guarantee that the element stays within a safe range of slenderness in order to prevent failure due to local buckling.

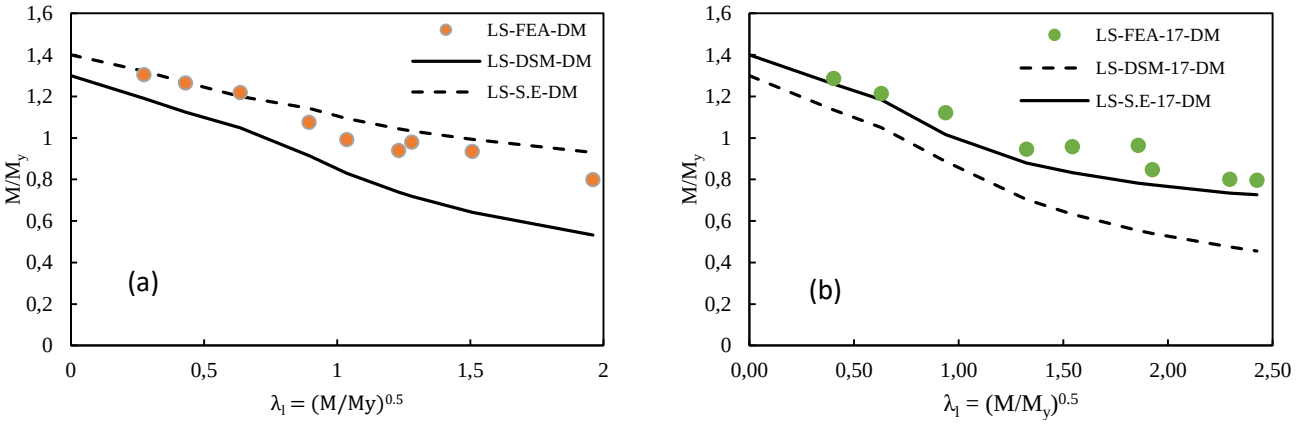

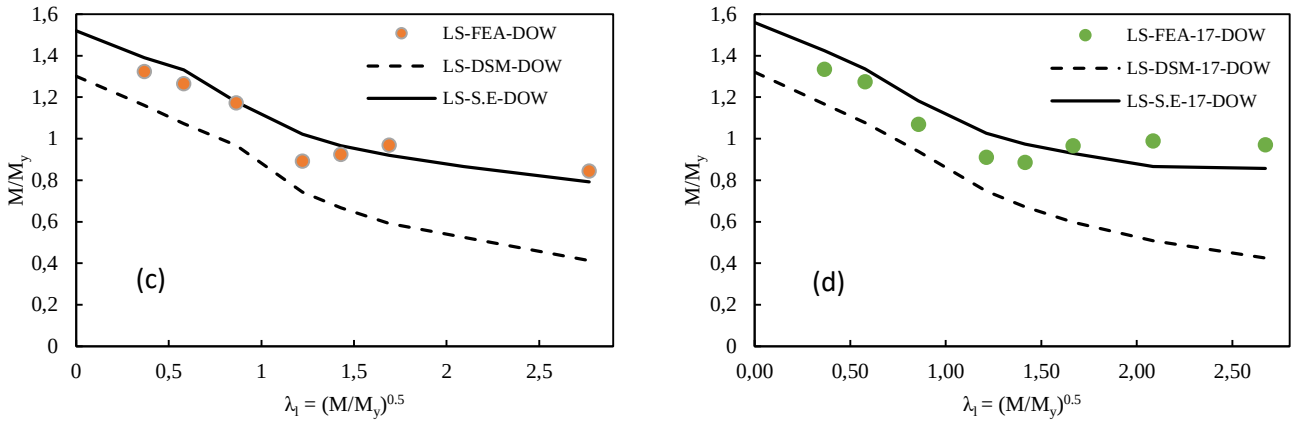

Figure 7.7: Local buckling design curves for: a) DM, b) 17-DM, c) DOW, d) 17-DOW.

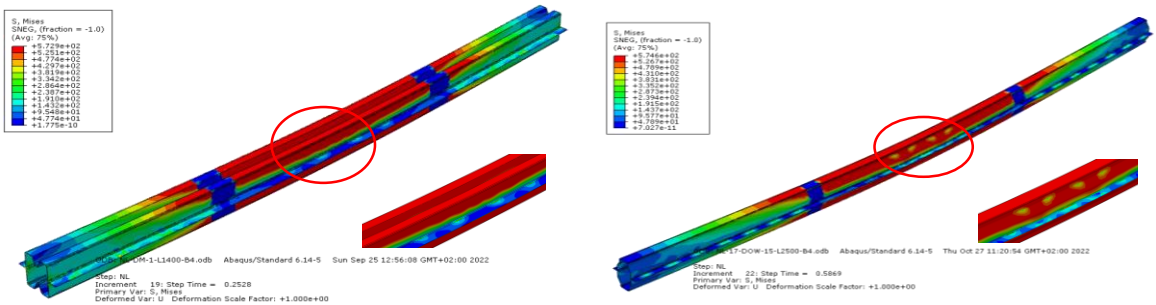

a) DM-1.0-L1400. b) 17-DOW-1.5-L2500.

Figure 7.8: Influence of local buckling collapse on: a) DM-1.0-L1400, b) 17-DOW-1.5-L2500 beams.

7.4.2 DSM-G validation against other Built-up sections

The goal behind developing a generalized Direct Strength Method for built-up sections was to avoid particular limited modified DSM equations, based on random parameters modifications. The current challenge requires the verification of this new method in covering design of a variety of built-up members. In this regard, an additional validation was carried using existing built-up open and closed sections, selected from tests and parametric study reported in [74,75] investigations. Figure 7.9 shows the cross-sectional geometry of four built-up open and closed sections. The label associated to these section was based on the cross-sectional geometry shape, the considered thickness and the loading type. egg: OV: is an open section with a middle

web stiffener that takes both the shape of an ‘O’ and ‘V’ simultaneously, COW: refer to a closed section ‘C letter’ with an overall rounded shape ‘O letter’ and an edge stiffener that forms ‘W’ shape, CV: is a closed section ‘C’ with ‘V’ shaped middle stiffeners, COF: is the inversed section of COW section. The application of DSM-G method on these sections aims to assess the potential of Eq 6.9 & 6.10 in predicting the design flexural strength. It is important to note that multiple configurations were considered by varying the dimensional properties of these sections, additionally to the wide range of thicknesses investigated in this study, this feature makes it convenient to validate the proposed method. The obtained results will be compared with the original DSM equation, and DSM modified equations proposed by [75].

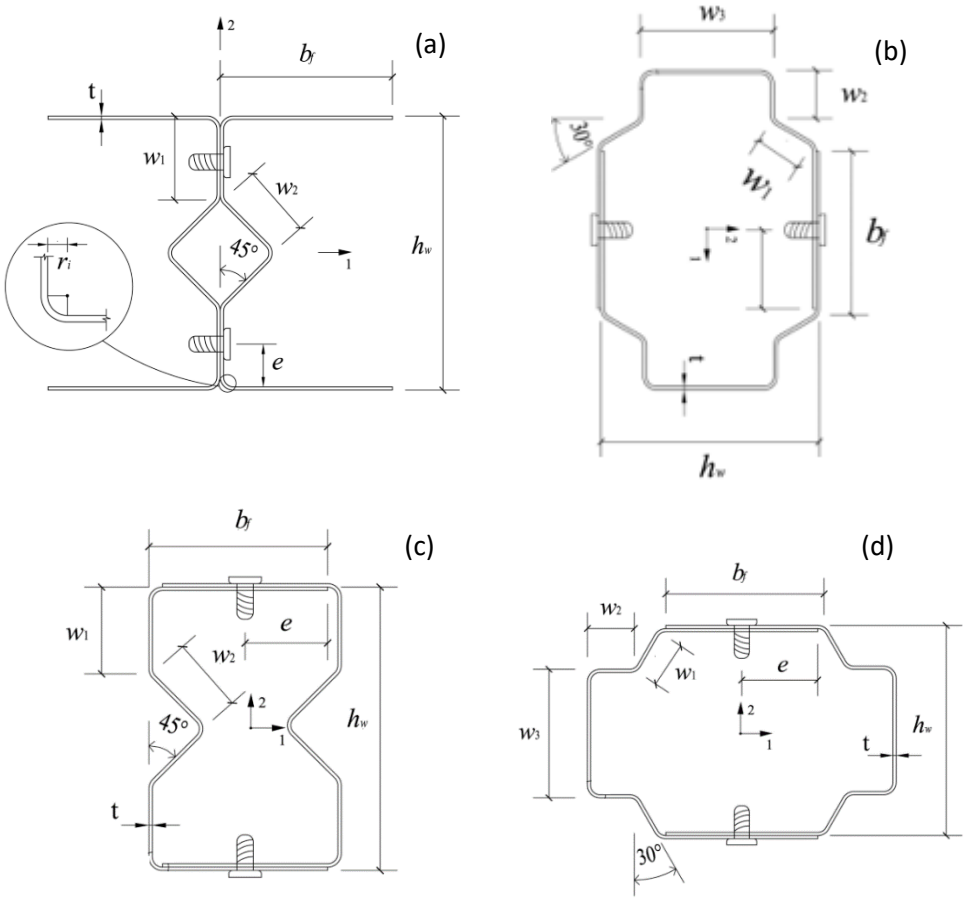

Figure 7.9: Definition of symbols and location of screws in cross section: (a) OV section; (b) COW section; (c) CV section; (d) COF section.

Table 7.9-7.11 present the results for the design flexural strength (M_{DSM-G}) in comparison to the critical flexural strength determined from numerical analysis (M_{FEA}) and the predicted flexural strength using DSM (Eq 6.1) (M_{DSM}), and the proposed equations by [75] (Eq 6.4-6.6) ($M_{DSM-W\&Y}$). on a total of 71 beams, the mean values of $M_{EXPorFEA}/M_{DSM-G}$ for the OV, COW, CV and COF sections is 1.00, 0.99, 1.02 respectively, with a coefficient of variation (COV) of 10.1 %, 9.8 % and 7.8 %, respectively, these degrees of variance in the specimens are considered as low, suggesting that the strength of the specimens is tightly gathred around the mean values. The proposed approach's reliability was confirmed by calculating the reliability indices (β1) and (β2), which exceeded the desired reliability of 2.5 as specified in [2]. The flexural strength values obtained from finite element analysis and tests ($M_{EXPorFEA}$) agree precisely with those calculated by the generalized (M_{DSM-G}), whether in the case of OV and COW sections, where the strength is predicted using Eq 6.9, or in the case of CV and COF sections using Eq 6.10. This emphasizes the precision and dependability of the design approach in giving precise estimates for the strength of built-up sections that are prone to failure due to sectional buckling.

Table 7.9: Comparison between DSM, W&Y, and DSM-G equations in bending strength determination for OV sections.

Specimen	M_{Test} or M_{FEA} (kN.mm)	M_{DSM}	$M_{DSM-W\&Y}$	M_{DSM-G}	M_{Test}/M_{DSM} or M_{FEA}/M_{DSM}	$M_{Test}/M_{DSM-W\&Y}$ or $M_{FEA}/M_{DSM-W\&Y}$	M_{Test}/M_{DSM-G} or M_{FEA}/M_{DSM-G}
12-OV-1.9	13844	12961	11446	17205	1.07	1.21	0.80
13-OV-1.9	13183	12797	11397	16988	1.03	1.16	0.78
12-OV-1.5	11271	8784	10315	11394	1.28	1.09	0.99
13-OV-1.5	10465	8670	10189	11246	1.21	1.03	0.93
2-OV-1.9	10290	8364	10352	11103	1.23	0.99	0.93
1-OV-1.9	9988	8318	10314	11042	1.2	0.97	0.90
9-OV-1.9	16971	13138	16313	17440	1.29	1.04	0.97
5-OV-1.9	22756	17544	21807	23289	1.3	1.04	0.98
10-OV-1.9	16480	12989	16152	17242	1.27	1.02	0.96
12-OV-1.0	7128	4439	5631	5844	1.61	1.27	1.22
13-OV-1.0	5271	4382	5565	5769	1.2	0.95	0.91
2-OV-1.5	6985	5596	7275	7259	1.25	0.96	0.96
1-OV-1.5	7584	5563	7248	7216	1.36	1.05	1.05
5-OV-1.5	16431	11719	15314	15201	1.4	1.07	1.08
7-OV-1.5	15346	11580	15153	15021	1.33	1.01	1.02
2-OV-1.0	4031	2781	3970	3661	1.45	1.02	1.10
9-OV-1.0	6571	4356	6249	5735	1.51	1.05	1.15
5-OV-1.0	8549	5814	8350	7654	1.47	1.02	1.12
10-OV-1.0	5952	4308	6189	5672	1.38	0.96	1.05
7-OV-1.0	7828	5743	8262	7561	1.36	0.95	1.04
9-OV-0.6	2861	1781	2909	2698	1.61	0.98	1.06
10-OV-0.6	2639	1762	2883	2670	1.5	0.92	0.99
7-OV-0.6	3614	2350	3851	3560	1.54	0.94	1.02
OV-0.48-B4	1246	774	1378	1278	1.61	0.9	0.98
OV-1.0-B4	4238	2811	4051	3701	1.51	1.05	1.15
				Mean (P_m)	1.36	1.03	1.00
				COV	0.123	0.083	0.101
				Reliability index β_1	3.87	3.00	2.85
				Reliability index β_2	4.06	3.84	3.74

Table 7.10: Comparison between DSM, W&Y, and Generalized DSM equation in bending strength determination for COW sections.

Specimen	M_{FEA} (kN mm)	M_{DSM} (kN mm)	$M_{DSM-W\&Y}$ (kN mm)	M_{DSM-G} (kN mm)	M_{Test}/M_{DSM} or M_{FEA}/M_{DSM}	$M_{Test}/M_{DSM-W\&Y}$ or $M_{FEA}/M_{DSM-W\&Y}$	M_{Test}/M_{DSM-G} or M_{FEA}/M_{DSM-G}
15-COW-2.4	11635	9242	11434	10769	1.26	1.02	1.08
14-COW-2.4	14185	11161	13798	13005	1.27	1.03	1.09
17-COW-2.4	19024	15835	19568	18451	1.20	0.97	1.03
19-COW-1.9	19407	16014	19354	19409	1.21	1.00	1.00
21-COW-2.4	16856	13468	15950	15693	1.25	1.06	1.07
15-COW-1.5	7002	5491	6446	6503	1.28	1.09	1.08
14-COW-1.5	8407	6628	7769	7850	1.27	1.08	1.07
17-COW-1.5	11232	9398	11007	11130	1.20	1.02	1.01
15-COW-1.0	4508	3259	3682	3918	1.38	1.22	1.15
19-COW-1.0	7674	7282	8229	8753	1.05	0.93	0.88
21-COW-2.4	16856	13468	15950	15693	1.25	1.06	1.07
17-COW-1.0	6745	5543	6268	6663	1.22	1.08	1.01
22-COW-2.4	19151	16554	19016	19289	1.16	1.01	0.99
22-COW-1.5	10410	7501	9062	8884	1.39	1.15	1.17
COW-0.48-B4	1699	1418	1735	2137	1.20	0.98	0.80
COW-1.0-B4	4691	4321	4888	5194	1.09	0.96	0.90
COW-1.0-B4R	4730	4321	4888	5194	1.09	0.97	0.91
				Mean (P_m)	1.22	1.04	1.02
				COV (V_P)	0.072	0.067	0.098
			Reliability index β_1		3.87	3.00	2.85
			Reliability index β_2		4.06	3.84	3.74

Table 7.11 Comparison between DSM, W&Y, and Generalized DSM equation in bending strength determination for CV & COF sections.

Specimens	M_{EXP} or M_{FEA} (kN mm)	M_{DSM} (kN mm)	$M_{DSM-W\&Y}$ (kN mm)	M_{DSM-G} (kN mm)	M_{EXP}/M_{DSM} or M_{FEA}/M_{DSM}	$M_{EXP}/M_{DSM-W\&Y}$ or $M_{FEA}/M_{DSM-W\&Y}$	M_{EXP}/M_{DSM-G} or M_{FEA}/M_{DSM-G}
6-CV-2.4	30827	34929	29554	27069	0.88	1.04	1.14
1-CV-1.9	9939	12924	10784	9629	0.77	0.92	1.03
4-CV-1.9	9840	12649	10485	9424	0.78	0.94	1.04
10-CV-1.9	16629	20150	15904	15012	0.83	1.05	1.11
1-CV-1.5	7145	9975	7711	7606	0.72	0.93	0.94
4-CV-1.5	7300	9759	7496	7441	0.75	0.97	0.98
6-CV-1.5	15638	20736	14994	15810	0.75	1.04	0.99
3-CV-1.0	3867	6216	4233	4670	0.62	0.91	0.83
7-CV-1.5	15343	20067	13640	15300	0.76	1.12	1.00
4-CV-1.0	3805	6138	4139	4611	0.62	0.92	0.83
10-CV-1.0	7482	9222	6178	6928	0.81	1.21	1.08
6-CV-1.0	8179	12251	8228	9203	0.67	0.99	0.89
7-CV-1.0	7609	10748	7415	8074	0.71	1.03	0.94
10-CV-0.6	2872	3968	2858	2590	0.72	1.01	1.11
7-CV-0.6	3807	4555	3403	2973	0.84	1.12	1.28
CV-0.48-B4	1266	2018	1501	1209	0.63	0.84	1.05
CV-1.0-B4	4088	6734	4460	5059	0.61	0.92	0.81
22-COF-2.4	31949	36259	29527	28100	0.88	1.08	1.14
14-COF-1.5	6216	7969	6284	6076	0.78	0.99	1.02
19-COF-1.9	9992	15630	11048	11645	0.64	0.9	0.86
15-COF-1.0	2934	4766	3352	3580	0.62	0.88	0.82
21-COF-1.0	5118	7100	4940	5334	0.72	1.04	0.96
17-COF-1.0	3582	5685	3906	4271	0.63	0.92	0.84
22-COF-1.0	9883	11967	8156	8990	0.83	1.21	1.10
21-COF-0.6	2542	3336	2308	2178	0.76	1.1	1.17
19-COF-1.0	3611	6150	4291	4620	0.59	0.84	0.78
COF-0.48-B4	1278	1915	1397	1147	0.67	0.91	1.11
COF-1.0-B4	3749	5523	3792	4149	0.68	0.99	0.90
COF-1.0-B4R	3884	5523	3792	4149	0.7	1.02	0.94
				Mean(P_m)	0.73	1.00	0.99
				COV(V_p)	0.113	0.094	0.129
				Reliability index β_1	1.55	2.80	2.94
				Reliability index β_2	1.74	3.00	3.14

7.5 Discussion and limitation of the proposed method

The proposed method presents a global improvement to the original DSM for built-up flexural members, by extending its applicability in successfully predicting the strength of built-up sections subjected to cross-sectional buckling, particularly the local

buckling failure. The results convergence is achieved through two approaches. The first, concerns the distribution of flexural strength against thickness variation, representing the generalized limitation of DSM for thin-walled sections subjected mainly to local buckling, the term generalized means that this concept is claimed to yield similar trends for any cross-sectional built-up section, fallen under the category of unpredicted results in the current design. Hence to prove this concept, a numerical investigation conducted on DM and DOW sections across a wide range of thicknesses, with a goal to develop a mathematical model with a polynomial cubic equation, the appropriateness of this model was thoughtfully examined and validated through a regression analysis.

The second concept, concerns the adjustment of the load capacity of built-up sections, by introducing a form coefficient to the equations, tailored to the specific built-up shape, considering that yielding and local buckling depend on the form and presence of stiffeners in the cross-section, instead of relying on relative local slenderness limits, which may not yield consistent results for built-up sections without modifying specific constants in the original equation. While this approach provides a more accurate adjustment, it is important to note that the new equation do not provide information on slenderness limits or inelastic reserves of the sections. Instead, it utilizes a fictive slenderness equivalent to the individual (CFS) sections limit. The actual slenderness limits are determined by specific slenderness curves corresponding to the section being investigated, as released for DM and DOW sections.

The curves presented in Figure 7.10 illustrate the distribution of the strength ratio M_{DSM}/M_{FEA} for all the investigated sections, along with the corresponding form coefficient for each curve. This representation enhances understanding and readability of the concept underlying the developed equations.

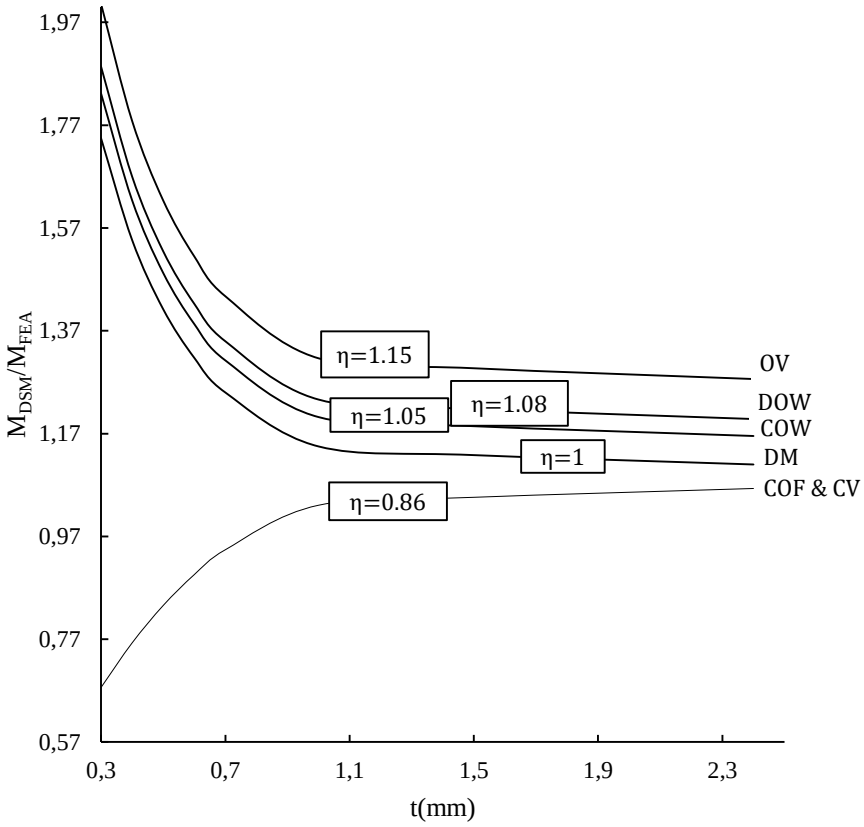

Figure 7.10: Mathematical models for the investigated built-up sections with corresponding shape coefficient η [106].

Prior to applying, DSM-G equations, the fulfillment of the following criteria has to be verified:

1- The elastic buckling modes pertaining to a built-up member has to be properly examined. Particular members may encounter failures when multiple buckling modes interacts. In these cases, the minimum buckling load may be identified for modes other than local buckling. The nominal buckling load may also be influenced by a variety of other factors, including member's length, boundary conditions, thickness, and geometrical characteristics. Prior to their extension, the applicability of the generalized equations must be evaluated in circumstances where these conditions may prevail.

2- The thickness utilized in the present study was restricted to 2.4 mm. Further research is required to assess the sufficiency within a specified range of increased thickness values.

7.6 Guidelines for DSM-G application

The use of the generalized method evolves around the application of Eq. 9&10 in the flexural design for built-up members, particularly for an innovative built-up sections, the present guidelines steps must be followed:

- Employ the original DSM by including the minimum local buckling moment M_{nl} (as defined in Eq 6.1), while taking into account a fictional local slenderness threshold $\lambda_{lf} \leq 0.776$.

- Determine the bending capacity ratio M_{FEA}/M_{DSM}, if DSM equations underestimate the flexural capacity of the built-up section $M_{FEA}/M_{DSM} > 1.00$, utilize the subsequent equation:

$$M_{DSM-G} = \frac{\eta}{0.1565t^3 - 0.774t^2 + 1.2178t + 0.2732} . M_{DSM} \qquad \text{Eq 6.13}$$

If DSM overestimate the bending strength of the built-up member $M_{FEA}/M_{DSM} < 1.00$, utilize the subsequent equation:

$$M_{DSM-G} = \eta . (0.1565t^3 - 0.774t^2 + 1.2178t + 0.2732) . M_{DSM} \qquad \text{Eq 6.14}$$

Eq 6.13&6.14 present a simplified version of Eq 6.9&6.10.

- Determine shape coefficient η thought experiencing, using at least three cross-section geometry alterations, to ensure covering a wide range of geometrical properties variations.

7.7 Conclusion

This study introduces a novel method for calculating the Design Strength of built-up flexural members. The method was created by an extensive numerical analysis on two closed sections in four-points bending, involving a total of 108 beams. To validate the

precision of the numerical model employed in this study, experiments conducted on multiple built-up closed and open members, as reported from literature experimental study. The verifies model was utilized to examine the influence of fasteners interconnection on the bending capacity and failure forms of two novel sections (DM & DOW) across a total of 56 specimens subjected to four-point bending. The goal of this analysis was to assess the suitability and practicality of the double thickness assumption in determining the design of bending capacity. In addition, the sections' elastic buckling behavior was examined by analyzing signature curves produced by the CUFSM software.

The formulation of the new equations is based on the analysis of 52 specimens in a comprehensive parametric investigation, specifically investigating the failure of sections due to local buckling. This was accomplished by altering factors that might affect the local buckling (LB) strength. Two alternative lengths, 1400 mm and 2500 mm, were utilized. Additionally, dimensional properties and a broad range of thicknesses [0.3-2.4mm] were examined.

This study has found that the existing DSM equations employed to determine the bending strength of the investigated sections underestimate their capacity, leading to overly cautious outcomes. Furthermore, the level of conservatism was notably elevated for very thin beams. The validity of this trend was thoroughly investigated using the findings from the present study results as well as prior investigations done on built-up sections. Regression analysis was undertaken to build a predictive model employed in the generalized equations for built-up members. The created equations evolve conservativeness-degree based approach, instead of the local slenderness limit ratio (λ_l) used in the original DSM equation. Two equations were established to account for both over-conservative and unconservative scenarios. By utilizing the generalized direct strength method for built-up flexural members, the following results can be emphasized:

- The proposed equation MDSM-G properly predicts the flexural strength of built-up closed and open sections that are prone to failure due to local buckling. Precision in forecasting the durability of extremely thin pieces.
- The modified DSM equations for built-up sections can be unified under two general equations, using the idea of conservativeness instead of local slenderness ratio limits.
- The local buckling strength of DM and DOW sections may be improved by considering post-yield buckling failure. This is particularly relevant when the ratio of applied moment to the yield moment (M/M_y) is more than 1, indicating slenderness limitations. These findings are consistent with the results obtained by finite element analysis (FEA).
- The spacing of the screws did not have an impact on the local buckling resistance of DM and DOW sections. However, it is necessary to have a minimum distance to prevent distortional deformation caused by the separation of the single components of the built-up sections.

Chapter 8
Conclusions and Recommendations

8.1 General Conclusion

This work presents a contribution into understanding the flexural behavior of innovative cold formed steel (CFS) built-up closed sections, subjected to cross-sectional buckling failure, and restricted against global buckling instability. Prior conducting an extensive comprehensive parametric study, the numerical model used was assiduously validated against a variety of built-up closed and open members in bending, subjected to cross-sectional instabilities. The selected cross-sectional shapes were obtained from an experimental study [74]. The goal of developing a Finite Element (FE) model capable of predicting the strength of a wide range of built-up members, was to broaden its applicability to the innovative sections investigated in this study, given the absence of experimental data on these sections. The developed FE model exhibited various levels of accuracy. The results were presented through comparisons of experimental and numerical maximum flexural strength, moment-displacement curves, and deformed shapes.

An overall of three parametric studies were conducted involving the validated numerical model, and comprising a total of 192 beams in four and three-points bending, each parametric study aimed to investigate a particular aspect of the proposed built-up closed sections. The first parametric study focused on studying the flexural behavior and buckling instabilities of built-up box section named as DH, thought conducting a comparative study against built-up box sections including a different assembling concept, the two considered section were named as DU and DC, where the later was chosen from [100] investigation in literature. all three sectional configurations underwent similar parameters variations, with the mechanical

properties applied to DH and DU sections following those used for DC section. The results of this investigation indicates a high accuracy for DH section in resisting bending load and sustaining local buckling instability, and thus for very thin sections (t=0.42 mm), with an overall strength increase of 50% compared to DC and DU sectional configuration. However, for thick specimens (t=1.9 mm) the advantage goes for DU section with an overall strength increase of 36% compared to DH and DC cross-sections.

The second parametric study concerns the investigation of the effect of fasteners; utilized in the new assembling concept, on the flexural strength, therefore, three built-up closed sections were adopted ranging from partially to fully stiffened sectional configuration, this aimed to assess the true contribution of fasteners in increasing/decreasing the flexural strength, and influencing the behavioral response of the sections in regards to buckling failure. The study concluded with the importance of including an adequate number of fasteners along the length of the beam to gain a full strength potential while improving the obtained failure shapes, indeed, in the case of partially stiffened sections DH and DO, the fasteners contributed to enhancing both the flexural strength and the deformation patterns, particularly by preventing the separation of individual components of the built-up section, however, for full stiffened section DOS the variation in strength due to fasteners spacing, was only recorded for three-points bending case, highlighting the unecessity of screws in four-points loading configuration.

The third parametric study comprise a total of 108 beams conducted on two innovative built-up stiffened sections named as DM and DOW, with a goal of assessing the direct strength method (DSM) in predicting the strength of built-up flexural members. The investigation was divided into two parts, the first, concerned the verification of the double thickness assumption in replacing the discrete fasteners modelling, in the design part, this assumption was made prior to non-existing provisions for fasteners in the current DSM, therefore the FEA including discrete

fasteners modelling focused on varying the fasteners spacing to capture any behavioral change in comparison with the deformed shapes obtained from the semi-analytical software CUFSM [101] based on the double thickness assumption. This investigation concluded with the small impact of fasteners on the bending strength, and hence opted for the double thickness assumption consideration in the analytical design of these built-up sections.

The second part of this parametric study focused primarily on varying the wall thickness of the sections, ranged from very thin to thick sections, hence, multiple thicknesses were considered [0.3-2.4 mm], this part comprised a total of 52 specimens in four-points bending. The obtained FEA results were compared with DSM predictions, the results revealed that DSM predictions were too conservative, to the point to underestimate the flexural capacity of the two sections, particularly for very thin sections. This inconsistency in DSM predictions was noticed as well in previous studies conducted on built-up flexural members, highlighting that DSM could not be faithfully considered for built-up sections subjected to bending, therefore, indicating the requirement of new design provisions in such case, that worth nothing that previous studies presented modified versions for DSM through modifying the original equations, however, these suggestions were limited to certain built-up cross-sectional shapes. In this study an earnest attempt was made following a new design concept based on extending the DSM applicability on built-up sections subjected to sectional buckling was presented. Firstly, a mathematical model was developed based on the obtained results from the two built-up sections investigated, the adequacy of this model in presenting the obtained results, was verified statistically. Subsequently, the model was included in DSM nominal flexural strength equation for local buckling, thus obtaining the first equation of the Generalized Direct Strength Method (DSM-G), this new equation was applied on DM and DOW sections which experienced over-conservative results when using the original DSM. The obtained design prediction from the new design equation was very accurate for both sections. Further, to validate

the applicability of the new equation in over-conservative DSM case, the equation was applied on more built-up open and closed sections issued from literature [74,75] and yielded high flexural strength predictions.

It is important to note that the proposed method is based on a convergence-degree assumption, hence, a second equation is needed to cover unconservative DSM prediction case, based on the same hypothesis and process followed for the first equation but in a reversed case. The second equation exhibited validation through comparing with (FEA/Test) results the built-up closed sections reported in [74,75], and the comparison yielded satisfactory results.

This study detailed the process of developing the Generalized Direct Strength Method (DSM-G) as well as the validation of its applicability on built-up sections undergoing local buckling failure, it is important to note that this method is gradually expanded and validated, by applying it on more built-up sections, therefore the following diagram illustrates the steps of DSM-G application in built-up sections:

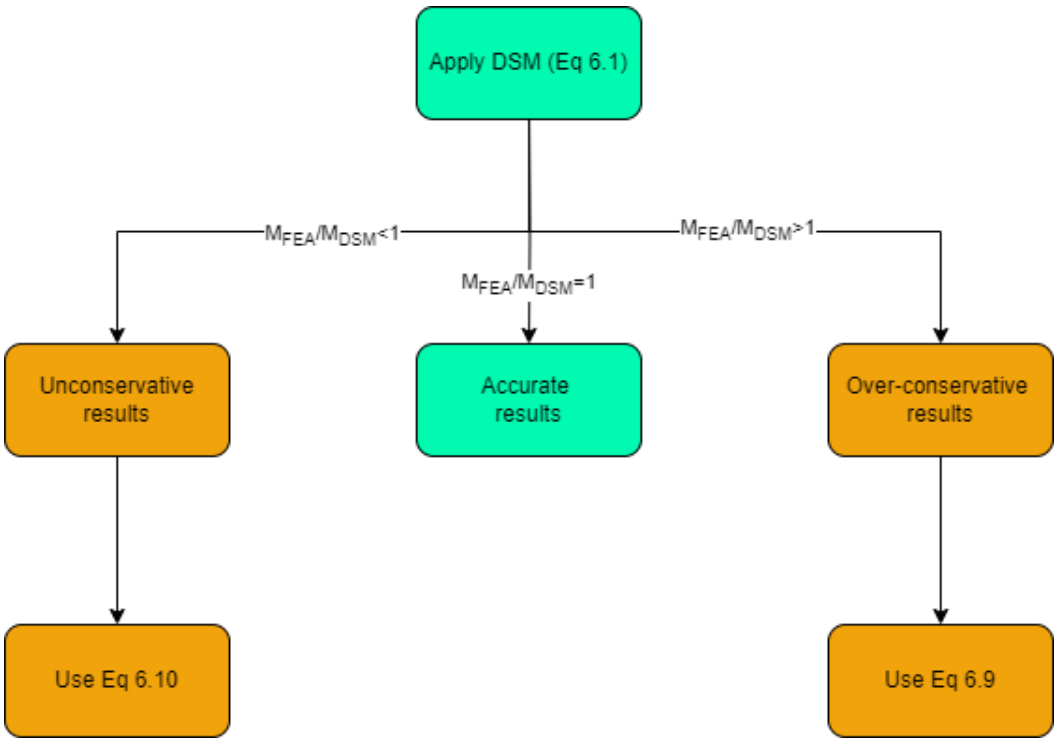

Figure 8.1: Diagram charts explaining DSM-G application [106].

8.2 Recommendations

The finite element model prescribed in this study has demonstrated its accuracy and performance through comparison with experimental results reported in the literature. As a result, it can be confidently utilized in future parametric studies involving variation in multiple parameters, such as cross-sectional shapes, loading types, and cross-sectional slenderness. This guarantees its applicability in studying different behavioral changes, such as global buckling of beams, and considering the magnitude of global and local imperfections when assessing their present determination criteria. The technic adopted for defining the interaction between individual components of the built-up member, as well as the virtual consideration of screws instead of physical modelling, was as well validated against tests particularly in visualizing the deformed shapes, this allowed for a better understanding of the impact of screws in the parametric study, this can open the door for more parametric studies regarding the impact of screws on built-up members, which consecutively could facilitates the elaboration of design provisions that handles the influence of screws spacing on the strength of built-up flexural members, considering the absence of such provisions in the current specifications.

The assessment of the present Direct Strength Method (DSM) as prescribed in (NAS) for flexural members, revealed a large inconsistency in predicting the flexural strength of built-up members. The Generalized Direct Strength Method (DSM-G) developed in this study was an earnest attempt to provide design provisions for built-up flexural members, however, its applicability was only investigated for members failing in local buckling or an interaction between local and distortional bucking, the consideration of global buckling must also be given attention, and the application of the DSM-G equations in case of specimens failing particularly in local-global interaction must be considered in future studies. The application of DSM-G equations on built-up sections with innovative cross-shapes is recommended further, to extend more its applicability in covering the design aspect for built-up flexural members.

Appendix

The following appendix presents two instances for the bending design capacity calculation of built-up members investigated in this study using DSM-G method, the specimens chosen are DM-1.5 and CV-0.48. To see material properties of the sections, refer to Table 4.2 (DM-1.5 uses COW-1.0 material properties).

- For DM section we use the following equation:

$$M_{DSM-G} = \frac{\eta}{0.1565t^3 - 0.774t^2 + 1.2178t + 0.2732} . M_{nl}$$

$$M_{nl} = \begin{Bmatrix} M_y + \left(1 - \frac{1}{C_{yl}^2}\right)(M_p - M_y) & for\ \lambda_{lf} \leq 0.776 \\ \left[1 - 0.15\left(\frac{M_{crl}}{M_y}\right)^{0.4}\right]\left(\frac{M_{crl}}{M_y}\right)^{0.4} M_y & for\ \lambda_{lf} > 0.776 \end{Bmatrix}$$

The determination of M_{crl} and M_p values should be aligned in accordance with the specifications presented in AISI-S100, specifically section F2.4.2.

λ_{lf}; is the fictive slenderness and its determined using the same steps for λ_l calculation;

$$\lambda_{lf} = \lambda_l = \sqrt{\frac{M_y}{M_{crl}}}$$

η: is determined from Figure 15 by selecting the correspondent distribution curve.

N.A on DM-1.5: for λ_{lf} = 0.43<0.776

$$M_{DSM-G} = \frac{\eta}{0.1565t^3 - 0.774t^2 + 1.2178t + 0.2732} . \left[M_y + \left(1 - \frac{1}{C_{yl}^2}\right)(M_p - M_y)\right]$$

M_{crl}= 32035359.4 N.mm; M_p = 7599992.4 N.mm; M_y= 5943480 N.mm; λ_{lf} = 0.43; $C_{yl} = 1.34$

t = 1.5 mm; η =1; Therefore:

$$M_{DSM-G} = \frac{1}{0.1565(1.5)^3 - 0.774(1.5)^2 + 1.2178(1.5) + 0.2732} . \left[5943480 + \left(1 - \frac{1}{(1.34)^2}\right)(7599992 - 5943480)\right]$$

$M_{DSM-G} = 7531663\ N.mm \approx 7532\ kN.mm$ (See Table 6.7).

For CV-0.48 beam we use the following equation:

$$M_{DSM-G} = \eta.(0.1565t^3 - 0.774t^2 + 1.2178t + 0.2732).M_{nl}$$

N.A on CV-0.48 beam:

η = 0.86; t = 0.48

For M_{nl} calculation in case of CV-0.48 we use the same steps as for DM-1.5 (basically a DSM calculation). In this example we directly used the value extracted from L. Wang & B. Young (2016) [75], Therefore:

$M_{DSM-G} = 0.86.(0.1565(0.48)^3 - 0.774(0.48)^2 + 1.2178(0.48) + 0.2732).2018 = 1209\ kN.mm$ (See Table 7.11)

References

[1] W.-W. Yu, *Cold-Formed Steel Design*. John Wiley & Sons, 2000.

[2] AISI (American Iron and Steel Institute). North American Specification for the Design of Cold-Formed Steel Structural Member. S100-16. Washington, DC: AISI; 2016.

[3] G. Winter, "Cold-Formed, Light Gage Steel Construction," *Journal of the Structural Division*, vol. 85, Nov. 1959.

[4] K. W. Karren, G. Winter, "Effects of Cold-Forming on Light-Gage Steel Members," *Journal of the Structural Division, ASCE Proceedings,* vol. 93, Feb. 1967.

[5] A. Chajes, S. J. Britvec, G. Winter "Effects of Cold-Straining on Structural Sheet Steels," *Journal of the Structural Division, ASCE Proceedings,* vol. 89, Apr. 1963.

[6] K. W Karren, "Corner Properties of Cold-Formed Steel Shapes," *Journal of the Structural Division, ASCE Proceedings,* vol. 93, Feb. 1967.

[7] G. Winter, J. Uribe, "Effects of Cold Work on Cold-Formed Steel Members Thin-Walled Steel Structures" *(K. C. Rockey and H. V. Hill, Eds.),* Gordon and Breach Science Publishers, New York, 1968.

[8] A. D. Martins, D. Camotim, and P. B. Dinis, "Local-distortional interaction in cold-formed steel beams: Behaviour, strength and DSM design," *Thin-Walled Structures*, vol. 119, pp. 879–901, Oct. 2017, doi: 10.1016/j.tws.2017.06.011.

[9] B. W. Schafer, *Distortional Buckling of Cold-Formed Steel Columns, AISI Report, American Iron & Steel Institute, Washington DC*. 2000.

[10] B. W. Schafer, "Local, Distortional, and Euler Buckling of Thin-Walled Columns," *Journal of Structural Engineering*, vol. 128, no. 3, pp. 289–299, Mar. 2002, doi: 10.1061/(asce)0733-9445(2002)128:3(289).

[11] B. Young, N. Silvestre, and D. Camotim, "Cold-Formed Steel Lipped Channel Columns Influenced by Local-Distortional Interaction: Strength and DSM Design," *Journal of Structural Engineering*, vol. 139, no. 6, pp. 1059–1074, Jun. 2013, doi: 10.1061/(asce)st.1943-541x.0000694.

[12] N. Silvestre, D. Camotim, and P.B. Dinis, "Direct strength prediction of lipped channel columns experiencing local-plate/distortional interaction," *Advanced Steel Construction*, vol. 5(1), no. 49–71, 2009.

[13] N. Silvestre, D. Camotim, and P.B. Dinis, "Post-buckling behaviour and direct strength design of lipped channel columns experiencing local-distortional interaction," *Submitted for publication*, 2011, **In-press**.

[14] E. S. Bernard, R. Q. Bridge, and G. J. Hancock, "Tests of Profiled Steel Decks with Flat-Hat Stiffeners," *Journal of Structural Engineering*, vol. 121, no. 8, pp. 1175–1182, Aug. 1995, doi: 10.1061/(asce)0733-9445(1995)121:8(1175).

[15] E. S. Bernard, R. Q. Bridge, and G. J. Hancock, "Tests of Profiled Steel Decks with V-Stiffeners," *Journal of Structural Engineering*, vol. 119, no. 8, pp. 2277–2293, Aug. 1993, doi: 10.1061/(asce)0733-9445(1993)119:8(2277).

[16] H. Wang and Y. Zhang, "Experimental and numerical investigation on cold-formed steel C-section flexural members," *Journal of Constructional Steel Research*, vol. 65, no. 5, pp. 1225–1235, May 2009, doi: 10.1016/j.jcsr.2008.08.007.

[17] M.-T. Chen, B. Young, A. D. Martins, D. Camotim, and P. B. Dinis, "Uniformly bent CFS lipped channel beams experiencing local-distortional interaction: Experimental investigation," *Journal of Constructional Steel Research*, vol. 170, p. 106098, Jul. 2020, doi: 10.1016/j.jcsr.2020.106098.

[18] N. Silvestre, D. Camotim, P.B. Dinis, and D. Camotim, "Direct strength method for lipped channel columns and beams affected by local-plate/distortional interaction," in *Proceedings of 18th International Specialty Conference on Cold- Formed Steel Structures*, W.-W. Yu, R. Laboube., vol. 26-27/10, Orlando, 2006, pp. 17–37.

[19] P. Borges Dinis, D. Camotim, "Local/distortional mode interaction in cold-formed steel lipped channel beams," *Thin-Walled Structures*, vol. 48, no. 10–11, pp. 771–785, Oct. 2010, doi: 10.1016/j.tws.2010.01.005.

[20] M. Anbarasu, "Local-distortional buckling interaction on cold-formed steel lipped channel beams," *Thin-Walled Structures*, vol. 98, pp. 351–359, Jan. 2016, doi: 10.1016/j.tws.2015.10.003.

[21] B. W. Schafer and T. Peköz, "Computational modeling of cold-formed steel: characterizing geometric imperfections and residual stresses," *Journal of Constructional Steel Research*, vol. 47, no. 3, pp. 193–210, Sep. 1998, doi: 10.1016/s0143-974x(98)00007-8.

[22] G. J. Hancock, "Nonlinear Analysis of Thin Sections in Compression," *Journal of the Structural Division*, vol. 107, no. 3, pp. 455–471, Mar. 1981, doi: 10.1061/jsdeag.0005658.

[23] B. S. I. Staff, *Structural Use of Steelwork in Building*. 2006.

[24] K. S. Sivakumaran and N. Abdel-Rahman, "A finite element analysis model for the behaviour of cold-formed steel members," *Thin-Walled Structures*, vol. 31, no. 4, pp. 305–324, Aug. 1998, doi: 10.1016/s0263-8231(98)00017-2.

[25] O. Kaitila, "Imperfection sensitivity analysis of lipped channel columns at high temperatures," *Journal of Constructional Steel Research*, vol. 58, no. 3, pp. 333–351, Mar. 2002, doi: 10.1016/s0143-974x(01)00060-8.

[26] M. Ashraf, L. Gardner, and D. A. Nethercot, "Finite element modelling of structural stainless steel cross-sections," *Thin-Walled Structures*, vol. 44, no. 10, pp. 1048–1062, Oct. 2006, doi: 10.1016/j.tws.2006.10.010.

[27] B. W. Schafer, M. Grigoriu, and T. Peköz, "A probabilistic examination of the ultimate strength of cold-formed steel elements," *Thin-Walled Structures*, vol. 31, no. 4, pp. 271–288, Aug. 1998, doi: 10.1016/s0263-8231(98)00019-6.

[28] J. Rondal, *Structure à parois mince*, Note de cours. Université de Liège, 2000.

[29] M. Batista, *Etude de stabilité des profils à parois minces et sections ouvertes de type U et C*, Thèse de doctorat. Université de Liège, 1988.

[30] H. C. Bui, *Analyse statique du comportement des structures à parois minces par la méthode des éléments finis et des bandes finis de type plaque et coque surbaissé déformables en cisaillement*. GB: Editions universitaires européennes, 2010.

[31] M. Grumbach and M. Prudhomme, *Propriétés des profilés à froids*, Construction métallique., vol. 1. 1974.

[32] N. Abdel-Rahman and K. S. Sivakumaran, "Material Properties Models for Analysis of Cold-Formed Steel Members," *Journal of Structural Engineering*, vol. 123, no. 9, pp. 1135–1143, Sep. 1997, doi: 10.1061/(asce)0733-9445(1997)123:9(1135).

[33] K. S. Sivakumaran and N. Abdel-Rahman, "A finite element analysis model for the behaviour of cold-formed steel members," *Thin-Walled Structures*, vol. 31, no. 4, pp. 305–324, Aug. 1998, doi: 10.1016/s0263-8231(98)00017-2.

[34] P. A. Matthey, *Comportement des poutres-colonnes métallique en double té*. Ecole polytechnique fédérale de Lausanne, 1985.

[35] Y. Itohi, *Ultimate strength variations of structural steel members*, Doctorat Dissertation. University of Nagoya, Department of civil engineering, 1984.

[36] C. M. Costa Ferreira and J. Rondal, *Etude expérimentale de la stabilité des cornières à parois minces profilées à froid*, Rapport N°149. Université de Liège, laboratoire de stabilité des constructions, 1985.

[37] C. M. Costa Ferreira, "Essais de cornière en acier pliées à froid," Université de Liège, laboratoire de stabilité des constructions, Liège, 155, Nov. 1986.

[38] G. W. Schulz and G. Alpsten, "Geometrical and cross-sectional properties of steel structures," *Manual on the stability of steel structures*. European Convention for Constructional Steelwork, 1976.

[39] S. M. Chou and J. Rhodes, "Review and compilation of experimental results on thin-walled structures," *Computers & Structures*, vol. 65, no. 1, pp. 47–67, Oct. 1997, doi: 10.1016/s0045-7949(96)00337-9.

[40] S. P. Timoshenko and J. M. Gere, *Theory of Elastic Stability*. Courier Corporation, 2012.

[41] N. W. Murray, *Introduction to the Theory of Thin-walled Structures*. Oxford University Press, USA, 1986.

[42] N. S. Trahair, *Flexural-Torsional Buckling of Structures*. CRC Press, 1993.

[43] F. Bleich, *Buckling Strength of Metal Structures*. London: Mc Grew-Hill, 1952.

[44] S. C. W. Lau and G. J. Hancock, "Distortional Buckling Formulas for Channel Columns," *Journal of Structural Engineering*, vol. 113, no. 5, pp. 1063–1078, May 1987, doi: 10.1061/(asce)0733-9445(1987)113:5(1063).

[45] G. J. Hancock, "Design for distortional buckling of flexural members," *Thin-Walled Structures*, vol. 27, no. 1, pp. 3–12, Jan. 1997, doi: 10.1016/0263-8231(96)00020-1.

[46] R. Schardt, "Lateral torsional and distortional buckling of channel- and hat-sections," *Journal of Constructional Steel Research*, vol. 31, no. 2–3, pp. 243–265, Jan. 1994, doi: 10.1016/0143-974x(94)90012-4.

[47] J. M. Davies and P. Leach, "First-order generalised beam theory," *Journal of Constructional Steel Research*, vol. 31, no. 2–3, pp. 187–220, Jan. 1994, doi: 10.1016/0143-974x(94)90010-8.

[48] J. M. Davies, P. Leach, and D. Heinz, "Second-order generalised beam theory," *Journal of Constructional Steel Research*, vol. 31, no. 2–3, pp. 221–241, Jan. 1994, doi: 10.1016/0143-974x(94)90011-6.

[49] *Eurocode 3 - Design of steel structures - Part 1-3: General rules - Supplementary rules for cold-formed members and sheeting*. 2006.

[50] J. Rondal, *Contribution à l'étude de la stabilité des profis creux à parois minces*, Thèse de doctorat. Belgique: Université de Liège, 2000.

[51] J. Rondal and R. Maquoi, *Formulation d'Ayrton-Perry pour le flambement des barres métalliques*, Construction métallique., vol. 41–53. 1979.

[52] B. W. Schafer, *Direct strength prediction of cold-formed steel members using numerical elastic buckling solution*, Second International Conference on Thin-

Walled Structures, Research and Development. Singapore: Elsevier Science Ltd, Oxford, pp. 137-144, 1998.

[53] B. W. Schafer, "Local, Distortional, and Euler Buckling of Thin-Walled Columns," *Journal of Structural Engineering*, vol. 128, no. 3, pp. 289–299, Mar. 2002, doi: 10.1061/(asce)0733-9445(2002)128:3(289).

[54] B. W. Schafer, *Elastic buckling analysis of thin-walled members using the classical finite strip method*, CUFSM Version 2.6. John Hopkins University, 2003.

[55] A. Rusch and J. Lindner, "Remarks to the Direct Strength Method," *Thin-Walled Structures*, vol. 39, no. 9, pp. 807–820, Sep. 2001, doi: 10.1016/s0263-8231(01)00023-4.

[56] S. Ádány and B. W. Schafer, "Buckling mode decomposition of single-branched open cross-section members via finite strip method: Derivation," *Thin-Walled Structures*, vol. 44, no. 5, pp. 563–584, May 2006, doi: 10.1016/j.tws.2006.03.013.

[57] Y. K. Cheung, *Finite strip method in structural analysis* . New york: Pergamon Press, 1976.

[58] B. W. Schafer, *Cold-formed Steel Behavior and Design*, PhD. dissertation. New York: Cornell University, 1997.

[59] X. Chu, Z. Ye, R. Kettle, and L. Li, "Buckling behaviour of cold-formed channel sections under uniformly distributed loads," *Thin-Walled Structures*, vol. 43, no. 4, pp. 531–542, Apr. 2005, doi: 10.1016/j.tws.2004.10.002.

[60] S. C. Fan and Y. K. Cheung, "Analysis of shallow shells by spline finite strip method," *Engineering Structures*, vol. 5, no. 4, pp. 255–263, Oct. 1983, doi: 10.1016/0141-0296(83)90004-4.

[61] H. Y. Yang and K. P. Chong, "Finite strip method with X-spline functions," *Computers & Structures*, vol. 18, no. 1, pp. 127–132, Jan. 1984, doi: 10.1016/0045-7949(84)90087-7.

[62] T. Mizusawa, T. Kajita, and M. Naruoka, “Buckling of skew plate structures using B-spline functions,” *International Journal for Numerical Methods in Engineering*, vol. 15, no. 1, pp. 87–96, Jan. 1980, doi: 10.1002/nme.1620150108.

[63] S. C. W. Lau and G. J. Hancock, “Buckling of thin flat-walled structures by a spline finite strip method,” *Thin-Walled Structures*, vol. 4, no. 4, pp. 269–294, Jan. 1986, doi: 10.1016/0263-8231(86)90034-0.

[64] L. G. Tham, “Application of spline finite strip method in the analysis of space structures,” *Thin-Walled Structures*, vol. 10, no. 3, pp. 235–246, Jan. 1990, doi: 10.1016/0263-8231(90)90066-8.

[65] J. Ye, F. J. Meza, I. Hajirasouliha, J. Becque, P. Shepherd, and K. Pilakoutas, “Experimental Investigation of Cross-Sectional Bending Capacity of Cold-Formed Steel Channels Subject to Local-Distortional Buckling Interaction,” *Journal of Structural Engineering*, vol. 145, no. 7, Jul. 2019, doi: 10.1061/(asce)st.1943-541x.0002344.

[66] R. Sujitha *et al.*, “Analytical and Experimental Study on Cold-Formed Steel Built-Up Sections for Bending,” *Materials*, vol. 15, no. 20, p. 7140, Oct. 2022, doi: 10.3390/ma15207140.

[67] R. A. Fitrah and A. P. Melinda, *Behaviour of Cold-formed Steel Back-to-Back Channel Built-Up Sections under Bending*, 2nd Conference on Innovation in Technology (CITES 2020) 4th-5th November 2020., vol. 1041. Padang, Indonesia: IOP Publishing Ltd, 2021. doi: 10.1088/1757-899X/1041/1/012006.

[68] K. Roy, H. Ho Lau, T. C. H. Ting, B. Chen, and J. B. P. Lim, “Flexural behaviour of back-to-back built-up cold-formed steel channel beams: Experiments and finite element modelling,” *Structures*, vol. 29, pp. 235–253, Feb. 2021, doi: 10.1016/j.istruc.2020.10.052.

[69] P. Manikandan and M. Thulasi, “Investigation on cold-formed steel lipped channel built-up I beam with intermediate web stiffener,” *International Journal*

of Advanced Structural Engineering, vol. 11, no. 1, pp. 97–107, Feb. 2019, doi: 10.1007/s40091-019-0220-x.

[70] X.-H. Zhou and Y. Shi, "Flexural Strength Evaluation for Cold-Formed Steel Lip-Reinforced Built-up I-Beams," *Advances in Structural Engineering*, vol. 14, no. 4, pp. 597–611, Aug. 2011, doi: 10.1260/1369-4332.14.4.597.

[71] J. Ye, F. J. Meza, I. Hajirasouliha, J. Becque, P. Shepherd, and K. Pilakoutas, "Experimental Investigation of Cross-Sectional Bending Capacity of Cold-Formed Steel Channels Subject to Local-Distortional Buckling Interaction," *Journal of Structural Engineering*, vol. 145, no. 7, Jul. 2019, doi: 10.1061/(asce)st.1943-541x.0002344.

[72] S. Selvaraj and M. Madhavan, "Design of Cold-Formed Steel Back-To-Back Connected Built-up Beams," *Journal of Constructional Steel Research*, vol. 181, p. 106623, Jun. 2021, doi: 10.1016/j.jcsr.2021.106623.

[73] L. Laím, J. P. C. Rodrigues, and L. S. da Silva, "Experimental and numerical analysis on the structural behaviour of cold-formed steel beams," *Thin-Walled Structures*, vol. 72, pp. 1–13, Nov. 2013, doi: 10.1016/j.tws.2013.06.008.

[74] L. Wang and B. Young, "Behavior of Cold-Formed Steel Built-Up Sections with Intermediate Stiffeners under Bending. I: Tests and Numerical Validation," *Journal of Structural Engineering*, vol. 142, no. 3, Mar. 2016, doi: 10.1061/(asce)st.1943-541x.0001428.

[75] L. Wang and B. Young, "Behavior of Cold-Formed Steel Built-Up Sections with Intermediate Stiffeners under Bending. II: Parametric Study and Design," *Journal of Structural Engineering*, vol. 142, no. 3, Mar. 2016, doi: 10.1061/(asce)st.1943-541x.0001427.

[76] M. Anbarasu, "Simulation of flexural behaviour and design of cold-formed steel closed built-up beams composed of two sigma sections for local buckling," *Engineering Structures*, vol. 191, pp. 549–562, Jul. 2019, doi: 10.1016/j.engstruct.2019.04.093.

[77] S. Selvaraj and M. Madhavan, "Structural Design of Cold-formed Steel face-to-face Connected Built-up beams using Direct Strength Method," *Journal of Constructional Steel Research*, vol. 160, pp. 613–628, Sep. 2019, doi: 10.1016/j.jcsr.2019.05.053.

[78] M. A. Dar, M. Yusuf, A. R. Dar, and J. Raju, "Experimental study on innovative sections for cold formed steel beams," *Steel and Composite Structures*, vol. 19, no. 6, pp. 1599–1610, Dec. 2015, doi: 10.12989/scs.2015.19.6.1599.

[79] B. El-Taly and M. El-shami, "Structural Performance of Cold-formed Steel Face-to-face and Back-to-back Beams," *International Journal of Civil Engineering*, vol. 19, no. 12, pp. 1427–1444, Jun. 2021, doi: 10.1007/s40999-021-00606-y.

[80] F. Muftah, M. S. H. Mohd Sani, and M. M. Mohd Kamal, "Flexural Strength Behaviour of Bolted Built-Up Cold-Formed Steel Beam with Outstand and Extended Stiffener," *International Journal of Steel Structures*, vol. 19, no. 3, pp. 719–732, Sep. 2018, doi: 10.1007/s13296-018-0157-0.

[81] C. Wang, Q. Guo, Z. Zhang, and Y. Guo, "Experimental and numerical investigation of perforated cold-formed steel built-up I-section columns with web stiffeners and complex edge stiffeners," *Advances in Structural Engineering*, vol. 22, no. 10, pp. 2205–2221, Mar. 2019, doi: 10.1177/1369433219836174.

[82] J. Ye, I. Hajirasouliha, J. Becque, and K. Pilakoutas, "Development of more efficient cold-formed steel channel sections in bending," *Thin-Walled Structures*, vol. 101, pp. 1–13, Apr. 2016, doi: 10.1016/j.tws.2015.12.021.

[83] D. Dubina, V. Ungureanu, and L. Gîlia, "Experimental investigations of cold-formed steel beams of corrugated web and built-up section for flanges," *Thin-Walled Structures*, vol. 90, pp. 159–170, May 2015, doi: 10.1016/j.tws.2015.01.018.

[84] A. R. Dar, M. Anbarasu, and G. Arun Kumar, "Cold-Formed Steel Built-Up I-Beam with the Trapezoidal Corrugated Web: Tests and Numerical Simulation,"

Journal of The Institution of Engineers (India): Series A, vol. 102, no. 4, pp. 943–958, Sep. 2021, doi: 10.1007/s40030-021-00571-8.

[85] Y. Wu, X. Du, and H. Yuan, "Structural performance of cold-formed steel box girders with C-section flanges and sinusoidal corrugated webs," *Structures*, vol. 34, pp. 4851–4866, Dec. 2021, doi: 10.1016/j.istruc.2021.10.066.

[86] D. Ravi, A. R. Ponsubbiah, S. S. Prabha, and J. P. Saratha, "Experimental, analytical and numerical studies on concrete encased trapezoidally web profiled cold-formed steel beams by varying depth-thickness ratio," *Frontiers of Structural and Civil Engineering*, vol. 14, no. 4, pp. 930–946, Aug. 2020, doi: 10.1007/s11709-020-0652-1.

[87] M. Sifan *et al.*, "Flexural behaviour and design of hollow flange cold-formed steel beam filled with lightweight normal and lightweight high strength concrete," *Journal of Building Engineering*, vol. 48, p. 103878, May 2022, doi: 10.1016/j.jobe.2021.103878.

[88] P. Hegyi and L. Dunai, "Experimental study on ultra-lightweight-concrete encased cold-formed steel structures Part I: Stability behaviour of elements subjected to bending," *Thin-Walled Structures*, vol. 101, pp. 75–84, Apr. 2016, doi: 10.1016/j.tws.2016.01.004.

[89] T. Valsa Ipe, H. Sharada Bai, K. Manjula Vani, and M. M. Zafar Iqbal, "Flexural behavior of cold-formed steel concrete composite beams," *Steel & Composite structures*, vol. 14, no. 2, pp. 105–120, Feb. 2013, doi: 10.12989/scs.2013.14.2.105.

[90] M. A. Dar *et al.*, "Development of lightweight CFS composite built-up beams: Tests and flexural response," *Journal of Constructional Steel Research*, vol. 209, p. 108041, Oct. 2023, doi: 10.1016/j.jcsr.2023.108041.

[91] M. A. Dar *et al.*, "Intermittently stiffened cold-formed steel GFRP composite lightweight built-up beams: Experimental investigation and performance assessment," *Thin-Walled Structures*, vol. 185, p. 110630, Apr. 2023, doi: 10.1016/j.tws.2023.110630.

[92] M. A. Dar, S. J. Fayaz, S. Rather, A. R. Dar, and I. Hajirasouliha, “Incremental stiffening approach for CFS built-up-beams with large imperfections: Tests and flexural-behaviour,” *Structures*, vol. 53, pp. 1318–1340, Jul. 2023, doi: 10.1016/j.istruc.2023.05.003.

[93] M. A. Dar, M. Anbarasu, A. R. Dar, N. U. Islam, A. F. Ghowsi, and H. Carvalho, “Stiffening schemes for CFS built-up I-beams with large global imperfections: Capacity and behaviour,” *Steel and Composite Structures*, vol. 42, no. 4, pp. 447–458, Feb. 2022, doi: https://doi.org/10.12989/scs.2022.42.4.447.

[94] M. A. Dar *et al.*, “Intermittently stiffened cold-formed steel GFRP composite lightweight built-up beams: Experimental investigation and performance assessment,” *Thin-Walled Structures*, vol. 185, p. 110630, Apr. 2023, doi: 10.1016/j.tws.2023.110630.

[95] Z. Li, J. Leng, J. K. Guest, and B. W. Schafer, “Two-level optimization for a new family of cold-formed steel lipped channel sections against local and distortional buckling,” *Thin-Walled Structures*, vol. 108, pp. 64–74, Nov. 2016, doi: 10.1016/j.tws.2016.07.004.

[96] B. W. Schafer, “Advances in the Direct Strength Method of cold-formed steel design,” *Thin-Walled Structures*, vol. 140, pp. 533–541, Jul. 2019, doi: 10.1016/j.tws.2019.03.001.

[97] J.-H. Zhang and B. Young, “Compression tests of cold-formed steel I-shaped open sections with edge and web stiffeners,” *Thin-Walled Structures*, vol. 52, pp. 1–11, Mar. 2012, doi: 10.1016/j.tws.2011.11.006.

[98] S. Kherbouche and A. Megnounif, “Numerical study and design of thin walled cold formed steel built-up open and closed section columns,” *Engineering Structures*, vol. 179, pp. 670–682, Jan. 2019, doi: 10.1016/j.engstruct.2018.10.069.

[99] R. S. Glauz, "Enhancements to the Direct Strength Method of cold-formed steel member design," *Thin-Walled Structures*, vol. 183, p. 110421, Feb. 2023, doi: 10.1016/j.tws.2022.110421.

[100] L. Wang and B. Young, "Behaviour and design of cold-formed steel built-up section beams with different screw arrangements," *Thin-Walled Structures*, vol. 131, pp. 16–32, Oct. 2018, doi: 10.1016/j.tws.2018.06.022.

[101] B. W. Schafer, "Constrained and unconstrained finite strip method," *(CUFSM). Version 5.01*, [Online]. Available: https://www.ce.jhu.edu/cufsm/

[102] M. Abbasi, M. Khezri, K. J. R. Rasmussen, and B. W. Schafer, "Elastic buckling analysis of cold-formed steel built-up sections with discrete fasteners using the compound strip method," *Thin-Walled Structures*, vol. 124, pp. 58–71, Mar. 2018, doi: 10.1016/j.tws.2017.11.046.

[103] ABAQUS version 6.14-5, *ABAQUS/CAE user's guide*, Dassault Systèmes Simulia Corp, Providence, RI, USA, 2014.

[104] ASCE, *Minimum design loads and associated criteria for buildings and other structures*, ASCE/SEI 7. ASCE, Reston, VA, 2016.

[105] AS-NZS 1170-2: *Structural design actions - Part 0: General principles* [By Authority of New Zealand Structure Verification Method B1/VM1], vol. 2, 2002.

[106] S.-E. Maizi, Y. Hadidane, and M. A. Dar, "Flexural design of cold-formed steel built-up sections failing by local buckling: Development of generalised direct strength method" Engineering Structures, vol. 308, p. 117967, Jun. 2024, doi: 10.1016/j.engstruct.2024.117967.

[107] F. Meza, 2018. "*The behaviour of cold-formed steel built-up structural members*", Doctoral dissertation, The University of Sheffield.